Gondwana Research 27 (2015) 459–485

Contents lists available at ScienceDirect

Gondwana Research

journal homepage: www.elsevier.com/locate/gr

Diamonds, native elements and metal alloys from chromitites of the Ray-Iz ophiolite of the Polar Urals

Jingsui Yang [a,*], Fancong Meng [a], Xiangzhen Xu [a], Paul T. Robinson [a], Yildirim Dilek [b], Alexander B. Makeyev [c], Richard Wirth [d], Michael Wiedenbeck [d], John Cliff [e]

[a] CARMA, State Key Laboratory of Continental Tectonics and Dynamics, Institute of Geology, Chinese Academy of Geological Sciences, Beijing 100037, China
[b] Department of Geology and Environmental Earth Science, Miami University, Oxford, OH 45056, USA
[c] Institute of Geology, Komi Scientific Center, Ural Division, Russian Academy of Sciences, Pervomaiskayaul. 54, Syktyvkar, 167982 Komi Republic, Russia
[d] Helmholtz Centre Potsdam, GFZ German Research Centre for Geosciences, D14473 Potsdam, Germany
[e] CMCA, The University of Western Australia, Crawley, WA 6009, Australia

ARTICLE INFO

Article history:
Received 19 October 2013
Received in revised form 14 July 2014
Accepted 14 July 2014
Available online 10 August 2014

Keywords:
Ophiolitic diamonds
UHP minerals
Native elements
Podiform chromitite
Tectonics

ABSTRACT

Diamonds and a wide range of unusual minerals were originally discovered from the chromitite and peridotite of the Luobusa ophiolite along the Yarlong–Zangbu suture zone in southern Tibet. To test whether this was a unique occurrence or whether such minerals were present in other ophiolites, we investigated the Ray-Iz massif of the early Paleozoic Voikar–Syninsk ophiolite belt in the Polar Urals (Russia) for a comparative study. Over 60 mineral species, including diamond, moissanite, native elements and metal alloys have been separated from ~1500 kg of chromitite collected from two orebodies in the Ray-Iz ophiolite. More than 1000 grains of microdiamond were recovered from the chromitite and, of particular importance, 2 grains were found as in-situ inclusions in chromite grains, proving that these minerals are intrinsic to the rock, and not the result of natural or anthropogenic contamination. The native elements include Cr, W, Ni, Co, Si, Al and Ta, commonly associated with carbides such as SiC and WC, and metallic alloys, such as CrFe, SiAlFe, NiCu, AgAu, AgSn, FeSi, FeP, and AgZnSn also occur. These minerals are accompanied by oxides (wüstite, periclase, eskolaite, rutile, baddeleyite, ilmenite, corundum, chromite, NiO and SnO_2) and silicates (kyanite, zircon, garnet, feldspar, and quartz). Sulfides of Fe, Ni, Cu, Mo, Pb, Ab, AsFe, FeNi, CuZn, and CoFeNi are common, as are various iron minerals, such as native Fe, FeO, and Fe_2O_3. Here, we focus on the composition and character of the diamonds, native elements and metal alloys.

All of the minerals discussed here are similar to those reported from chromitites of the Luobusa ophiolite, Tibet, indicating that they are not restricted to one ophiolite or one geographic region; rather, they may be widespread in the oceanic mantle. The diamonds recovered from these ophiolites are completely different from most of those in kimberlites and ultra-high pressure (UHP) metamorphic rocks, and represent a new occurrence of diamonds on Earth. A three-stage model is proposed to explain the source of the diamonds and highly-reduced minerals, their formation, and their preservation in ophiolites.

1. Introduction

Ophiolites are fragments of ancient ocean lithosphere emplaced on continental margins, in island arcs and/or in accretionary prisms, and have long been studied to better understand the Wilson Cycle evolution of ocean basins, plate boundary processes, collision tectonics, and the occurrence of valuable ore bodies, such as podiform chromitites and massive sulfide deposits (Coleman, 1977; Pearce et al., 1984; Nicolas, 1989; Dilek, 2003; Dilek and Furnes, 2011, 2014; Furnes et al., 2014a, b). The melt evolution of ophiolites are generally thought to take place at shallow mantle levels beneath the spreading axes in different tectonic settings (Pearce et al., 1984; Dilek et al., 1999; Proenza et al., 1999; Yumul, 2001; Flower and Dilek, 2003; Pearce, 2003; Dilek and Thy, 2009). The podiform chromitites hosted in ophiolites are currently interpreted as magmatic deposits formed during melt–rock reaction in mid-ocean ridge (MOR) or suprasubduction zone (SSZ) environments (Stockman and Hlava, 1984; Talkington et al., 1984; Zhou et al., 1994, 1996; Arai, 1997; Edwards et al., 2000; Rollinson, 2008; Rollinson and Adetunji, 2013). However, in-situ diamonds and other UHP minerals, highly reduced phases and native elements in ophiolitic peridotites and chromitites of southern Tibet (Bai et al., 2000a,b; Bai et al., 2003; Robinson et al., 2004; Yang et al., 2007, 2009; Dobrzhinetskaya et al., 2009; Ren et al., 2009; Trumbull et al., 2009; Xu et al., 2009; Yamamoto et al., 2009; Xu et al., 2011; Yang and Robinson, 2011)

* Corresponding author. Tel.: +86 10 68997804; fax: +86 10 68999698.
E-mail addresses: yangjsui@163.com, yangjsui@cags.ac.cn (J. Yang).

http://dx.doi.org/10.1016/j.gr.2014.07.004
1342-937X/

strongly suggest that some of these bodies formed at mantle depths of 150–300 km or greater, perhaps near the mantle transition zone (Yang et al., 2014). For example, recently discovered coesite in the Luobusa chromitites is thought to be pseudomorphic after stishovite, formed initially at pressures >10 GPa, which are much higher than the pressures under which coesite is formed during prograde metamorphism in UHP orogenic belts (Yang et al., 2007). Dobrzhinetskaya et al. (2009) reported grains of osbornite (TiN), cubic boron nitride (cBN) (>300 km depth) and α-PbO_2-structured TiO_2 (TiO_2 II) intergrown with the coesite. Exsolution lamellae of coesite and clinopyroxene in chromite grains have also been reported by Yamamoto et al. (2009), suggesting a depth of formation >370 km.

Diamonds in the Luobusa chromitites occur both as inclusions in OsIr alloy, and as in-situ grains in chromite (Yang et al., 2007, 2009; Yang and Robinson, 2011; Yang et al., 2014), confirming their mantle origin and indicating ultrahigh temperatures and pressures of formation T > 2000 °C and P > 5 GPa. Importantly, UHP minerals, such as diamond, as well as many highly reduced phases have been separated from peridotites of many other ophiolites in the Yarlung–Zangbo suture zone of Tibet, including, Zedang, Xigaze, Dangqiong, Purang and Dongbo (Xu et al., 2009, 2011; Yang et al., 2011, 2014). These massifs consist mainly of harzburgite and minor dunite–lherzolite of mid-ocean ridge (MOR) origin that were later modified in a suprasubduction zone (SSZ) environment (Xiong et al., 2011; Xu et al., 2011), typical of the upper mantle sequences in many other Tethyan ophiolites (Hoeck et al., 2002; Dilek and Flower, 2003; Saccani and Photiades, 2004; Dilek and Furnes, 2009; Moghadam et al., 2010; Goodenough et al., 2014; Sarifakioglu et al., 2014; Uysal et al., 2014).

Diamonds from ophiolites of different massifs show many similarities in their morphology, carbon isotopes and mineral inclusions, but are distinctly different in all these respects from most diamonds occurring in kimberlites and UHP metamorphic belts (Sobolev and Shatsky, 1990; Dobrzhinetskaya et al., 1995; Stachel et al., 2000; Cartigny, 2005; Xu et al., 2011; Yang et al., 2013). These findings indicate a completely new environment for diamond formation in ophiolitic mantle peridotites.

The discovery of UHP and highly reduced minerals in the Tibetan ophiolites has raised many questions regarding the origin of ophiolites and chromitites, and the composition of the upper mantle. Are these unusual minerals restricted to ophiolites in Tibet or do they occur in ophiolites of different ages, geographic locations and tectonic environments of formation? How can the formation and preservation of UHP minerals in oceanic lithosphere be explained, and what are the mantle dynamics involved in this process? The Paleozoic Ray-Iz ophiolite of the Polar Urals was selected for comparison with the Luobusa ophiolite because it is a large, well-exposed body of different age that lies in a completely different orogenic belt far from the Tibetan ophiolites (Fig. 1).

The Uralide orogenic belt is a major early Paleozoic suture zone extending more than 2500 km in a N–S direction that divides Europe from Asia (Chemenda et al., 1997). Ophiolites, podiform chromitites and high-pressure metamorphic rocks are well developed in the orogen (Brown et al., 1998; Leech and Ernst, 1998, 2000; Spadea et al., 2003). The Ray-Iz ophiolite occurs at the northeast end of the Paleozoic Voikar–Syninsk ophiolite belt in the Polar Urals (Fig. 1; Moldavantsev and Kazak, 1977; Garutis et al., 1999), where it consists chiefly of mantle peridotite containing over 200 podiform chromitite orebodies.

We sampled ophiolite peridotites and associated chromitites in Ray-Iz for comparison with the Tibetan ophiolites. In this paper, we document many similarities between the two ophiolites and confirm that the diamonds and highly reduced minerals previously discovered in Tibetan ophiolites are not unique, suggesting that such minerals may occur widely in the oceanic mantle. We discuss the conditions

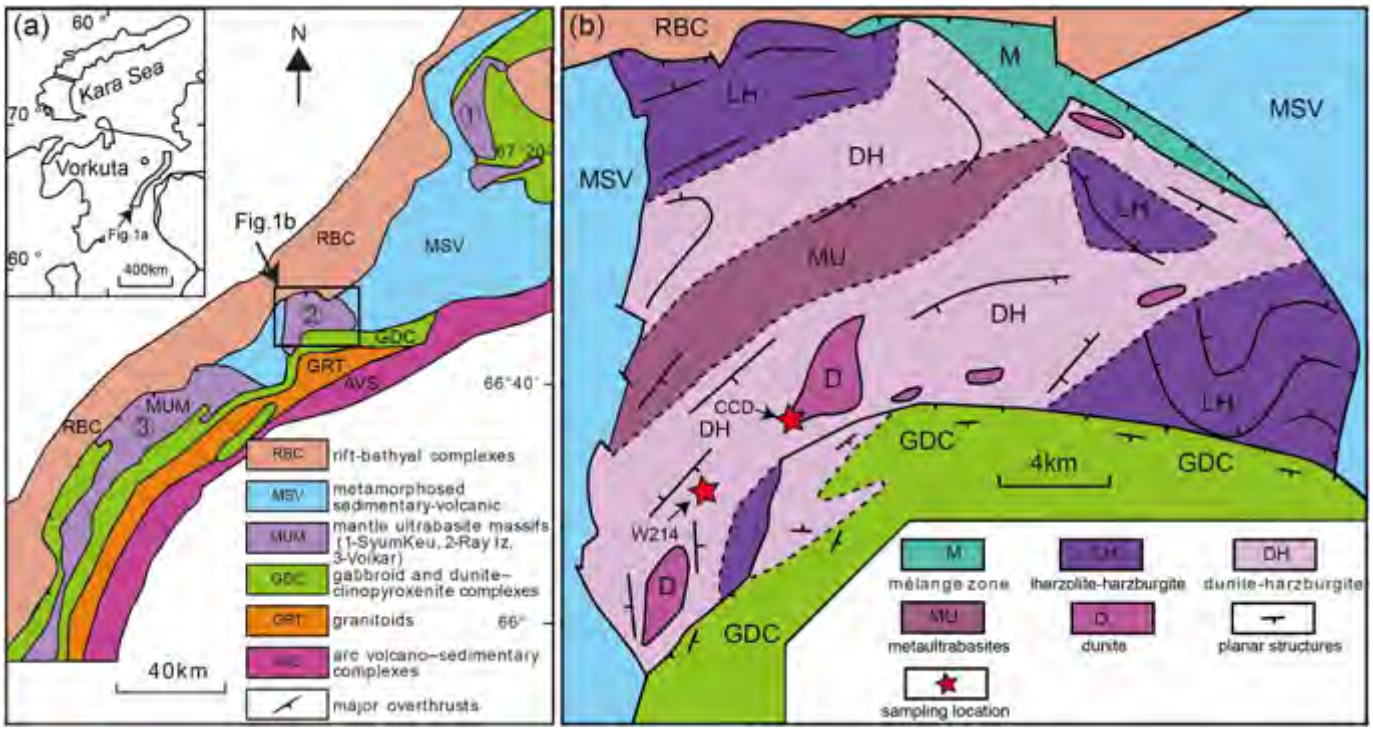

Fig. 1. Sketch geological maps of the Vorkuta ophiolite belt and Ray-Iz ophiolite in the Polar Urals. a) Map of the northern Ural Mountains. RBC: Lower–Middle Paleozoic rift–bathyal complexes (paleocontinental sector); MSV: metamorphosed sedimentary–volcanic Paleozoic rocks with Precambrian basement blocks; MUM: mantle ultrabasite massifs (1—Syum–Keu, 2—Ray-Iz, 3—Voikar); GDC: gabbroid and dunite–clinopyroxenite complexes; GRT: granitoids; AVS: Paleozoic arc volcano-sedimentary complexes of the Voikar–Shchuchya megazone. The inset shows the location of the Polar Ural Ophiolite Zone. b) Geologic map of the Ray-Iz ophiolite. M: mélange zone; LH: major lherzolite and harzburgite; DH: dunite and harzburgite; MU: meta-ultrabasites, D: dunite; Red stars: sample locations.

of formation of these UHP minerals in the oceanic mantle and of diamond-bearing ophiolitic peridotites and chromitites in the last part of the paper.

2. Geology of the Ray-Iz chromite deposit

2.1. Ray-Iz ophiolite

The Ural Mountains mark a 2500-km-long, linear, mid-Paleozoic orogenic belt that developed as a result of an arc–continent collision (Magnitogosrk arc–East European Block) followed by a continent–continent collision (East European block–Siberian Continent) (Savelieva and Nesbitt, 1996; Brown et al., 1998). The Polar Ural region is the northern sector of the Uralian Mountains, which extends NE–SW and is about 50–100 km wide. In this region, the Polar Urals consist of a series of westward-directed thrust stacks in which oceanic–arc sequences lie on the continental margin of the European plate. The main structural units in the region are subdivided into 5 sectors, which consist from west to east of: Lower–middle Paleozoic, rift–bathyal complexes (paleocontinental sector); Paleozoic metasedimentary–metavolcanic rocks with Precambrian basement units; mantle ultramafic massifs with gabbro and dunite–clinopyroxenite complexes; granitoids; and Paleozoic arc volcanic–sedimentary complexes of the Voikar–Shchuchya megazone (Fig. 1a).

The Paleozoic Voikar–Syninsk ophiolite belt in the Polar Urals consists of the Syum–Keu, Ray-Iz, and Voykar–Syn'ya massifs, containing ultramafic bodies, gabbros and granitoids. The ophiolites, along with Paleozoic metasedimentary–metavolcanic rocks and Precambrian basement units, occur as a tectonic sheet regionally controlled by the Main Ural Fault. The ophiolite belt is bordered by two thrust sheets, one on the west that consists of lower–middle Paleozoic, rift–bathyal complexes, and one on the east, consisting of Paleozoic, arc volcanic–sedimentary complexes (Fig. 1a) (Puchkov, 1990; Matte, 1995; Savelieva and Nesbitt, 1996; Savelieva et al., 1999). Subduction-related, high pressure, metamorphic rocks, such as eclogite, blueschist, amphibolite and albite–lawsonite facies rocks, whose protoliths were volcanic–sedimentary country rocks and ophiolitic gabbro and diabase, are spatially associated with the ophiolites (Savelieva, 1987; Dobretsov, 1991). Ultramafic rocks, gabbro, and mafic lavas, which were metamorphosed to the greenschist facies, were strongly deformed by late Vendian folding. The metamorphic mineral lineation in amphibolites suggests a sinistral shear sense and a south to southwestern direction of early movement for the allochthons. The ophiolite massifs of the Voikar–Syninsk belt and their associated metamorphic rocks were thrust westward over Paleozoic passive continental margin sequences of the East European block (Shmelev, 2011).

The Ray-Iz massif is a funnel-shaped body, about 20 × 30 km, with an outcrop area of ~380 km^2, and forms a south-dipping thrust sheet whose dip angle increases from 35–40° in the north to 75–90° in the south (Fig. 1b). Geophysical data show that this sheet is about 1–1.5 km thick in the north and 4–7 km thick in the south (Moldavantsev and Kazak, 1977; Makeyev et al., 1985; Makeyev and Braynchaninova, 1999). The Ray-Iz massif has an undulating topography, most likely created by glaciation. Vegetation is absent on the mountaintops, and large blocks (meters to tens of meters in size) of ultramafic rock are exposed on the weathered surface (Fig. 2a).

A 300- to 500-m-thick mélange zone containing blueschist and jadeite occurs along the northeast margin of the Ray-Iz massif (M in Fig. 1b) (Kazak et al., 1976; Moldavantsev and Kazak, 1977; Makeyev et al., 1985; Perevozchikov et al., 1990a), and Precambrian metamorphic rocks of the basement crop out on both the northeast and northwest sides (Makeyev et al., 1985; Puchkov, 1990). To the south, the massif is overthrust by a basement complex composed of dunite, websterite, pyroxenite, metagabbro and amphibolite (DCG in Fig. 1b) (Kazak et al., 1976; Makeyev et al., 1985). Sheeted dikes and pillow lavas are absentin the Ray-Iz massif, although they do occur locally along the eastern margin of the ultramafic–mafic sequence in the southern part of the Voikar–Syninsk belt (Garutis et al., 1999). Some jadeite–albite metasomatic dikes occur within the ultramafic bodies, and ruby-bearing veins near the base of the Ray-Iz massif have a Rb–Sr isochron age of 358 ± 3 Ma (Glodny et al., 2000). Metasomatic veins in the Ray-Iz ophiolite have a Rb–Sr isochron age of 373.1 ± 5.4 Ma. They are interpreted as evidence for suprasubduction zone metasomatism in an oceanic setting, prior to subduction of the East European margin and associated formation of eclogites in the Marun–Keu complex (Glodny et al., 2003).

It is currently widely acknowledged (Tektonika, 1977) that the ophiolites in the Uralides were produced during opening of the Ural paleo-ocean in the early Paleozoic. However, isotopic data indicate that the Polar Ural ophiolites could have been produced over a broad age range, from the Proterozoic and Cambrian (Gurskaya and Smelova, 2003; Savelieva et al., 2006; Vakhrusheva, 2007) to the Devonian (Sharma et al., 1995). Shmelev and Meng (2013) reported a zircon U–Pb age of 418 ± 2 Ma from the gabbro-diorite in the Ray-Iz massif, thought to represent a late Silurian island arc magmatic activity.

The Ray-Iz ophiolite consists mainly of lherzolite–harzburgite with about 10% dunite (Zavaritsky, 1932; Moldavantsev and Kazak, 1977; Makeyev et al., 1985). Some crustal cumulates, including dunite, websterite, and pyroxenite, as well as metagabbro and amphibolite, occur locally in the southern part of the body (Fig. 2e, f). The harzburgite is regarded as SSZ-type mantle peridotite, formed in a mantle wedge above a subduction zone (Perevozchikov et al., 2005; Shmelev, 2011). Whole-rock/mineral Sm–Nd isotope dating yielded a formation age of 409 ± 26 Ma for the harzburgite and 410 ± 15 Ma for the dunite (Ronkin et al., 2000), whereas Re–Os isotope dating yielded an age of 470 Ma for formation of the chromite (Walker et al., 2002). The massif has a complex metamorphic and deformation history, involving several different types of serpentinization (Perevozchikov et al., 1990a; Shmelev et al., 1990; Makeyev and Braynchaninova, 1999; Perevozchikov et al., 2005).

The chromite deposits occur mainly in the western and southwestern parts of the massif, where they are associated with dunite (Makeyev et al., 1985; Perevozchikov et al., 1990b; Makeyev, 1992; Perevozchikov et al., 2005). Some of the chromitites are enclosed in dunite envelopes, whereas others are in direct contact with the harzburgite.

The Central Chromite Deposit (CCD) is the largest of the more than 200 ore bodies in the massif. It consists of several parallel bodies with both massive and disseminated ores, which extend to a depth of 500 m. More than 40 million tons of chromite was mined from this deposit between 1996 and 2005. The chromite ore contains a variety of PGE minerals (Makeyev, 1992; Garutis et al., 1999; Walker et al., 2002; Pasava et al., 2011), which have features showing that fluids played an important role in their formation (Garutis et al., 1999).

The W214 orebody is approximately 100 m long and 5 m wide, and extends to over 100 m depth, indicating that it contains about 10 million tons of chromite ore. The orebody is partly surrounded by a thin dunite envelope and is locally in direct contact with coarse-grained, weakly serpentinized harzburgite. In this study, chromitite samples were collected from both the CCD and W214 orebodies. The sample locations are 66°52.06′N; 65°15.72′E for the CCD (900 kg in weight, sample number R) and 66°49.62′N; 65°07.45′E for the W214 orebody (600 kg in weight, sample number P).

2.2. Petrography and mineralogy

The harzburgites are coarse-grained and massive, and composed of 80–85 vol.% olivine (Ol), 5–15% orthopyroxene (Opx), 1–2% clinopyroxene (Cpx), and minor spinel or chromite (Cr). Olivine grains show a bimodal grain size; coarse olivine grains are mostly 1–5 mm across, whereas fine-grained varieties are <0.2 mm. The small grains show evidence of recrystallization, perhaps related to deformation during emplacement; similar features are seen in the Luobusa ophiolitic

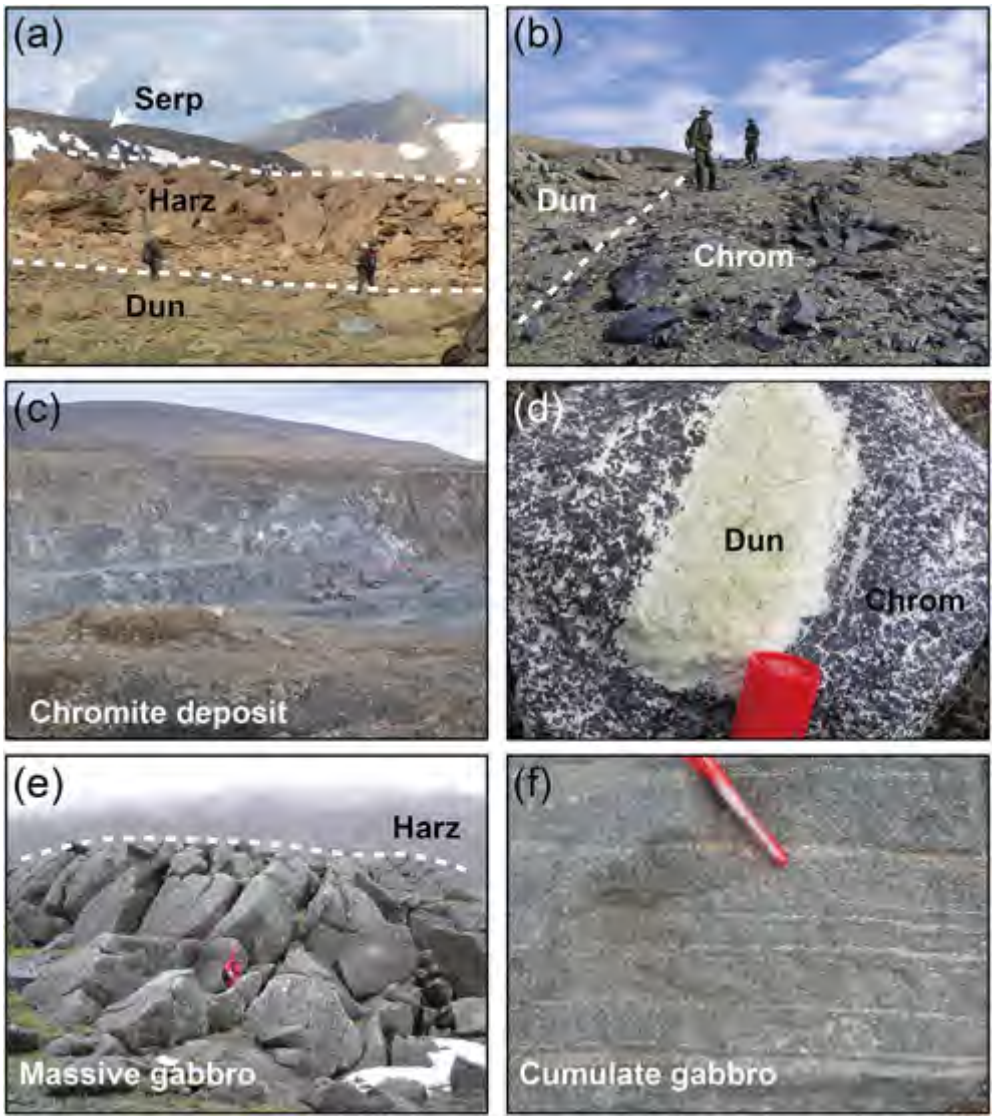

Fig. 2. Landscape of the Ray-Iz ultramafic massif, which is composed chiefly of harzburgite with less than 10% dunite. (a) Harzburgite and lens of dunite with a sharp boundary; (b) chromite orebody with a thin envelope of dunite; (c) open-pit mine of the central chromite deposit (CCD); (d) massive chromitite from the W214 chromite orebody (see photomicrograph in Fig. 3c) (e) coarse-grained, massive gabbro and (f) layered cumulate gabbro within the harzburgite massif.

peridotites (Xu et al., 2009). Orthopyroxene crystals range up to 10 mm in length, and are evenly distributed in the rocks. Clinopyroxene crystals are similar in size to the orthopyroxene grains. Spinel or chromite crystals are evenly distributed in the rocks, mostly as very small, euhedral grains (Fig. 3a, b). Two types of chromitite are present, massive and disseminated. The massive varieties are coarse grained, fresh, and red (with high-Cr#) in plane-polarized light under the microscope (Fig. 3c), whereas some disseminated chromitites are dark (with high iron contents) under plane-polarized light (Fig. 3d).

On the basis of 141 EPMA (electron probe micro-analyzer) analyses (see Table 1 for representative data), olivine compositions vary from Fo_{90-91} in the harzburgites to Fo_{90-95} in the dunites, although both have low NiO contents (0.3–0.7 wt.%) (Fig. 4a). Olivines in massive chromitite or as inclusions in chromite grains are more magnesian (Fo_{95-98}) and have significantly higher NiO contents (0.5–1.4 wt.%) (Fig. 4a). These compositions are essentially the same as those of olivines in the Luobusa ophiolite (Xu et al., 2009), indicating significant mineralogical similarities between the two ophiolites of different ages formed in different orogenic belts.

Eighty-seven analyses (Table 1) show that massive chromite in chromitite is characterized by very high Cr#s = [100Cr / (Cr + Al)] (80–95) and wide range of Mg#s = [100Mg / (Mg + Fe)] (~65–15). In contrast, chromite grains in the lherzolites, disseminated chromitites and some of the dunites have low Cr#s (~25–60) and high Mg#s (~60–75). The disseminated chromitites are characterized by high contents of Al_2O_3 (21–28 wt.%), intermediate Cr#s and high Mg#s (66–73). Interestingly, chromite grains in the harzburgites have extremely high Cr#s (~80–97) and low Mg#s (~9–21). These compositions are due to the very high iron contents in the chromite grains. Such high iron contents are typically the result of alteration, but neither the chromite grains nor the silicate minerals show significant alteration in these rocks.

3. Sample preparation and analytical techniques

3.1. Mineral separation

Mineral separation was carried out at the Institute of Multipurpose Utilization of Mineral Resources, Chinese Academy of Geological Sciences, Zhengzhou, which was selected because of its experience in mineral separation. Since the early 1980s, mineral separation has been carried out for over 20 large samples (about 1 ton each) of chromite ore and ultramafic rock in the Institute (e.g., Bai et al., 2001; Yang

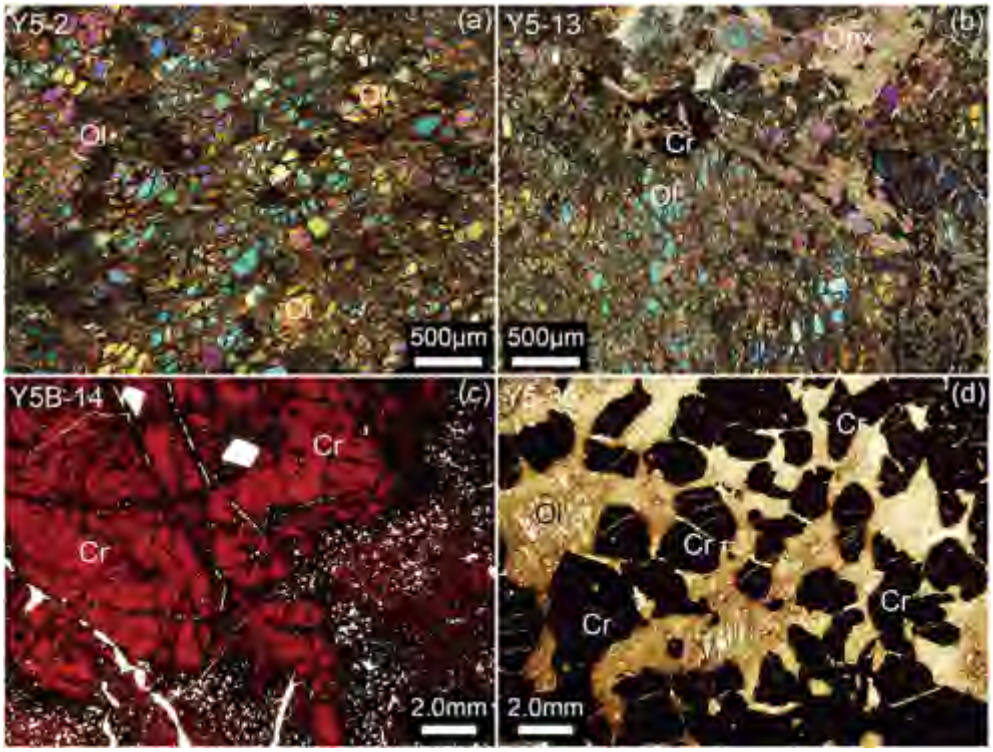

Fig. 3. Photomicrographs of ultramafic rocks and chromitites from the Ray-Iz massif. (a) Dunite associated with a chromite orebody; (b) harzburgite containing 10–15% orthopyroxene; (c) massive chromitite from the W214 chromite orebody. (d) Disseminated chromitite ore from CCD outcrop; Ol—olivine; Cr—chromite; Opx—orthopyroxene.

et al., 2005, 2007, 2008; Xu et al., 2009). Before processing, all work sites and equipment were carefully cleaned to avoid any contamination. The samples were crushed and divided into three sizes: <1 mm to >0.5 mm, <0.5 mm to >0.3 mm, and <0.3 mm, after which the minerals were separated using a combination of gravity and magnetic and electrostatic techniques (Bai et al., 2001; Yang et al., 2005; Xu et al., 2009). The minerals were finally handpicked under a binocular microscope.

Detailed processing includes: (1) Dry magnetic separation using moderate (3.19 kA) and strong (955 kA) magnetic fields with a frequency of 5.0 Hz. (2) Shaking table separation with a stroke of 10 mm, and a frequency of 280 times/min. (3) Electrostatic separation at 20 kV, using a rotation speed of 70 times/min. (4) Treatment by alkali solution at temperatures of 700–800 °C using an alkali/ore ratio of 4:1.

Using these procedures, 13 types of mineral separates were obtained; (1) strongly magnetic and dense minerals (mostly ferrous iron-bearing magnetic minerals); (2) strongly magnetic and less dense minerals; (3) strongly magnetic and light minerals; (4) nonmagnetic and heavy minerals, e.g., noble metallic minerals; (5) nonmagnetic and less dense minerals, e.g., pyroxenes; (6) nonmagnetic minerals and light minerals, e.g., serpentine, chlorite and mica; (7) weakly magnetic and heavy minerals, e.g., metallic oxides and metallic sulfides; (8) weakly magnetic and less heavy minerals, e.g., pyroxene and olivine; (9) weakly magnetic and light minerals, e.g., chlorite and mica; (10) nonmagnetic and heavy minerals; (11) nonmagnetic and less dense minerals, e.g., pyroxene; (12) nonmagnetic and light minerals, e.g., pyroxene and apatite; and (13) nonmagnetic, nonconductive, and relic minerals after alkali solution treatment, e.g., diamond and moissanite (Hu, 1999; Yang et al., 2005; Xu et al., 2009).

The difficulty in retrieving diamond from chromitites and peridotites is that their abundancies are very low. Based on our experience,

Table 1
Representative compositions of olivine and chromite in chromitites of the Ray-Iz ophiolite.

Minerals	Olivine	Olivine	Olivine	Olivine	Olivine	Olivine	Chromitite	Chromitite	Chromitite	Chromitite
Sample	05y-1.15	05y-18.2	05y-2.3	05y-2.5	05y-15.3	05y-274.4	05y-7.1	05y-7.6	05y-15.4	05y-15.9
Host rock	Harzburgite	Harzburgite	Dunite	Dunite	Chromitite	Chromitite	Disseminated	Disseminated	Massive	Massive
SiO_2	41.20	40.84	42.13	42.02	42.50	42.34	0.00	0.00	0.00	0.00
TiO_2	0.02	0.00	0.00	0.00	0.00	0.00	0.11	0.08	0.06	0.05
Al_2O_3	0.00	0.00	0.00	0.00	0.00	0.00	26.17	28.22	8.32	8.48
Cr_2O_3	0.04	0.00	0.01	0.00	0.05	0.05	38.64	38.05	58.22	58.40
FeO	10.17	9.57	6.71	6.71	3.64	2.44	16.15	13.29	21.78	21.03
MnO	0.12	0.13	0.15	0.11	0.04	0.01	0.21	0.19	0.39	0.38
MgO	48.80	48.58	50.89	51.26	53.10	52.97	17.57	18.13	10.49	10.85
NiO	0.36	0.38	0.32	0.28	0.56	0.90	0.22	0.21	0.08	0.06
CaO	0.00	0.03	0.00	0.01	0.00	0.02	0.00	0.00	0.00	0.00
Na_2O	0.00	0.00	0.03	0.01	0.00	0.00	0.00	0.04	0.00	0.03
K_2O	0.01	0.02	0.00	0.02	0.00	0.01	0.00	0.00	0.00	0.00
P_2O_5	0.02	0.00	0.00	0.01	0.02	0.00	0.01	0.00	0.02	0.00
Total	100.74	99.53	100.24	100.43	99.91	98.75	99.08	98.22	99.35	99.28
Fo/Mg#	90	90	93	93	96	97	66	71	46	48
NiO/Cr#	0.36	0.38	0.32	0.28	0.56	0.90	50	47	82	82

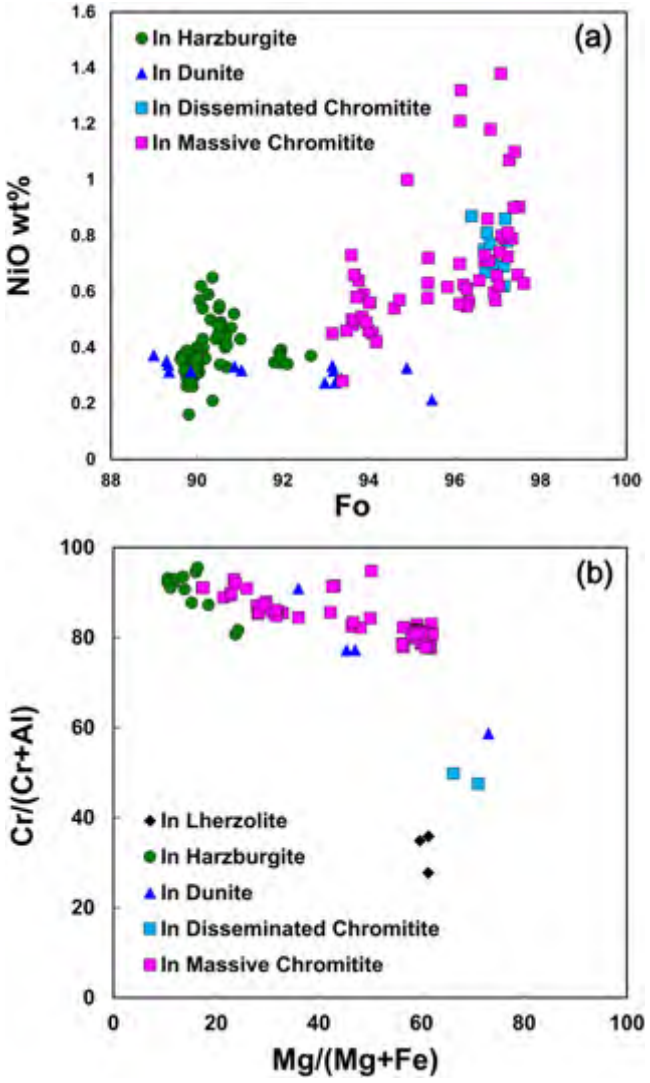

Fig. 4. Olivine and chromite compositions in the peridotites and chromites of the Ray-Iz ophiolite. (a) Fo–Ni composition of the olivines in the harzburgite, dunite and chromitite from the Ray-Iz massif; (b) Cr# vs. Mg# diagram of chromites from different lithologies in the Ray-Iz ophiolite, except chromites in lherzolite are from the Syum–Keu massif.

the maximum concentration of diamond in chromitite is 0.03 g/t, or 30 ppb. Diamond has nearly the same specific gravity as olivine and pyroxene (diamond = 3.52, olivine = 3.5 and pyroxene = 3.1–3.5), so complex procedures are required for diamond separation. Normally, it takes more than one month to separate a 1-ton sample and approximately 7 months for one person to hand-pick the resulting output.

3.2. Analytical techniques

3.2.1. Scanning electron microscope (SEM) and microprobe (EMP) analyses

Selected minerals were analyzed with an S-3500N scanning electron microscope with an energy-dispersive spectrometer at the Beijing General Research Institute of Mining and Metallurgy, a JEOL JSM-5610LV energy-dispersive electron microprobe and a RENISHAW-1000 Laser Raman in the State Key Laboratory of Continental Tectonics and Dynamics. The operating conditions for the SEM were a voltage of 20 kV and a beam current of 15 nA. Cobalt metal was used for calibration. Microprobe analyses of magnesiochromite, olivine and orthopyroxene were carried out on polished thin sections using a JEOL JXA-8100 electron-probe micro-analyzer (EPMA) at the State Key Laboratory Breeding Base of Nuclear Resources and Environment, Nanchang, China. This instrument is equipped with 3 wavelength-dispersive spectrometers and an energy-dispersive Oxford INCA spectrometer. Analytical conditions were 15 kV accelerating voltage, 20 nA beam current and 10 s counting time for silicates. A beam diameter of 1 μm was applied, with a detection limit for oxide species of ~0.01 wt.%. Well-characterized natural minerals and synthetic oxide standards were used for calibration. Raw data were reduced with an online correction procedure including background, dead time and a ZAF calculation. Accuracy and precision were tested on SPI standards and are within ~2% relative for the major elements.

3.2.2. Carbon isotope analysis

The carbon isotopes were analyzed originally by secondary ion mass spectrometry (SIMS) at the GeoForschungsZentrum (GFZ), Potsdam, Germany. Count rate data were corrected for a 16 ns deadtime. Instrument drift was monitored with a diamond having a $\delta^{13}C$ value of −4.4‰, and another diamond with a mean $\delta^{13}C$ value of −23.0 ± 0.4‰ (1 s) was used as a primary reference (William Griffin, personal communication). On the basis of repeated analyses of the primary reference material, our results are reliable at the ±1.5‰ to ±2.0‰ level.

Additional carbon isotope ratios ($^{13}C/^{12}C$) were later determined using a Cameca IMS 1280 multi-collector ion microprobe located at the Centre for Microscopy, Characterisation and Analysis (CMCA), University of Western Australia. A static 1 nA Cs^+ beam with an impact energy of 20 keV was focused to a 10 μm spot on the sample surface. Instrument parameters included: a magnification of ×130 between the sample and field aperture, 400 μm contrast aperture, 4000 μm field aperture, 150 μm entrance slit, 500 μm exit slits, and a 40 eV band pass for the energy slit with a 5 eV gap. Secondary C ions were accelerated to 10 keV and analyzed with a mass resolving power of approximately 2200 (10% max peak height) using dual Faraday cup detectors. Care was taken to avoid interference on ^{13}C due to ^{12}CH by offsetting the detector slightly to the low mass side to avoid the hydride. A normal incidence electron gun was used for charge compensation.

Each analysis spot was pre-sputtered for 10 s before automated peak centering in the field and contrast apertures was performed. Analyses consisted of 12-four second cycles, which gave an average internal precision of less than 0.1‰ (1 SD mean). Bracketing standards allowed correction for instrumental mass fractionation (IMF), which was corrected using an in house standard DVK125b with a $\delta^{13}C$ value of −4.59‰ relative to VPDB. The spot-to-spot reproducibility (external precision) of the standard was 0.1‰ for the in-situ analyses and 0.2‰ for the analyses in which the standard was analyzed on a separate mount. Values in Table A3 are reported relative to VPDB, and uncertainties are propagated to include internal precision, external precision, and the uncertainty of the standard relative to VPDB.

3.2.3. Identification of mineral inclusions

The inclusions within diamond were investigated at the GFZ, Potsdam, Germany. Transmission electron microscopy (TEM) foils 15 × 10 × 0.150 μm were prepared using the focused ion beam (FIB) technique and studied with a Tecnai F20 X-Twin TEM operated at 200 kV with a field emission gun as the electron source. This TEM is equipped with a Gatan imaging filter GIFTM (Tridiem), a Fishione HAADF detector and an EDAX X-ray analyzer. The TEM images were acquired as filtered images by applying a 20 eV window to the zero loss peak of the energy-loss spectrum. Energy dispersion X-ray (EDX) analyses were performed by scanning a pre-selected area, thus avoiding mass loss. The sample was tilted 20° towards the detector during data acquisition and the counting time was 60–120 s. The analytical data were processed using the TIATM software package, and were quantified using the kab factors provided. The NiMnCo alloys were calculated in at.% with error bars of ±3%. Electron diffraction data of nanocrystals were acquired as selected area diffraction (SAED) images or derived from high-resolution lattice fringe images.

Table 2
Species, analyses and formulae of minerals separated from chromitite of the Ray-Iz ophiolite.

	Numbers of analysis	Average formula
Native elements		
Diamond	83	C
Cr	17	Cr
Ni	2	Ni
W	2	W
Cu	1	Cu
Si	10	Si
Fe	13	Fe
Zn	1	Zn
Zr	1	Zr
Al	6	Al
Ta	7	Ta
Pb	1	Pb
Co	2	Co
Carbides		
Moissanite	20	SiC
WC	14	WC_2; W_2C_3; WC; $W_{4.4}C_{5.6}$; W_3C_7; $W_{3.5}C_{6.5}$;
WCoC	9	$W_{3.1-4}Co_{0.9-1.5}C_{4.9-5.8}$; $W_{0.8}Co_{6.6}C_{2.6}$
WCoFeNiC	1	$W_{1.3}Co_{2.1}Fe_{0.5}Ni_{0.9}C_{5.1}$
Cu–Ni	1	$Cu_{8.9}Ni_{1.1}$
Metal alloys		
Pt–Fe–Ni–Cu	12	$Pt_{5.6-7.1}Fe_{2.2-2.9}Ni_{0.3-0.5}Cu_{0.4-1}$; $Pt_{6.6-6.7}Rh_{0.4}Fe_{2.8}Ni_{0.1-0.2}$; $Pt_{5.2-6.2}Rh_{0.1-0.4}Fe_{2.4-2.7}Ni_{0.5-1}Cu_{0.3-1.3}$
Pt–Pd–Fe–Cu	3	$Pt_{4.8-5.2}Pd_{1.8-2.3}Fe_{2.7-2.8}Cu_{0.2-0.3}$
Fe–Cr–Ni	15	$Fe_{6.5-7.3}Cr_{1.6-2.8}Ni_{0.7-1.3}$; $Fe_{1.4}Cr_{6.7}Ni_{1.9}$; $Fe_{7.5}Cr_{2.4}Mn_{0.1}$
Fe–Cr–Si	1	$Fe_8Cr_{1.8}Si_{0.2}$
Fe–Si	5	$Fe_{2.3-3.7}Si_{6.3-7.7}$; $Fe_{6.4}Si_{3.6}$;
Fe–Cr–Ni–Si(Mn,Ti)	24	$Fe_{1.7}Cr_{3.2}Ni_{1.7}Si_3Mg_{0.3}$; $Fe_{6.6-7.0}Cr_{1.7-1.9}Ni_{0.9}Si_{0.2-0.8}$; $Fe_{6.9-7.4}Cr_{1.4-2}Ni_{0.8-1.1}Mn_{0.1-0.3}$; $Fe_{6.7-7}Cr_{1.7-1.9}Ni_{0.9-1.1}Mn_{0.2}Si_{0.2}$; $Fe_{6.5-6.8}Cr_{1.8-1.9}Ni_{0.9-1}Mn_{0-0.2}Ti_{0.1-0.8}$;
Fe–Al–Si	17	$Fe_{3.9-6}Al_{2.3-3.5}Si_{1.6-2.6}$; $Fe_{8.2-8.3}Al_{0.1}Si_{1.6-1.7}$
Ag–Au	6	$Ag_{2.4-3.8}Au_{6.2-7.6}$; $Ag_{0.9}Au_{9.1}$
Ag–Au–Fe	1	$Ag_{2.2}Au_{5.9}Fe_{1.2}Ni_{0.2}Cu_{0.3}Zn_{0.2}$
Os–Ir–Ru	29	$Os_{2.2-3.3}Ir_{2.5-4.1}Ru_{2.2-5.2}$; $Os_{1.0-2.2}Ir_{0.3-0.6}Ru_{6-7.6}Fe_{0.5-0.9}Ni_{0.5-0.6}$; $Os_{5.1-5.2}Ir_{4.1-4.2}Ru_{0.6-0.8}$; $Os_{5.9}Ir_{1.7}Ru_{2.4}$; $Os_{2.3-4.1}Ir_{2.0-3.2}Ru_{1.8-5}Cu_{0.8-0.9}$; $Os_{3.2}Ir_{3.2}Ru_{2.6}Fe_{0.3}Cu_{0.7}$; $Os_{3.9}Ir_{3.6}Ru_{2.3}Fe_{0.2}$;
Pb–Sn	1	$Pb_{4.5}Sn_{5.5}$
Sn–Zn–Ag	2	$Sn_7Zn_{2.6}Ag_{0.4}$; $Sn_{5.4}Ag_{4.6}$
Pb–Zn–Cu–Fe	1	$Pb_{4.8}Zn_{1.9}Cu_{2.8}Fe_{0.5}$
Ta–Co	1	$Ta_{5.4}Co_{4.5}$
Fe–P–As	1	$Fe_{8.5}P_{1.3}As_{0.2}$
Fe–P	4	$Fe_{7.9-9.4}P_{0.6-2.1}$
Ni–As	1	$Ni_{7.3}As_{2.7}$
Oxides		
wüstite	54	FeO
Chromite	30	$(Mg,Fe)(Fe,Cr)_2O_4$
Eskolaite	3	Cr_2O_3
Quartz	35	SiO_2
Hematite	27	Fe_2O_3
Periclase	16	MgO
Cassiterite	4	SnO_2
Corundum	20	Al_2O_3
Bunsenite	5	NiO
Rutile	59	TiO_2
Baddeleyite	4	ZrO_2
	1	Cu_3O_2
Cuprite	1	Cu_2O
Tenorite	2	CuO
	1	Ni_2O_3
	3	NiO_2
	1	ZnO
Ilmenite	9	$FeTiO_3$
Sulfides		
Pyrite	16	FeS_2
Chalcopyrite	5	$CuFeS_2$
Troilite	12	FeS
Covellite	1	CuS
Arsenopyrite	6	FeAsS
	49	Ni_3S_2
	13	NiS
	3	Ni_2S
Molybdenite	7	MoS_2
Stibnite	2	Sb_2S_3
Irarsite	1	(Ir,Rh)AsS
Galena	7	PbS
Sphalerite	1	ZnS
	1	$(Fe,Ni,Co)_{5.3}S_{4.7}$
Dienerite	4	Ni_3As

3.3. Main identified minerals

Diamond and a wide variety of exotic and common minerals have been handpicked from the chromitite separates. About 60 species of recovered minerals fall into six major groups, including native elements, carbides, metal alloys, oxides, sulfides and silicates (Table 2). The native elements include diamond, Cr, W, Co, Si, Al, Ta and Fe; carbide minerals are WC and SiC; PGE minerals are OsIr, OsIsRu, and FePt; metal alloys are Fe–Cr–Ni, Fe–Al–Si, Ni–Cu, Ag–Au, Ag–Sn, Fe–Si, Fe–P and Ag–Zn–Sn; oxide minerals are NiCrFeO, TiO_2, Si-rutile, corundum, wüstite, ferrite, Fe_2O_3, ZnO, MnO and an unknown TiFe-oxide; sulfide minerals are pyrite, galena, pyrrhotite, stibnite and molybdenite; and silicate minerals are kyanite, octahedral pseudomorphs of serpentine, garnet, andalusite, quartz, zircon, monazite and feldspar, along with abundant olivine, orthopyroxene and clinopyroxene. Small amounts of carbonate and apatite are also present.

The exotic minerals normally have simple compositions, consisting of 1 or 2 elements, and some of them have specific shapes, e.g. spherical native Fe associated with wüstite. The minerals and their features are similar to those reported from the Luobusa chromitites and peridotites in the Tibetan ophiolites (Robinson et al., 2004; Bai et al., 2006, 2007a; Xu et al., 2009). Specific features of the most important minerals are described in the next sections.

4. Mineral descriptions

4.1. Diamond

We collected two large chromite samples from two chromite orebodies as described above, and found over 1000 grains of diamond from each individual sample. The diamond grains are colorless, transparent and small (ca. 0.2–0.5 mm) (Fig. 5a). They are typically euhedral with well-developed crystal forms, and some are polycrystalline aggregates. The common growth forms are octahedral, cubic and cubo-octahedral. SEM images show that most faces have sharp edges, but some grains are slightly rounded with eroded or pitted surfaces, indicating a post-crystalline process (Fig. 5b, c). Laser Raman shifts are all around 1332 cm^{-1} (Fig. 5d).

Chrome and other native metals occur as thin films, mostly 0.1–1 μm, on many of the diamond grains (Fig. 6). EDS analysis identified native Zr, ZrO, Ta, CrFe, NaCl, SiO_2, and copper sulfide in these films, all of which have been reported on kimberlitic diamond, particularly coated grains from 5 kimberlite pipes in Siberia where they can be accompanied by Cr, Fe, Ni, W, Au, Ag, Cu, Zn, Sn and minor Al, Ti, Mg, Zr and Pb (Makeev and Kriulina, 2012). These metal films can be used for tracing the formation mechanism of mantle diamond (Makeev, 2000, 2010).

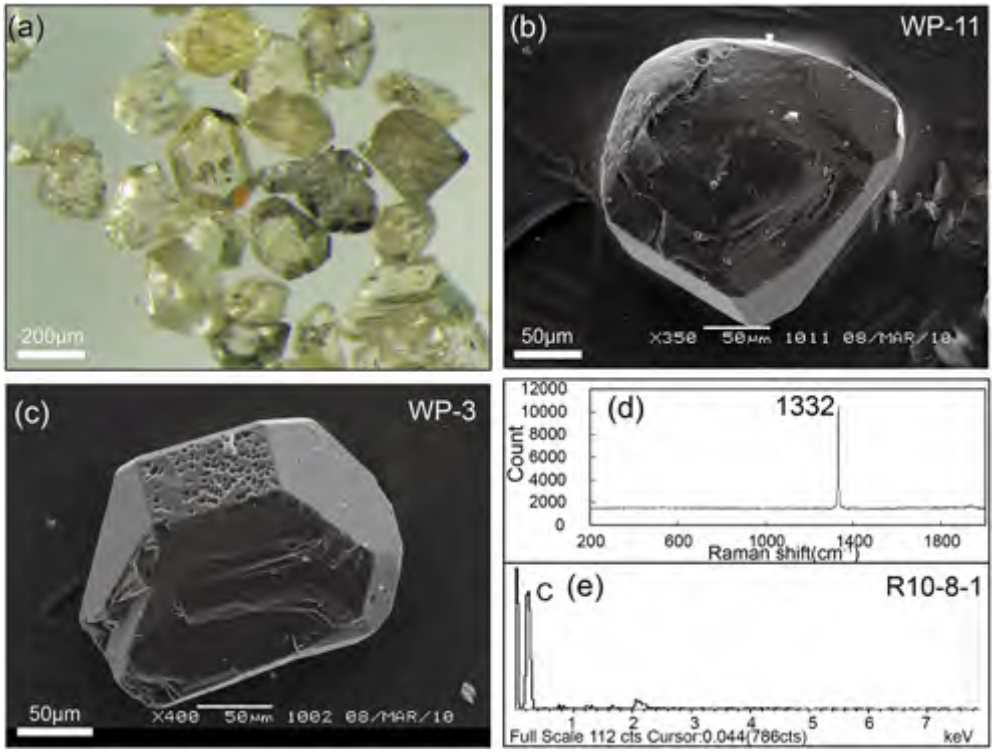

Fig. 5. Diamonds separated from podiform chromitite of the Ray-Iz ophiolite, Russia; (a) diamonds under a binocular microscope; (b) SEM image of diamond with rounded shape; (c) SEM image of diamond with flat and pitted surface; (d) typical laser Raman pattern of diamond with 1332 shift peak; (e) pure C composition of diamond by EDS.

4.1.1. Discovery of insitu diamond within chromitite

The recovery of more than 1000 diamond grains from each of the two samples collected from the Polar Urals indicates a much higher diamond concentration than previously reported for the Tibetan chromitites. Thus, we used these relatively diamond-rich chromitites to search for in situ grains. We cut 40 pieces of chromitite, each 4 cm^2 in area and encased them in epoxy (Fig. 7a). We then used a Buehler Phoenix Beta Twin Plate Grinder/Polisher to grind the samples down in 100 μm increments (Fig. 7b). Diamond-coated disks, with a maximum grain size of 37 μm, were used in the grinding/polishing. After each increment, the samples were checked with a binocular microscope and laser Raman to identify diamond and other unusual minerals. Over a period of 1 year, we found 6 in situ grains of diamond in chromite, 2 from Ray-Iz and 4 from Tibet; in addition, we found 1 in situ grain of corundum and 1 of moissanite in peridotite from Tibet. It takes a great deal of work to identify in situ grains. In total, we polished approximately 9.6 m^2 of sample, equal to making 24,000 polished thin sections.

The two in-situ diamond grains from the Polar Urals occur in small patches of carbon hosted in chromite grains within podiform chromitite (Fig. 8). The carbon patches are generally 0.5–1 mm across, spherical to irregular (Fig. 8b, d), and consist chiefly of amorphous carbon based on element mapping and the absence of a Raman pattern. Small grains of chromite, olivine, serpentine and chlorite are also present in some patches. Where the host grains are fractured, the carbon is in small (10–100 μm), irregular patches (Fig. 8d). The diamonds occur as subhedral to euhedral grains ~200–500 μm in diameter, much larger than any of the diamond grinding/polishing grit. Diamond YSB-17-2 is a tabular, yellowish, translucent grain about 300 μm across, whereas grain Y5B-16-2 is euhedral, colorless and transparent with a length of about 400 μm. Both consist of pure C with no discernable inclusions (Fig. 8d).

4.1.2. Carbon isotopes of diamond

Thirty-two carbon isotope analyses of 17 separated diamond grains from the Ray-Iz ophiolite were carried out by SIMS at the GFZ, Potsdam, Germany, and by ion microprobe at the University of Western Australia. These analyses yielded $\delta^{13}C_{PDB}$ values ranging from −18.9‰ to −28.3‰, with an average of −25.1 ± 2.5‰ (Table 3, Fig. 9), significantly different from those of typical kimberlitic diamond, most of which have $\delta^{13}C_{PDB}$ values of −1‰ to −8‰ (Mathez et al., 1995). Light carbon isotopes are rare but have been previously reported from UHP metamorphic diamond, eclogitic diamond and carbonado (Cartigny, 2005), and diamond from the Jagersfontein (Tappert et al., 2005) and Juina-5 (Walter et al., 2011) kimberlites. The only known source of isotopically light carbon on Earth is organic material and we suggest that such material was subducted to near the mantle transition zone, where the diamond apparently grew. This interpretation is strongly supported by the presence of common crustal minerals in the chromitites hosting the diamond (Robinson et al., in this issue). Diamonds from the Jagersfontein kimberlite of South Africa have $\delta^{13}C$ values of −17‰ to −24‰ (Tappert et al., 2005), slightly heavier than the values reported here. These diamonds are interpreted as having formed at depths of 250 to 500 km from organic matter contained in a subducted slab. Similarly, $\delta^{13}C$ values as low as −24‰ are reported from superdeep diamonds in the Juina-5 kimberlite pipe of Brazil and are also interpreted as reflecting subduction of surface carbon (Walter et al., 2011). Another possible origin of isotopically light carbon is fractionation of the main mantle reservoir, which has an average $\delta^{13}C_{PDB}$ value of about −5‰, but it is unlikely that such a process could produce the range of values reported here (Deines, 1980; Trumbull et al., 2009; Walter et al., 2011).

4.1.3. Mineral inclusions in diamond

Many grains of diamond contain metallic minerals up to 50 μm in size that can be clearly seen under the microscope (Fig. 10a). EDS analysis of an inclusion (sample WDR-8) indicates that it is a NiMnCo alloy, with a relative uniform composition (Ni 72.2–75.6 wt.%, Mn 17.8–19.3 wt.%, Co 5.0–5.6 wt.%), and lesser amounts of Fe (0.56 wt.%) and Si (0.41 wt.%). A preliminary FIB and TEM study of the diamonds confirmed that they contain inclusions of nanometer-size NiMnCo alloys associated with graphite (Fig. 10b–f). The presence of NiMnCo

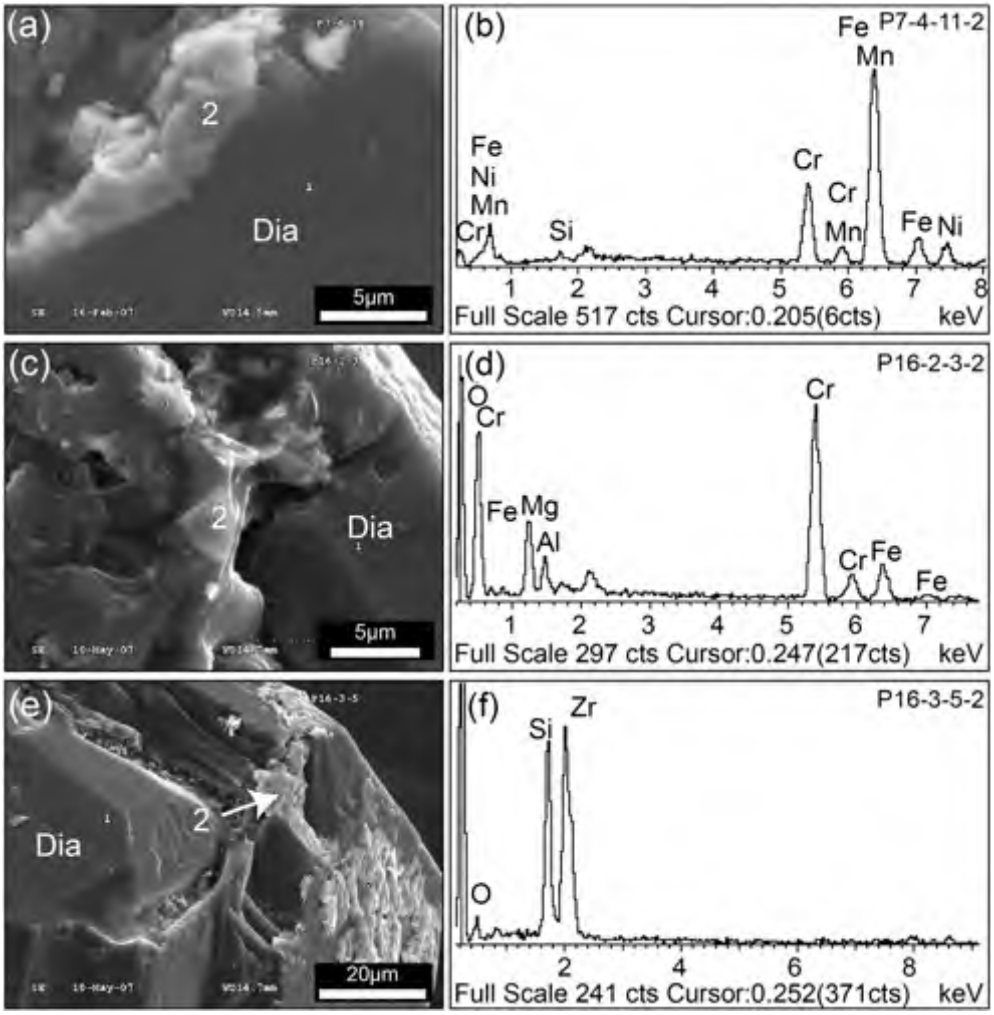

Fig. 6. Metal films (2) on the surfaces of diamonds as revealed by SEM (a, b) CrFeMnNi alloy and EDS analysis; (c, d) chromite on the surface of diamond and EDS analysis; (e, f) ZrSi alloy on surface of diamond and EDS analysis.

inclusions further distinguishes the diamonds from those found in metamorphic rocks and kimberlites (Gurney et al., 2005). An inclusion of coesite, about 500 nm across, in diamond (WDR-8) was identified using a combination of EDS and high resolution, transmission electron microscopy (HRTEM) lattice fringe imaging (0.621 nm (020) reflection) (Fig. 11).

Wirth et al. (2009) recently reported unusual micro- and nano-size inclusions in diamonds from the Juina area, Brazil, including TiO_2 with an α-PbO_2 structure, native Fe and coesite, which are included in a diamond with a light, 'organic' carbon isotopic composition ($\delta^{13}C_{PDB}$ ranges from −14 to −25‰). They proposed that diamonds from the Juina area may have formed as a result of subduction of the crustal material to depths of at least the lower transition zone or even the lower mantle. The pressure estimates for the investigated diamonds vary from 3 to 10 GPa.

The presence of coesite as an inclusion in a Polar Ural diamond confirmsthat both minerals are natural and cannot be synthetic. Coesite has previously been reported twice in aTibetan diamond-bearing chromitite. One example occurs together with kyanite rimming a grain of Ti–Fe alloy in chromitite. On the basis of its morphology and crystal orientation, these coesite grains are considered to be pseudomorphs after stishovite, which must have formed originally at a depth >300 km (Yang et al., 2007). The other occurrence is as coesite and clinopyroxene exsolution lamellae in chromite grains from a podiform chromitite in the Luobusa ophiolite. This assemblage suggests crystallization of a chromite precursor with a $CaFe_2O_4$ structure that was stable at pressures over 12.5 GPa (>380 km deep) (Yamamoto et al., 2009).

Coesite is widely known as a typical high-pressure mineral in UHP metamorphic rocks formed by deep subduction of continental crust (Yang et al., 2001; Liou et al., 2009). However, it commonly occurs as inclusions in zircon and garnet, not in diamond. Thus, the ophiolite occurrence is very different from coesite in UHP metamorphic rocks.

4.2. Other native element minerals

4.2.1. Native Cr

Eleven grains of native Cr were analyzed (P18-10, P18-12, P6-6-8, P6-6-2, R26-14, R12-3, R24-21, R19-2, P19-20, P23-11, P23-24). These grains are euhedral to anhedralwith prismatic to irregular forms, and are about 0.5 mm × 0.2 mm in size (Fig. 12a). EMP and EDS analyses indicate that they consist of pure Cr (100 wt.%); no other elements were detected (Fig. 12b). Native Cr has also been reported in the ophiolitic chromititesof Tibet, where it also consists of pure chromium with no impurities (Zhu et al., 1981; Bai et al., 2004).

Native chromium is now recognized as a mineral. The first specimens were separated from a podiform chromitite in northern Tibet (Zhu et al., 1981). Those grains also consists of pure Cr, are 50–100 μm in size, and belong to the isometric system with $a_0 = 2.889$ Å (Zhu and Liu, 1981). Two grains of native chromium were reported from

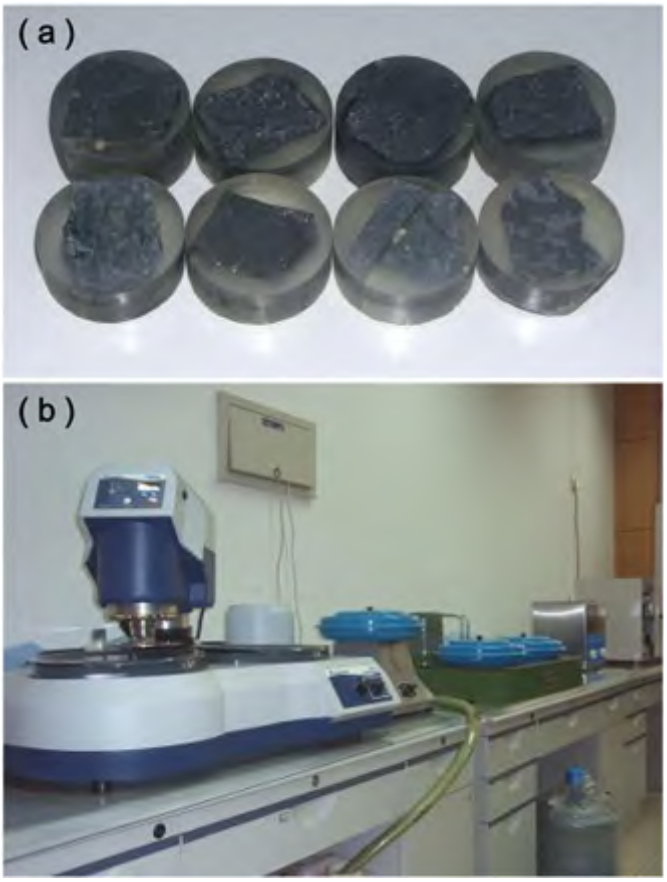

Fig. 7. Equipment for finding in situ diamonds in chromitite. (a) Epoxy plugs, each containing a piece of chromitite about 4 cm^2,were used to search for in situ diamonds; (b) a Buehler Phoenix Beta Twin plate Grinder/Polisher was used to grind the surface of the plugs in 100-μm increments. The diamond-coated disks used to grind the plugs had a maximum grain size of 37 μm.

the Luobusa podiform chromite deposit, as well, that are similar to those from northern Tibet (Bai et al., 2004). Native chromium has yet to be reported from kimberlite pipes rich in diamond, although two Cr–Fe alloys have been described from the Udachnaya (Lucky) Mine in Russia: ferchromide ($Cr_3Fe_{0.4}$) and chromferide ($Fe_3Cr_{0.4}$). Both minerals are structurally similar to chromium.

The native chromium from the Ray-Iz chromitites suggests a highly reducing environment of formation that is consistent with that from Tibet.

4.2.2. Native Al

Four grains of native Al were analyzed (P24-11, R16-12, P32-1-14, P11-2-2). The grains are irregular to anhedral in shape, 0.4–0.8 mm across and silver-white in color with a metallic luster (Fig. 12c). An EDS analysis indicates that it consists of pure Al (Fig. 12d).

Makeyev (1992) reported a single grain of native aluminum from the Voikar ultramafic massif in the Polar Urals that contains 94.7–99.15 wt.% Al, 0.16–0.36 wt.% Si and 0.15–0.44 wt.% Cr, with traces of Os and Pt up to 0.11 wt.%. Native Al has also been reported from ophiolitic chromitite of Tibet, where it is commonly associated with moissanite (Robinson et al., 2004; Trumbull et al., 2009), and a few of those grains contain up to 2.5 wt.% Cr_2O_3, suggesting a mantle origin (Bai et al., 2004).

Native aluminum has also been reported in Siberian trap rocks (Okrugin et al., 1981), skarn-ore deposits (Novgorodova et al., 1982), in potassicrhyolites (Filimonova and Trubkin, 1996) and in metasomatised sediments of the EPR (13° N, Davydov and Aleksandrov, 2001). Small spherules and particles of native Al have also been described in sedimentary cores from the Central Indian Basin (Iyer et al., 2007). These native aluminum particles are all similar in morphology and composition, prompting Iyer et al. (2007) to suggest their formation by fluxing of the sediments with methane and hydrogen to account for the very low oxygen fugacity.

4.2.3. Native Fe and FeO

Grains of native Fe occur as small spheres, generally ranging from 0.5 to 1 mm in diameter (Fig. 13a, c). Six grains of native Fe were analyzed, showing that some spheres are rimmed by wüstite (FeO) (Fig. 13a, b), or include some small droplets of wüstite within them (Fig. 13). Some grains are associated with complex oxide minerals, such as sample P20-3 (Fig. 13b), which contains both spheres of native Fe and wüstite, with sharp contacts between them. SEM images show that the wüstite consists of micro-crystals, but that the native Fe is homogeneous. Hematite occurs along the contact of the two minerals, indicating an increase in oxygen fugacity, probably related to alteration. Sample P20-14 (Fig. 13c, d) shows many small, spherical droplets of wüstite, about 10 μm across, hosted in native Fe. These droplets have a complex composition, namely $Fe_{42}Si_4Mn_3Ti_1)O$. Some silicate droplets (about 10 μm across) that occur in the native Fe of sample P20-8 also have complex compositions consisting of 39 wt.% TiO_2, 19 wt.% SiO_2, 4 wt.% Al_2O_3, 22 wt.% FeO, 8 wt.% MnO, 6 wt.% CaO and 1 wt.% K_2O. These droplets are most likely a quenched glass.

Similar spherical droplets of wüstite in native Fe have also been reported from the Luobusa chromitite, where they have compositions of $Fe_{98.2-100}Cu_{0.1}Mn_{0.02-0.71}Si_{0-0.09}$. However, some of the native Fe from Luobusa contains 20% Mn and 80% Fe (Bai et al., 2004).

Native Fe was reported many years ago from the Yakutia kimberlite (Sobolev et al., 1981), and Sloan kimberlitic diamond (Meyer and MccaUum, 1986). A grain of native Fe surrounded by wüstite was also reported in a kimberlitic diamond from Tanzania (Stachel et al., 1999). Native Fe has also been identified in kimberlitic diamond from Rio Soriso (Hayman et al., 2005) and from the Pandrea-1 pipe of the Juina area, Brazil,where it occurs with ferropericlase and chrome spinel (Kaminsky et al., 2009). It has also been described from the Kankan placer in Guinea (Stachel et al., 2000). However, these minerals can be easily distinguished from those of the chromitites of Tibet and the Polar Urals, because they contain complex and variable compositions (Kaminsky, 2012).

4.3. Carbides

4.3.1. W–(Co)–C

Tungsten carbide occurs as a 400 μm diameter ball (Fig. 14a), which consists of an intergrowth of small, euhedral crystals, about 2–10 μm in size (light gray material in Fig. 14b) containing many small, angular grains of metal or oxide materials (dark grains in Fig. 14b). Most of the WC grains contain approximately 90 wt.% W and 10 wt.% C (point 1 in Fig. 14b and analyses P17-1-1 and P17-1-2 in Table 4). However, compositions can vary widely, particularly with the addition of Co (Table 4). Five major compositional groups are recognized (Table 4); WC (e.g., P17-16), (WCo)C (e.g., P17-4, P17-170), W_2C_3 (e.g. P17-2-1), $(W,Co)_9C_{11}$(P17-3) and W_3C_7 (R23-21). The small (1–3 μm) angular grains between the WC crystals are chiefly Cr_2O_3 (point 3 in Fig. 14b), native Co (point 4 in Fig. 14b and P17-1-4 in Table 3) and W_3C_7 (R23-21) (Table 4). Three similar subgroups, i.e., WC, W_2C_7, and TiWC, as well as CoC are recognized in the Luobusa chromitites (Bai et al., 2004). One of these subgroups (WC) has recently been approved as a new mineral, called qusongite (Fang et al., 2009). The qusongite is associated with chromian chlorite, calcite, (W, Ti)C and (Ti,W)C alloys, and chromite. It occurs as angular grains generally 4–8 μm in diameter, but some are as large as 0.2 × 0.3 × 0.25 mm (Fang et al., 2009).

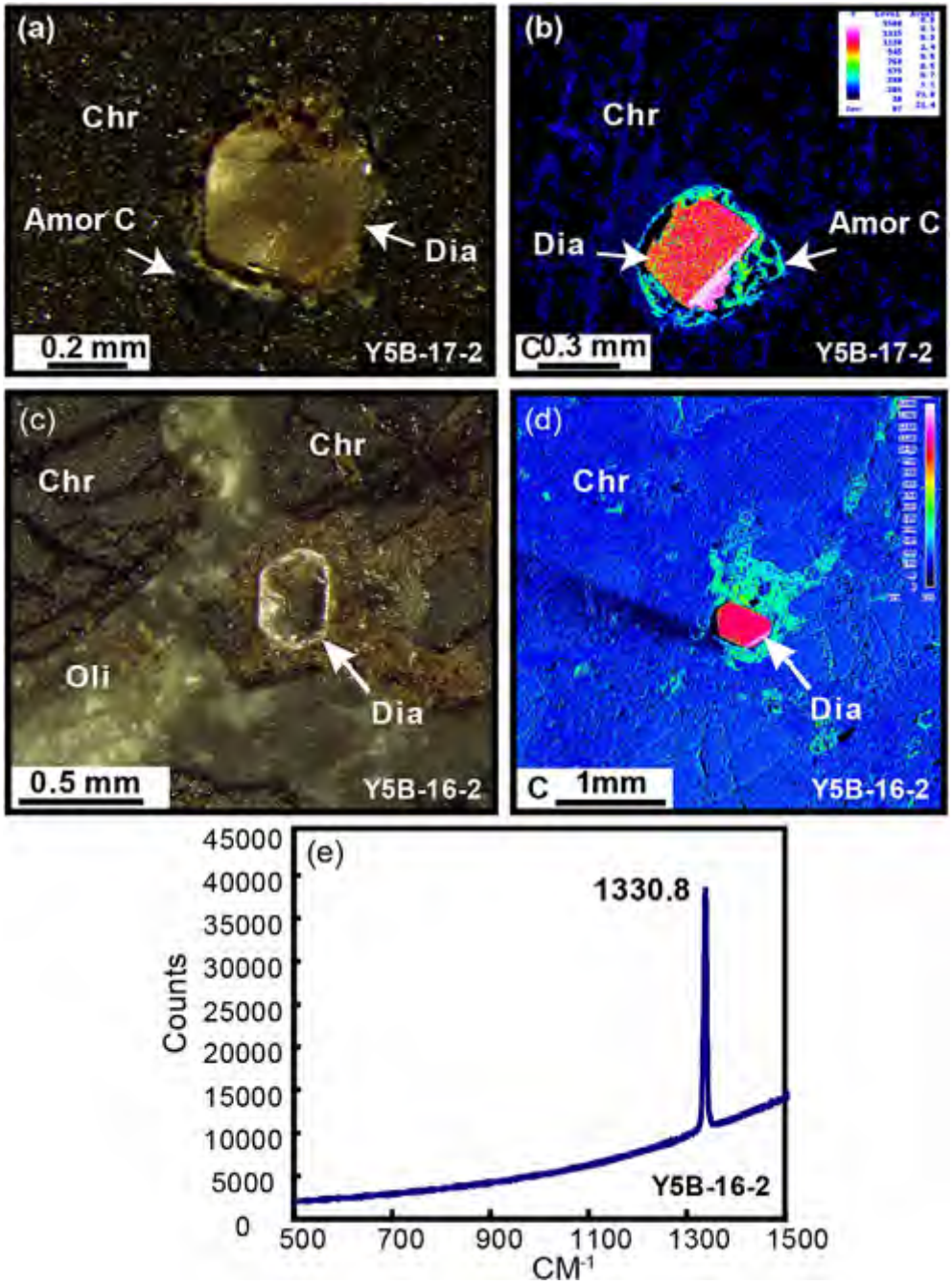

Fig. 8. Photomicrographs (a, c) and, carbon element maps (b, d) of diamonds from the Ray-Iz ophiolite and (e) laser Raman pattern of diamond. The in-situ diamonds are hosted in spherical (sample 05B-17-2) to irregular (sample 05B-16-2) patches of amorphous carbon within chromitite of the Ray-Iz ophiolite. Chr—chromite, Oli—olivine, Dia—diamond. The dark blue color is chromite and olivine and the light blue color is amorphous carbon.

4.3.2. Moissanite

Thirteen grains of moissanite (SiC) were recovered from the Ray-Iz chromitite. These are light blue to green, irregular to subhedral, transparent crystals, ranging from 0.2 to 0.4 mm across (Fig. 15). The grains are relatively uniform in composition (SiC) (e.g., P25-23, P21-14-1 and R26-9-1 in Table 3), but some contain minute inclusions of Fe_3Si_7, Si and SiO_2. These grains are similar to those recovered from the Luobusa chromitites (Bai et al., 2000a,b; Robinson et al., 2004).

Moissanite has also been found as inclusions in kimberlitic diamond as well as other mantle-derived magmatic rocks and volcanic breccias (Jaques et al., 1989; Moore and Gurney, 1989; Leung et al., 1990; Klein-BenDavid et al., 2007). They commonly contain native Si, Fe-, Mg-, Ti-, or Cr-silicates, which imply formation under extremely reducing conditions, well below the iron-wüstite buffer as a lower limit on fO_2 of the mantle (Shiryaev et al., 2011). Five analyzed SiC grains from Ray-Iz yielded consistent C isotope values, i.e., $\delta^{13}C_{PDB} = -19.2$ to -24.7, nearly identical to moissanite grains from other ophiolites and kimberlites (Trumbull et al., 2009). This finding hints that moissanite, whether in ophiolitic mantle or in kimberlitic mantle, has a similar process of formation.

4.4. PGE and base-metal alloys

4.4.1. OsIrRu alloy

PGE alloys typically occur as euhedral to anhedral grains, 0.2–0.4 mm in size (Fig. 16), but some are spherical. They are silver white

Table 3
Carbon isotope compositions of diamonds from ophiolitic chromitites in Polar Urals.

Analysis	Sample locality	No.	Grain	$^{13}C/^{12}C$ Meas.[c]	$^{13}C/^{12}C$ Absolute[d]	$\delta^{13}C$[a]	Unc.[b]	CL image
YJ080	Ray-Iz Chr	WP	C028 g8 pt1	0.01060	0.01096	−24.2	0.97	Dark
YJ081	Ray-Iz Chr	WP	C028 g7 pt1	0.01057	0.01094	−26.7	0.99	Dark
YJ082	Ray-Iz Chr	WP	C028 g6 pt1	0.01060	0.01097	−24.0	0.92	Bright
YJ083	Ray-Iz Chr	WP	C028 g5 pt1	0.01056	0.01093	−27.7	0.94	Dark
YJ084	Ray-Iz Chr	WP	C028 g4 pt1	0.01057	0.01094	−26.8	0.80	Bright
YJ086	Ray-Iz Chr	WP	C028 g3 pt1	0.01055	0.01092	−28.3	0.93	Dark
YJ087	Ray-Iz Chr	WP	C028 g2 pt1	0.01060	0.01096	−24.2	0.88	Bright
YJ088	Ray-Iz Chr	WP	C028 g1 pt1	0.01062	0.01099	−22.2	1.07	Bright
YJ001	Ray-Iz Chr	WR	g1 pt1	0.01055	0.01094	−26.3	0.73	Dark
YJ002	Ray-Iz Chr	WR	g1 pt2	0.01057	0.01096	−24.4	0.84	Patchy
YJ003	Ray-Iz Chr	WR	g2 pt1	0.01055	0.01094	−26.3	0.85	Light
YJ004	Ray-Iz Chr	WR	g2 pt2	0.01055	0.01094	−26.2	0.89	Dark
YJ005	Ray-Iz Chr	WR	g3 pt1	0.01053	0.01092	−28.0	0.79	Dark
YJ010	Ray-Iz Chr	WR	g4 pt1	0.01058	0.01097	−23.9	1.04	Bright
YJ011	Ray-Iz Chr	WR	g5 pt1	0.01063	0.01102	−18.9	1.09	Bright core
YJ012	Ray-Iz Chr	WR	g5 pt2	0.01060	0.01100	−21.5	0.92	Dark rim
YJ013	Ray-Iz Chr	WR	g6 pt1	0.01057	0.01096	−24.6	0.94	Dark core
YJ014	Ray-Iz Chr	WR	g7 pt1	0.01056	0.01096	−24.9	1.25	Dark
YJ015	Ray-Iz Chr	WR	g7 pt2	0.01057	0.01096	−24.6	0.90	Bright
YJ016	Ray-Iz Chr	WR	g8 pt1	0.01061	0.01100	−21.0	0.94	Dark
WR-3-1	Ray-Iz Chr	WR	pt1	0.01063	0.01095	−25.1	0.19	
WR-3-2	Ray-Iz Chr	WR	pt2	0.01063	0.01096	−24.9	0.21	
WR-4-1	Ray-Iz Chr	WR	pt1	0.01062	0.01095	−25.6	0.20	
WR-4-2	Ray-Iz Chr	WR	pt2	0.01062	0.01095	−26.0	0.20	
WR-5-1	Ray-Iz Chr	WR	pt1	0.01063	0.01095	−25.2	0.20	
WR-5-2	Ray-Iz Chr	WR	pt2	0.01063	0.01096	−25.0	0.20	
WR-6-1	Ray-Iz Chr	WR	pt1	0.01062	0.01094	−26.4	0.18	
WR-6-2	Ray-Iz Chr	WR	pt2	0.01062	0.01094	−26.1	0.18	
WR-7-1	Ray-Iz Chr	WR	pt1	0.01061	0.01093	−27.1	0.19	
WR-7-2	Ray-Iz Chr	WR	pt2	0.01061	0.01093	−27.0	0.19	
WR-8-1	Ray-Iz Chr	WR	pt1	0.01063	0.01095	−25.3	0.19	
WR-8-2	Ray-Iz Chr	WR	pt2	0.01063	0.01095	−25.3	0.21	

[a] Value in per mil relative to VPDB $^{13}C/^{12}C = 0.0112372$.
[b] Propagated 1σ uncertainty.
[c] Raw isotope ratio without corrections.
[d] Corrected isotope ratio.

in color, and have various combinations of Os–Ir–Ru (Table 5). Grain R22-10 (Fig. 16b) has a formula of $Os_{5.1}Ir_{4.1}Ru_{0.8}$ (Fig. 16c). However, 12 analyses of various grains show a compositional range of 3–36 wt.% Ru (average 19 wt.%), 25–66 wt.% Os (average 42 wt.%), and 18–45 wt.% Ir (average 38 wt.%). On the basis of these analyses, four groups are recognized; the most common are OsIrRu and RuIrOs, whereas RuOsIr and IrOsRu are relatively rare. In the triangular diagram of OsIrRu components (Fig. 17), the alloys are all relatively low in Ru, unlike grains from the Luobusa chromitites of Tibet (Bai et al., 2007b) and the Kempirsa chromitites of Kazakstan in the southern Ural Mountains (Melcher et al., 1997; Nakagawa and Franco, 1997).

Small (3–4 μm) silicate mineral inclusions are present in some of the OsIrRu alloys (Fig. 16a, b), and these have compositions similar to those of "Si-spinel" in PGE alloys of the Luobusa ophiolite (Bai et al., 2007b) (SiO_2 = 54.6 wt.%, Al_2O_3 = 7.4 wt.%, Cr_2O_3 = 3.1 wt.%, MgO = 19.7 wt.%, FeO = 0.9 wt.%, CaO = 13.3 wt.% and Na_2O = 1.0 wt.%) (Fig. 16d).

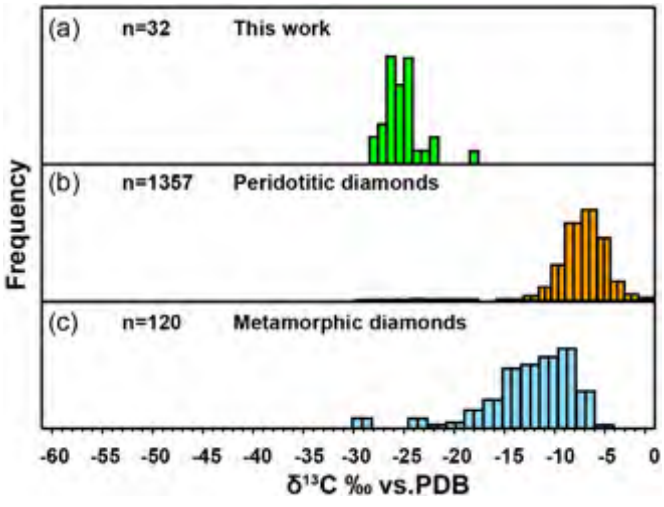

Fig. 9. Histograms of $\delta^{13}C$ values for diamonds from the Ray-Iz ophiolite and from other occurrences in the world for comparison. (a) Ray-Iz diamonds; (c) peridotitic diamond in kimberlite (Cartigny, 2005); (c) metamorphic diamond in ultrahigh presuure subduction zone (Cartigny, 2005).

4.4.2. PtFe alloys

Three grains of PtFe alloy were identified from the Ray-Iz chromitite. They are anhedral in shape, 0.2–0.4 mm in size and silver-white in color. They consist of 86–89 wt.% Pt and (8–10 wt.%) Fe, with minor Rh, Cu and Ni (Table 6). The mineral formula of samples R22-31B and R22-4 is $Pt_7(Fe,Cu,Ni)_3$ (Fig. 18). The latter is intergrown with an OsRhIr alloy (Fig. 18b). Although PtFe alloys occur in the Luobusa chromitite, they are not common. Sample R14-18 contains small amounts of Rh, Cu and Ni (Table 6), and its formula can be written as (Pt,Rh)(Fe,Cu,Ni)–$(Pt,Rh)_3(Fe,Cu,Ni)_2$.

Most of the PtFe alloys from the Luobusa chromitite have 52–72 wt.% Pt and 17–29 wt.% Fe (Bai et al., 2004), similar to a PtFe alloy from the Josephine ophiolite in the USA with an iron content of 33 wt.% (Stockman and Hlava, 1984). The Fe content of the alloy from Ray-Iz is much lower, suggesting a different origin.

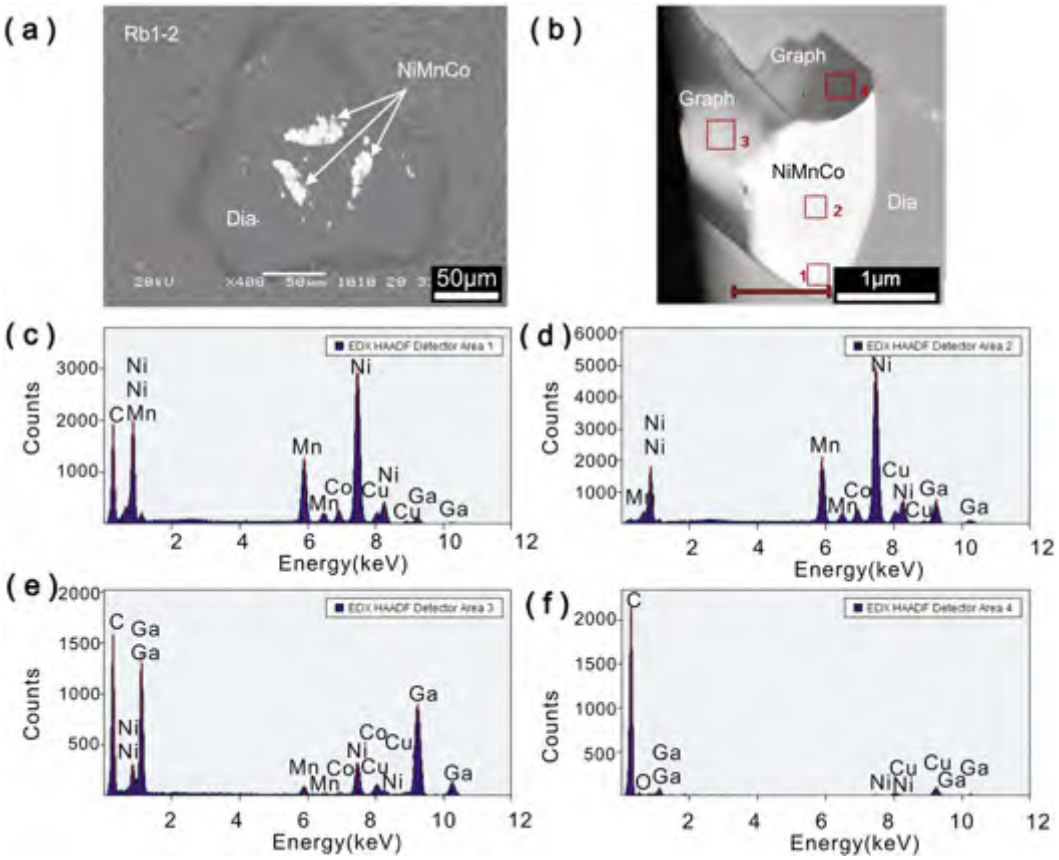

Fig. 10. Micrometer- and nanometer-size NiMnCo alloy and graphite inclusionsin diamons. (a) NiMnCo alloy up to 50 μm in size under the microscope; (b) nano-size graphite associated with NiMnCo alloy inclusions in diamond; (c–f) EDS analysis of NiMnCo alloys associated with graphite.

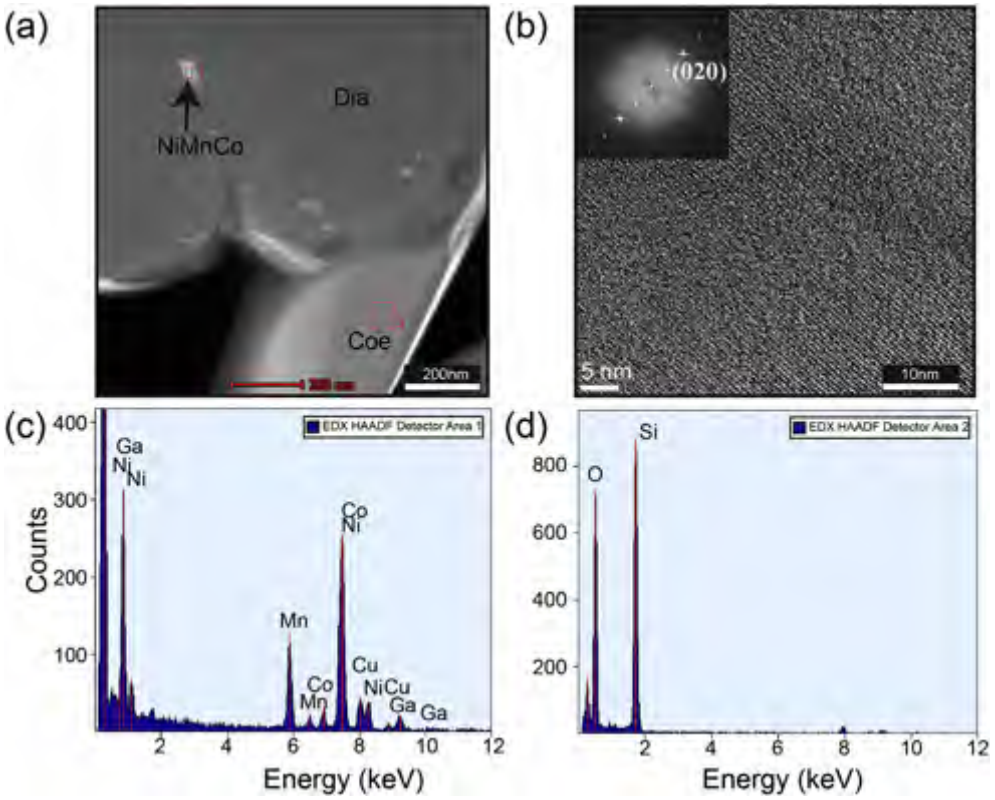

Fig. 11. Nanometer-size inclusions of coesite and NiMnCo in diamond WDR-8 hosted in chromite of the Ray-Iz ophiolite; (a) HAADF image of the inclusions. Small white grain in upper left is NiMnCo alloy; (b) HREM lattice fringe image of coesite inclusion with diffraction pattern in upper left hand corner. The lattice fringes display the (020) planes with a spacing of 0.621 nm. (c–d) EDX spectrum of NiMnCo and coesite inclusions, respectively.

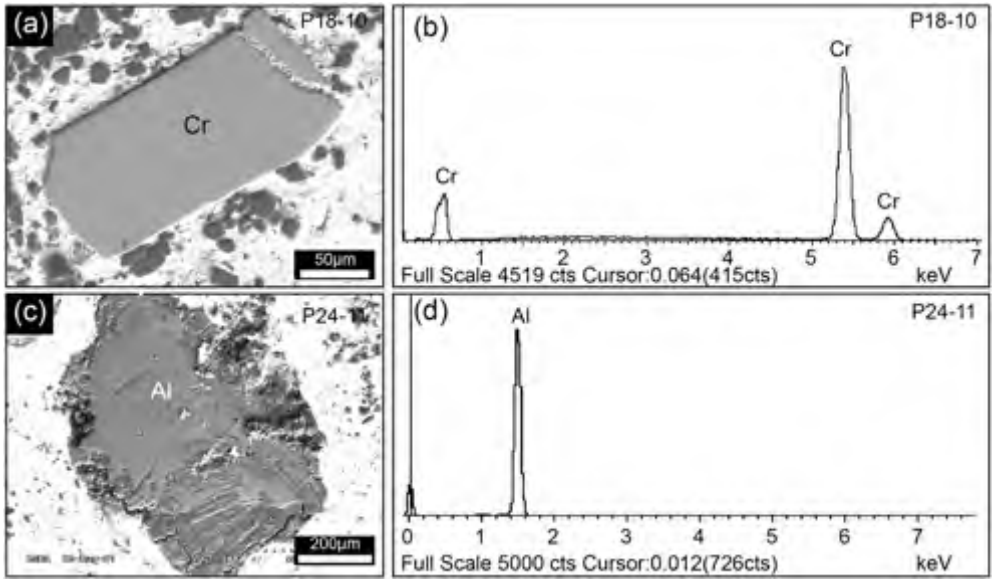

Fig. 12. SEM image and EDS analysis of native Cr and native Al from the Ray-Iz ophiolite. (a, b) Native Cr, and (c, d) native Al.

4.4.3. FeCr alloys

FeCr alloys occur as individual grains, or as microcrystals associated with rutile, diamond and WC. Two grains of FeCr alloy were analyzed. Sample P19-1 has a somewhat rounded form, is about 0.1 × 0.2 mm in size (Fig. 19a), and has a formula of $Fe_{0.8}Cr_{.18}Si_{.02}$. Sample P19-1 also contains a spherical inclusion about 3 μm in diameter (Fig. 19b) with a composition of SiO_2 = 24 wt.%, Al_2O_3 = 28%, CaO = 44%, and MgO = 4%. It is inferred to be amorphous glass formed by fast cooling. SampleP34-5-7 is black in color, anhedral and about 0.2 mm in diameter. It has a formula of $Fe_{0.7}Cr_{0.2}Ni_{0.1}$ but also contains traces of Mn and Si.

4.4.4. FeSi(Al, Ti) alloys

FeSi(Al,Ti) alloys form anhedral grains generally 0.05–0.2 mm in size. The 3 analyzed samples (P23-2, P23-4, and P31-5) show a range of compositions but Fe is the major component in all of them. Sample P23-2 (Fig. 20a) has 65–75 wt.% Fe, 14–21 wt.% Al and 10–13 wt.% Si. Some small patches of different colors are seen in Fig. 20b, but they have essentially the same composition as the host grain. They may reflect minor structural differences produced by cooling. Sample P31-5 contains 90 wt.% Fe, 9 wt.% Si, and traces of Al (Table 6).

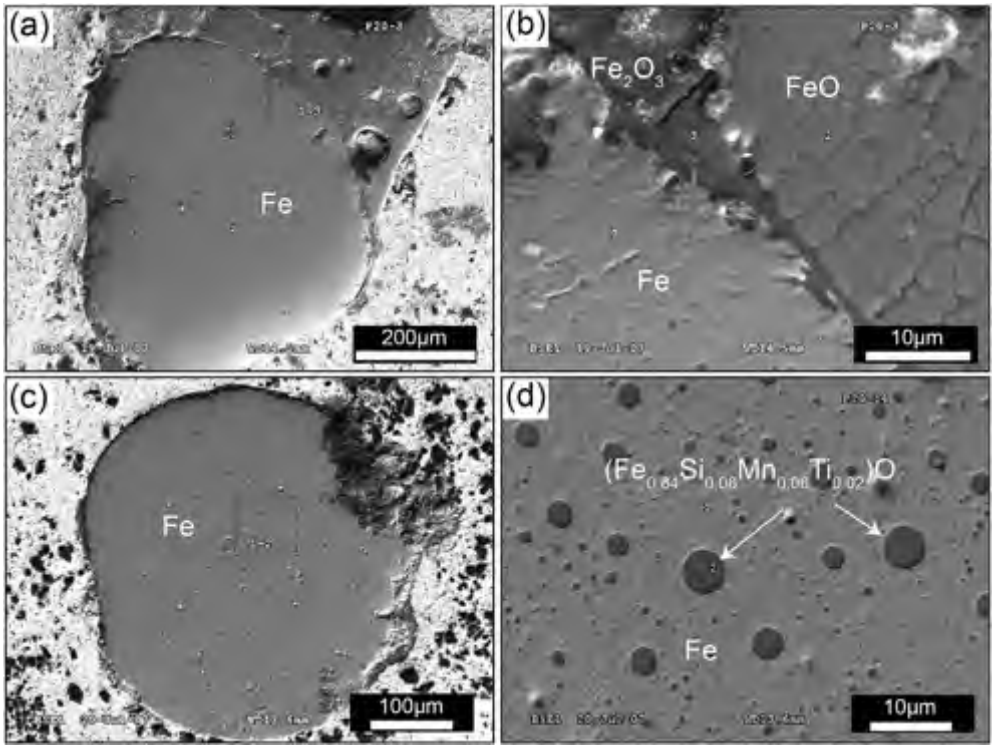

Fig. 13. Spheres of native Fe with small drops of wüstite within them; (a) sphere of native Fe partly rimmed with FeO; (b) Fe_2O_3 occurs between native iron and wüstite; (c, d) sphere of native Fe containing small droplets of wüstite.

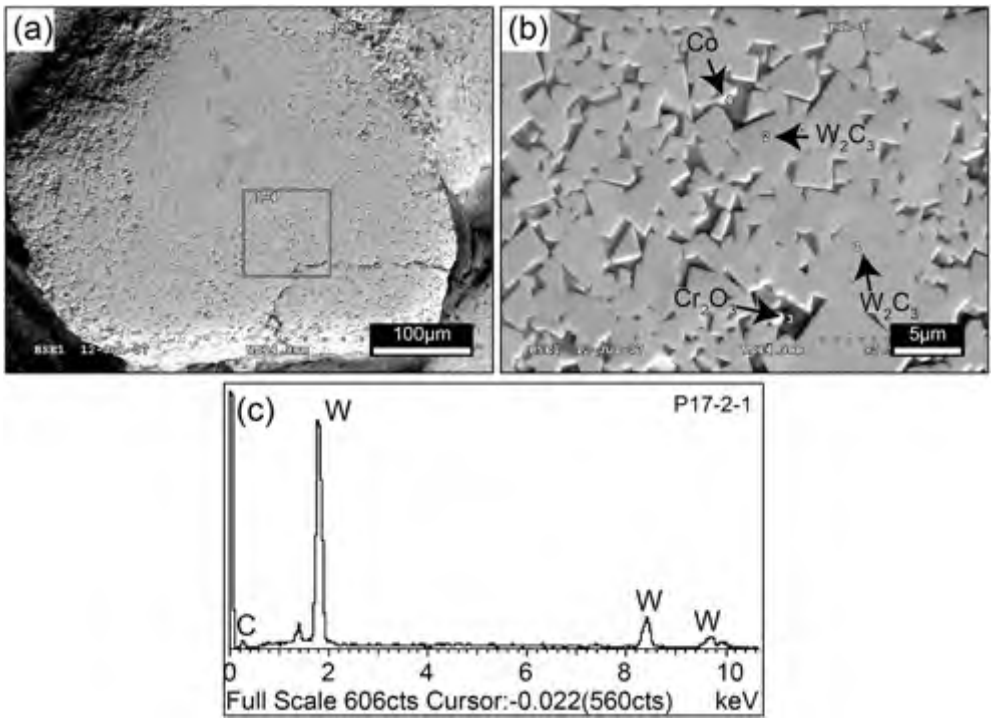

Fig. 14. WC minerals occur as an assemblage of small grains, with Cr_2O_3 filling interstices between the grains. (a,b) SEM images, and (c) EDS analysis of WC.

Similar minerals have been reported from Luobusa chromitites, which contain major Fe–Si components and minor Al and Ti. Analyses of Tibetan samples show 44.4% Fe and 55.5–56.2% Si, giving a formula of Fe_3Si_7 (Hu, 1999). X-ray powder diffraction analyses of an alloy with a pure Si and Fe composition (Fe_3Si_7) indicate an orthorhombic system, and the mineral has been approved to be a new mineral, luobusaite (no. IMA.2005-052a) (Bai et al., 2007b).

An Fe–Si alloy with minor Al and Ti, as well as grains of Fe_3Si_7, have also been reported from the Yakutia kimberlite (Mathez et al., 1995), indicating a deep formation for the ophiolitic Fe–Si minerals, as well as a highly reduced environment.

4.4.5. NiCu and AuAg

The only grain of NiCu alloy recovered (sample P21-3; Fig. 21a) is anhedral and 0.1–0.2 mm in size. Its bulk composition is 90 wt.% Cu and 10 wt.% Ni (Table 7) (Fig. 21b), but it contains a small patch of CuNi sulfide (P21-1-3; Table 7) and is rimmed by CuNi oxide (21-2 and 21-4, Table 7). Two grains of AuAg alloy (R26-23, R21-29) were recovered; both are anhedral and 0.2 mm in size. Sample R26-23 (Fig. 21c) has a composition of 80 wt.% Au and 20 wt.% Ag (Table 7) (Fig. 21d).

4.4.6. FeP alloy

Only one grain of FeP alloy (P30-23-1) was recovered from the Ray-Iz chromitites (Fig. 22a). It is sub-spherical in shape, about

Table 4
Microprobe analyses of tungsten carbides and moissanite.

Sample	wt.%					at.%				
	C	W	Co	Si	Total	C	W	Co	Si	Total
P17-2-1	9.86	90.14			100	62.6	37.4			100
P17-2-2	7.97	92.03			100	57.02	42.98			100
P17-1	12.07	87.93			100	67.75	32.25			100
P17-3	7.38	92.62			100	54.96	45.04			100
P17-4	7.64	84.7	7.66		100	51.83	37.56	10.6		99.99
P17-5	8.94	91.06			100	60.05	39.95			100
P17-6	10.02	89.98			100	63.02	36.98			100
P17-7	9.94	80.31	9.75		100	57.88	30.55	11.58		100.01
P17-8	8.83	83.9	7.27		100	55.92	34.7	9.38		100
P17-9	9.85	90.15			100	62.59	37.41			100
P17-10	8.03	83.7	8.26		99.99	52.9	36.01	11.09		100
P17-13	6.92	93.08			100	53.22	46.78			100
P17-14	8.94	78.65	12.42		100.01	53.82	30.94	15.24		100
P17-16	6.86	93.14			100	53	47			100
P17-17	6.88	7.72	85.41		100.01	49.02	11.21	39.77		100
P18-15	8.54	83.11	8.34		99.99	54.51	34.64	10.85		100
R23-21	13.34	86.66			100	70.2	29.8			100
R23-19	7.55	92.45			100	55.56	44.44			100
P17-2-4			100		100			100		100
P25-23	33.87			66.13	100	54.5			45.5	100
P21-14-1	31.61			68.39	100	51.94			48.06	100
R28-9-1	29.45			70.55	100	49.39			50.61	100

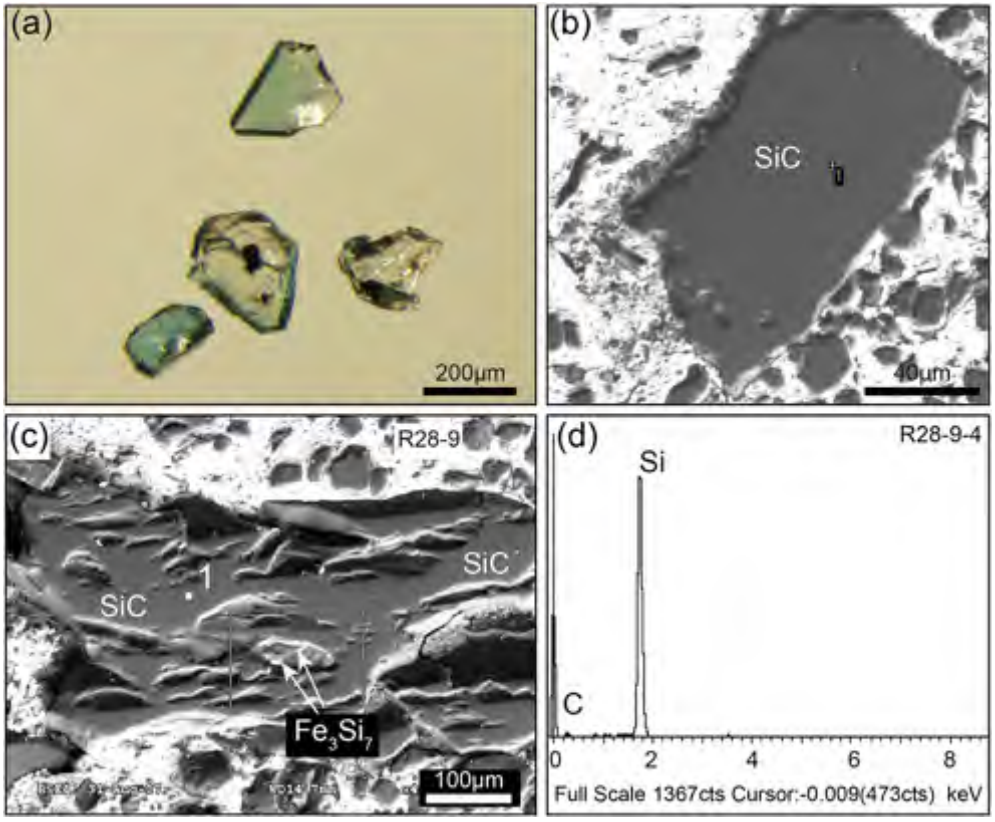

Fig. 15. Moissanite (SiC) and FeSi alloy (R28-9); (a) SiC crystals are euhedral to subhedral and light blue or green under the microscope; (b) SEM image of SiC polished surface; (c) FeSi inclusions in SiC; (d) typical laser Raman pattern of SiC.

0.2 mm across, and has several small fractures. It consists of 87–96 wt.% Fe and 4–13 wt.% P (Fig. 22b). FeP alloys are not common in nature, but have been reported from a garnet peridotite in the Sulu ultrahigh pressure metamorphic belt. That grain has a composition of 73.4 wt.% Fe and 23.7 wt.% P, with small amounts of Cr, Ni and Co (Yang et al., 2005). Some grains of an alloy with a composition of $Fe_4Ti_3Si_2P$ have also been reported from the Tibet podiform chromitites (Bai et al., 2003).

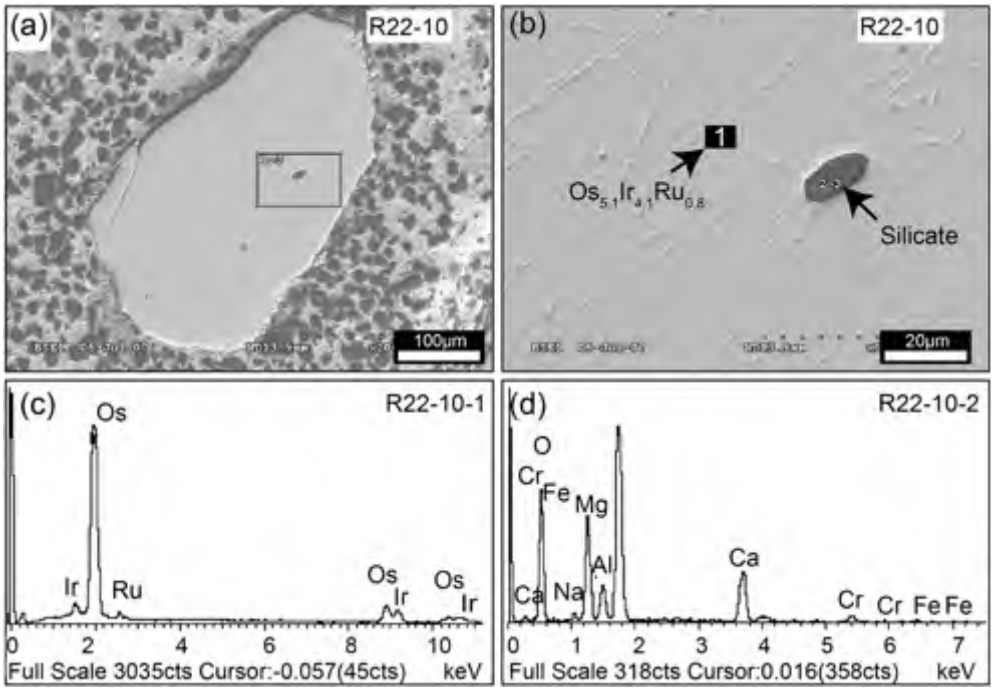

Fig. 16. SEM and EDS analysis of Os–Ir–Ru sample (R22-10). (a) SEM image of OsIrRu grain with small silicate 'inclusion'; (b) composition of the grain based on the EDS analysis in (c); (d) EDS analysis of silicate inclusion in (b).

Table 5
Representative compositions of OsIrRu alloys from the Ray-Iz chromitites.

Sample	wt.%				at.%			
	Ru	Os	Ir	total	Ru	Os	Ir	total
P15-6-2	24.53	39.45	36.02	100	38.07	32.54	29.4	100.01
P30-24	36.83	29.56	33.61	100	52.45	22.38	25.17	100
R14-15-1	16.56	42.98	40.46	100	27.3	37.64	35.07	100.01
R14-15-2	16.03	43.63	40.34	100	26.53	38.36	35.1	99.99
R14-15-3	16.51	43.34	40.14	99.99	27.23	37.97	34.8	100
R14-16-1	25.37	35.78	38.85	100	39.14	29.34	31.52	100
R14-16-2	25.03	36.48	38.49	100	38.72	29.98	31.3	100
R14-16-3	23.97	37.88	38.15	100	37.36	31.38	31.27	100.01
R14-17-1	14.12	41.1	44.78	100	23.73	36.7	39.57	100
R14-17-2	13.32	40.8	45.88	100	22.53	36.67	40.8	100
R14-17-3	13.23	40.42	46.34	99.99	22.4	36.35	41.25	100
R22-4-3	22.29	44.44	33.27	100	35.16	37.25	27.59	100
R22-4-4	22.73	44.1	33.17	100	35.73	36.84	27.43	100
R22-8	23.62	37	39.37	99.99	36.92	30.73	32.35	100
R22-9	3.07	53.32	43.62	100.01	5.64	52.14	42.21	99.99
R22-10-1	4.2	52.68	43.11	99.99	7.66	51.02	41.32	100
R22-30	14.25	41.37	44.38	100	23.92	36.91	39.17	100
R22-31	14.46	66.82	18.73	100.01	24.17	59.36	16.47	100
R22-32	31.29	32.67	36.04	100	46.29	25.68	28.03	100
R22-33	13.23	44.86	41.91	100	22.38	40.33	37.29	100

5. Discussion

5.1. Comparison of unusual minerals from the Ray-Iz and Luobusa chromitites

Ophiolitic diamond was originally discovered in the Luobusa massif of southern Tibet (IGCAGS, 1981), where they are accompanied by a wide range of other unusual minerals (Bai et al., 2000a,b; Bai et al., 2004; Robinson et al., 2004; Yang et al., 2007; Xu et al., 2008, 2014). As documented above, the podiform chromitites of the Ray-Iz ophiolite also contain a collection of UHP and highly reduced minerals similar to those found in the Luobusa ophiolite (Table 8). Both contain a wide variety of native elements, carbides, metal alloys, oxides and sulfides. Nearly all of the native elements recovered from the Luobusa ophiolite have also been identified in the Ray-Iz ophiolite, including native C (diamond), Cr, Ni, W, Cu, Fe, Si, Zn, Al, Pb and Co (Yang et al., 2008, 2014). The Ray-Iz chromitites also contain native Zr and Ta, but lack the native Os, Ir, Ru, Rh, Pd, Au, Ag, Sn, Ti and S, which have been identified in the Luobusa ophiolite.

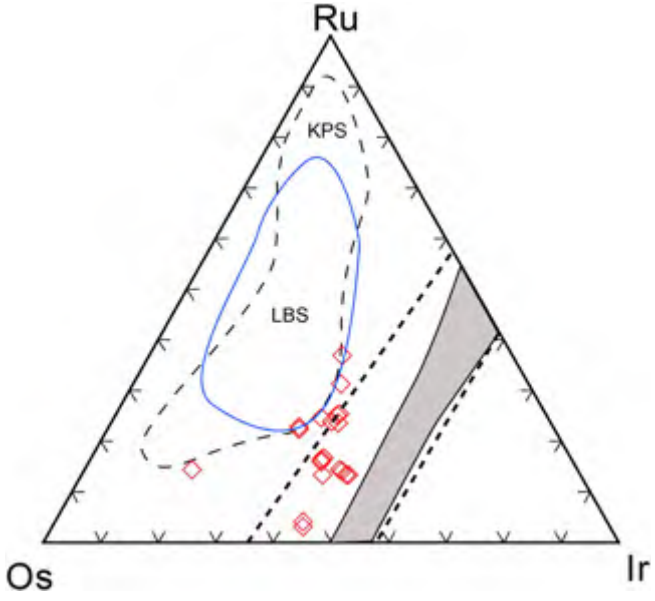

Fig. 17. Triangular diagram showing compositional variations of OsIrRu alloys in the Ray-Iz chromitites. The shaded miscibility gap is from Harris and Cabri (1991). The solid outlined field represents compositions of OsIrRu alloys from the Luobusa ophiolite (Bai et al., 2004), and the dashed outlined field represents compositions from Kempirsai, southern Urals, and Samar in the Philippines.
Data are from Nakagawa and Franco (1997) and Melcher et al. (1997).

Both localities have a similar collection of carbides, including SiC (moissanite), W(Co)C, and Ni- and Fe-bearing carbides. Cr-bearing carbides, which are present in Luobusa, have yet to be found in the Ray-Iz ophiolite. Interestingly, no Cr-bearing mineral inclusions have been found in diamond from either the Polar Urals or Luobusa (Yang et al., 2011).

Many metal alloys have been identified from both the Ray-Iz and Luobusa ophiolites (Table 8). The most common varieties are Fe–Ni–Cr-bearing alloys and Pt- or Os-bearing alloys. These alloys are accompanied by various combinations of P, Pb, Co, Ta, As, Sn, Zn, Au and Ag alloys, present in small quantities.

FeSi alloys are common in both ophiolites but with slightly different compositions. Both contain Fe_3Si_7, and Fe_3Si_4, but the Luobusa chromitites also contain FeSi, which has not yet been discovered in Ray-Iz.

The largest group of alloys in both ophiolites consists of variable proportions of FeCrNi, with or without Mn or Si (Table 8). However, several simple NiFe alloys, such as Ni_3Fe and $NiFe_3$ that are common in Luobusa, have not been observed in Ray-Iz.

FeAlSi alloys are common in the Ray-Iz chromitites but have not been found in the Luobusa ophiolite. In contrast, SiTiFe and SiCaFe alloys, which may also contain Ni and Al, occur in Luobusa but not in Ray-Iz.

A wide variety of PGE alloys occurs in both ophiolites but there are distinct differences in composition. For example, Pt-bearing alloys, typically containing various combinations of Fe, Ni, Cu, Rh or Pd are common in Ray-Iz but scarce in Luobusa, where only two types have been reported, $PtFe_3$ and $Pt_5Fe_4Pd_2$. On the other hand, many OsIr-bearing alloys, with or without Ru, Fe, Ni or Cu, have been recovered from the Ray-Iz chromitites but only a few, mostly IrFe varieties, have been found in Luobusa.

Au- and Ag-bearing alloys in Ray-Iz typically contain variable proportions of Fe, Ni, Cu, Zn and Sn. However, only two types, Ag_6Au and Ag_4Sn, are known from Luobusa. Sparse P-bearing alloys, including $Fe_{8.5}P_{1.3}As_{0.2}$, $Fe_{7.9-9.4}P_{0.6-2.1}$, have been recovered from Ray-Iz (Table 8) but are unknown in Luobusa. FeP alloys are rare in nature but have been reported from ultramafic rocks of the Sulu UHPM belt of eastern China (Yang et al., 2005).

5.2. Conditions of formation of the unusual minerals in ophiolites

Because the chromitites in Ray-Iz and Luobusa contain a wide variety of different minerals, all of which were separated from the host rock, it is impossible to use typical geothermometers or geobarometers to determine their P–T conditions of formation. It is clear that the minerals do not represent any sort of equilibrium assemblage but rather must reflect a mixture of minerals from different sources that formed under various P–T conditions.

The abundance of native elements and metal alloys, such as SiC, indicates derivation from a highly reduced section of the mantle. The redox conditions in the deep mantle are not well constrained, but the mean fO_2 is thought to decrease with depth, possibly reaching conditions near the iron-wüstite (IW) buffer (ca. FMQ-5) at the deepest levels (Frost and McCammon, 2008). Experimental studies suggest that SiC in the mantle requires fO_2 values several log units below the IW buffer (Shiryaev et al., 2011). Even lower fO_2 is indicated by the presence of native Si and $FeSi_2$, both of which are present in the chromitites. Such extreme reducing conditions (fO_2 equal to IW −8) are also indicated by the very low Sm and Eu contents of the diamonds (Griffin et al., 2013). Diamonds from both ophiolites are associated with small patches of amorphous carbon within chromite grains.

Table 6
Representative compositions of Si(Al)Fe, FePt, and FeP alloys from the Ray-Iz chromitites.

Sample	wt.%									
	Al	Si	Fe	P	Cr	Ni	Cu	Pt	Rh	Total
R28-9-2		52.67	47.22							99.89
R28-9-3		53.86	46.14							100
R22-31B			7.97			1.12	1.47	89.44		100
R22-4-1			10.32			0.93		86.11	2.64	100
R22-4-2			10.3			0.51		86.48	2.7	99.99
R14-18-1			9.66			2.55	1.31	83.96	2.53	100.01
R14-18-2			10.32			2.02	1.69	83.3	2.66	99.99
R14-18-3			10.04			2.03	2.18	83.27	2.48	100
R14-18-4			10.74			3.89	6.36	78.44	0.57	100
R14-18-5			10.53			3.71	6.23	79.17	0.36	100
R14-18-6			10.11			4.08	7.02	77.81	0.98	100
R14-18-7			10.58			4.57	6.41	76.99	1.45	100
P19-1-1		0.72	81.82		17.46					100
P23-2-1	14.16	10.37	75.47							100
P23-2-2	20.15	13.39	66.46							100
P23-2-3	20.37	13.85	65.78							100
P23-2-4	21.21	13.57	65.23							100.01
P23-2-5	14.57	10.97	74.46							100
P23-2-6	14.6	10.29	75.11							100
P31-5-1	0.7	9.11	90.19							100
P31-5-2	0.62	8.92	90.46							100
P31-5-3	0.55	9.08	90.37							100
P30-23-1			95.2	4.8						100
P30-23-2			96.31	3.69						100
P30-23-3			87.22	12.78						100
P30-23-4			87.46	12.54						100
	at.%									
	Al	Si	Fe	P	Cr	Ni	Cu	Pt	Rh	total
R28-9-2		68.88	31.12							100
R28-9-3		69.89	30.11							100
R22-31B			22.18			2.96	3.59	71.26		99.99
R22-4-1			27.68			2.38		66.11	3.84	100.01
R22-4-2			27.83			1.32		66.88	3.97	100
R14-18-1			25			6.27	2.98	62.21	3.55	100.01
R14-18-2			26.45			4.93	3.81	61.11	3.7	100
R14-18-3			25.7			4.93	4.91	61.01	3.45	100
R14-18-4			25.09			8.64	13.07	52.47	0.72	99.99
R14-18-5			24.85			8.32	12.92	53.46	0.46	100.01
R14-18-6			23.53			9.02	14.37	51.84	1.23	99.99
R14-18-7			24.38			10.02	12.98	50.8	1.82	100
P19-1-1		1.4	80.21		18.39					100
P23-2-1	23.38	16.44	60.18							100
P23-2-2	30.95	19.75	49.3							100
P23-2-3	31.12	20.32	48.55							99.99
P23-2-4	32.26	19.82	47.93							100.01
P23-2-5	23.85	17.25	58.9							100
P23-2-6	24.02	16.27	59.71							100
P31-5-1	1.32	16.51	82.17							100
P31-5-2	1.18	16.2	82.62							100
P31-5-3	1.04	16.49	82.48							100.01
P30-23-1			91.67	8.33						100
P30-23-2			93.55	6.45						100
P30-23-3			79.11	20.89						100
P30-23-4			79.46	20.54						100

The highly reduced minerals are accompanied by a number of UHP phases, suggesting depths of formation at, or near, the top of the transition zone. Diamonds can form over a range of depth in the mantle, generally >150 km. Coesite grains interpreted as pseudomorphs after stishovite suggest formation at depths of at least 300 km (Yang et al., 2007). Diamonds from both the Ray-Iz and Luobusa ophiolites contain inclusions of coesite and highly reduced metallic alloys; some chromite grains from Luobusa have exsolution lamellae of coesite and clinopyroxene suggesting crystallization at depths >380 km (Yamamoto et al., 2009).

Also present in the chromitites of both ophiolites are many silicate and oxide minerals, including coesite (as mentioned above), kyanite, andalusite, almandine garnet, zircon, rutile and corundum, all of which have a crustal affinity (Robinson et al., 2014).

We suggest that the presence of highly reduced andUHP phases, together with silicates and oxides in the chromitite, reflect interaction of the peridotites and chromitites with reduced fluids near the top of the transition zone.

5.3. A new occurrence of diamond on Earth

Natural diamonds are widespread in the Earth's crust and mantle, occurring principally in kimberlites and lamproites (Cartigny, 2005; Stachel et al., 2000; Gurney et al., 2010), ultrahigh-pressure metamorphic (UHPM) rocks (Sobolev and Shatsky, 1990; Dobrzhinetskaya et al., 1995) and impact structures (Hough et al., 1995, 1997; Koeberl et al., 1997).

Kimberlite diamonds, which have both ornamental and industrial uses, have been studied for a long time. These diamonds are thought to have originated from subcontinental (cratonic) mantle at depths of 200 km or greater (Shirey et al., 2004; Gurney et al., 2010; Walter et al., 2011). Kimberlites normally occur as pipes, dikes or veins, formed when alkaline magmas formed by low-degrees of partial melting of subcontinental lithosphereic mantle, are injected into the overlying crust (Stachel et al., 2005; Harte, 2010). Lamproites are regarded as counterparts of kimberlite because of their similar components and formational environment. Kimberlite diamonds are formed under high temperatures and pressures, and low oxygen fugacities. Such diamonds were generally thought to have crystallized from the kimberlite magmas in which they occur. However, age dating of mineral inclusions within diamonds suggests that the diamonds crystallized earlier than the kimberlites, and that the latter are simply carriers of the UHP minerals (Richardson et al., 1984). It has recently been shown that diamonds originally formed in the lower mantle at depths of at least 700 km can be entrained in kimberlites and carried to the surface (Walter et al., 2011). Some diamond grains, after being captured by kimberlite magmas, can continue to grow as new pulses of magma are added, so fluids and melts are clearly important in diamond formation.

Formation of kimberlite diamond is a lengthy process as shown by the zoning of these crystals, their various morphologies, and their common inclusions. Cubic and coated diamond commonly contain fluid inclusions, thought to have formed during capture of the diamond by kimberlite magma (Field et al., 2008; Burgess et al., 2009; Fedortchouk et al., 2010; Skuzovatov et al., 2012). Solid inclusions are also common and are used to subdivide diamonds into peridotite-type (P-type) and eclogite-type (E-type) that must have originated from different sources. P-type diamonds mainly include typical mantle minerals, such as Cr-pyrope, Mg-olivine, Cr-clinopyroxene, orthopyroxene and chromite (Gurney, 1989), whereas E-type diamond commonly contain inclusions of omphacite, Fe–Al garnet, phlogpite, coesite and rutile (Sobolev et al., 1997). Carbon isotope of kimberlite diamond generally show a variable range of $\delta^{13}C$ values, in which P-type varies mainly from −1‰ to −10‰, whereas E-type has a relatively larger range of $\delta^{13}C$ values (Bulanova et al., 2002; Deines et al., 2009; Melton et al., 2013). Nitrogen isotope $\delta^{15}N$ varies from −1.2‰ to −8‰ (Burgess et al., 2009). Fluids such as CO_2, H_2 and H_2O have also been discovered in kimberlite diamond, indicating crystallization in a reduced environment enriched in liquid and melt (Burgess et al., 2009; Zedgenizov et al., 2009; Fedortchouk et al., 2010; Basu et al., 2013).

Inclusions of lower mantle minerals in diamond are of great interest and importance. P-type inclusions contain ferri-wustite (wustite and periclase assemblage), iron and nitrogen carbide, majorite (high-Si garnet) (Harte, 2010), MgSi-perovskite, CaSi-perovskite, and CaTi-perovskite, TAPP (tetragonal almandine-pyrope and pyrope phase) (Harte and Harris, 1994), Mn-ilmenite, low-Mg chromite, as well as moissonite, native Ni and Fe (Kaminsky, 2012). E-type mineral inclusions contain 'phase Egg'($AlSiO_3OH$) (Schmidt et al., 1998; Wirth et al., 2007), which is stable up to 40 GPa (Vanpeteghem et al., 2003), as well as stishovite (Ono, 1999; Sano et al., 2004), Ca–Si perovskite and majorite garnet (Kaminsky, 2012). These diamonds commonly contain

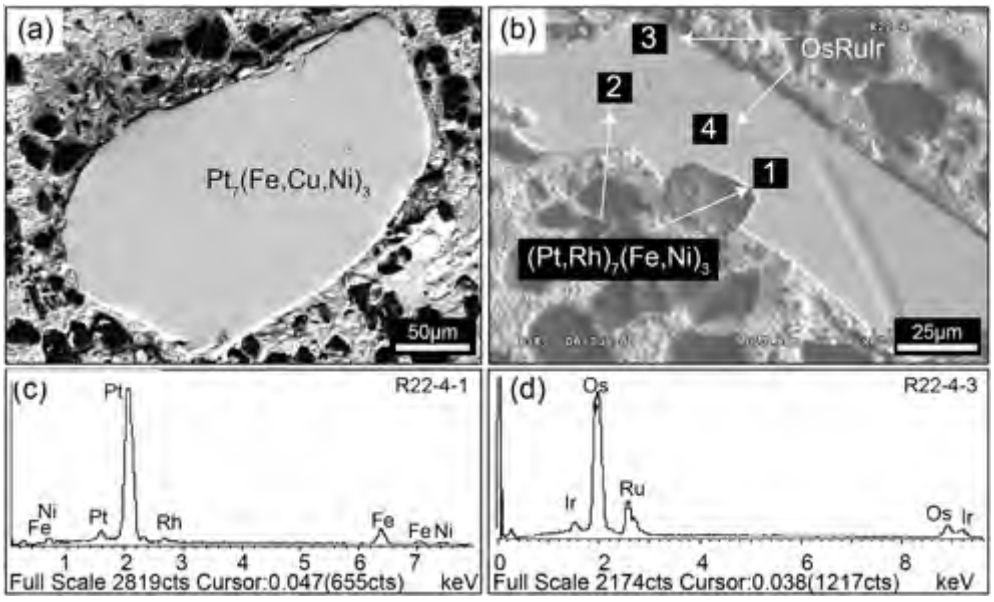

Fig. 18. SEM and EDS of PtFe alloys from the Ray-Iz chromitites. (a) Slightly rounded grain of PtFe alloy; (b) PtFe alloy intergrown with an OsRuIr alloy (sample R22-4); (c) EDS analysis PtFe alloy in (b); (d) EDS analysis of OsRuIr alloy in (b).

a large range of $\delta^{13}C$ (from ~− 1‰ to − 24‰), different from the typical values of P-type diamond ($\delta^{13}C$ ~ − 5‰) (Stachel et al., 2005; Tappert et al., 2009). On the basis of mineral inclusions and C isotope values, Walter et al. (2011) proposed that this type of diamond may have formed from surface carbon that was subducted into the lower mantle, then brought back to the surface as diamond by upwelling kimberlite magma.

Over the last 30 years, UHPM diamonds have been discovered from 6 locations in the Earth; the Kokchetavmassif in Kazakstan (Sobolev et al., 1990), the Dabie–Sulu and Qinling orogenic belt in China (Xu et al., 1992; Yang et al., 2003), the Northwest Gneiss Province, Norway (Dobrzhinetskaya et al., 1995), the Erzgebirge massif in Germany (Massonne, 1999), and the Rhodope complex in Greece (Mposkos and Kostopoulos, 2001). The UHPM diamonds in Kokchetav occur as micro-grains, mostly 10–80 μm in size, with an average of 30–50 μm. These micro-diamonds generally have C isotope $\delta^{13}C$ values of − 9.3‰ to − 13‰, but some small grains have $\delta^{13}C$ values of − 17.2‰ to − 26.9‰. Such low $\delta^{13}C$ values are thought to be the result of isotope fractionation at mantle temperatures (Ogasawara, 2005). The diamonds in the Erzgebirge UHPM terrane formed in two stages; early stage grains have

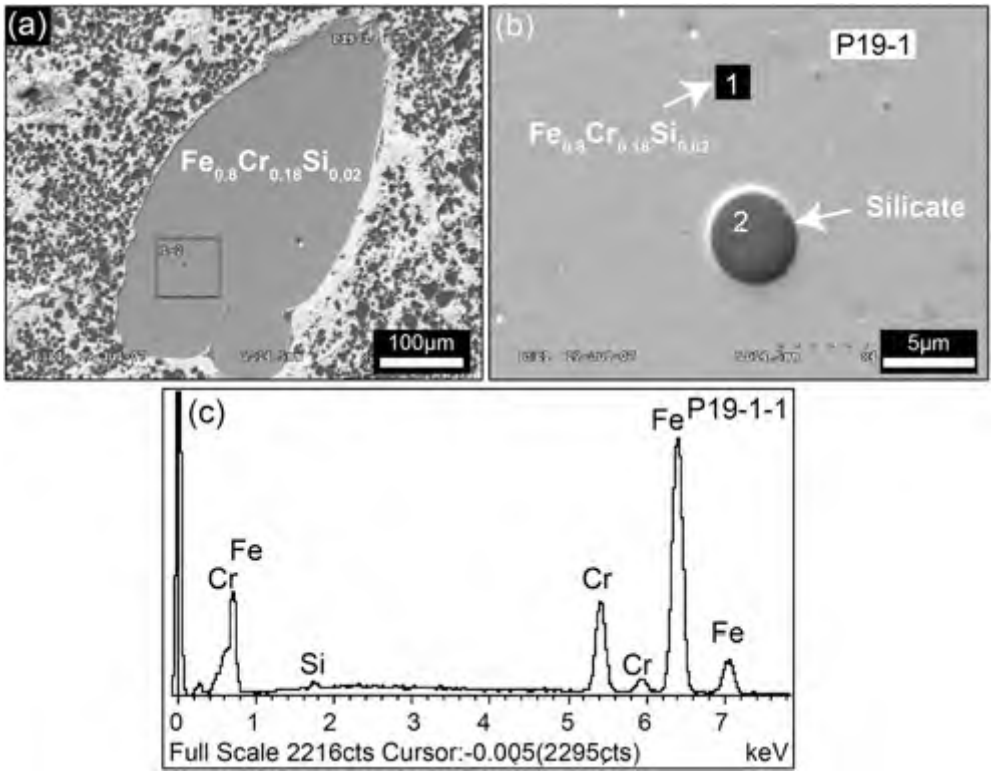

Fig. 19. SEM and EDS of a FeCr alloy (a) SEM image of an FeCr alloy; (b) a silicate inclusion within the grain; (c) EDS analysis of the FeCr grain.

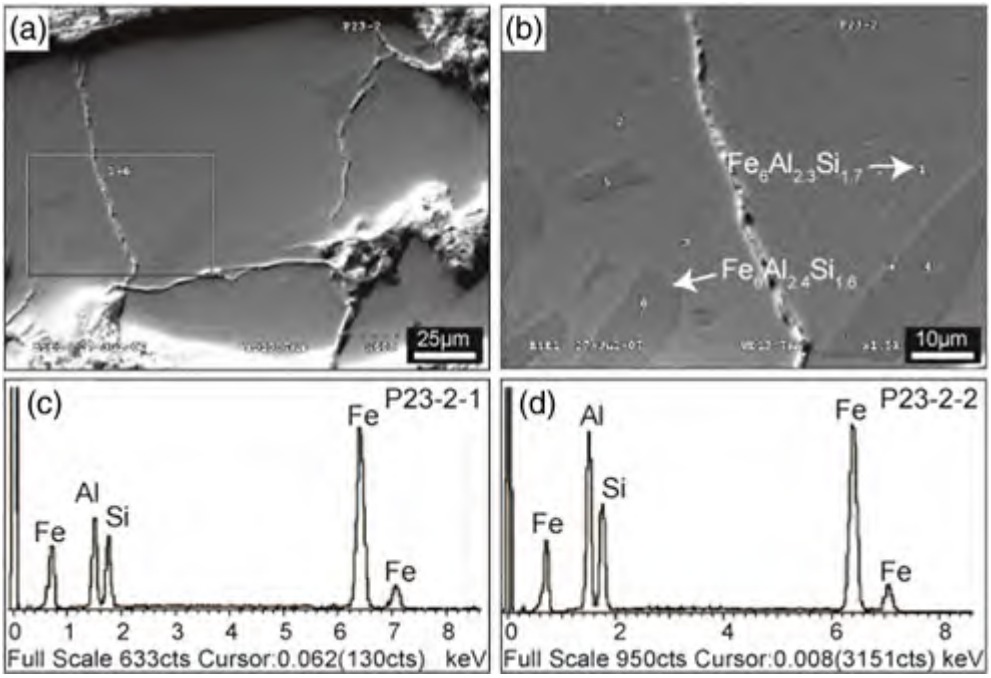

Fig. 20. SEM images and EDS analyses of Fe(Al)Si alloys from the Ray-Iz chromitites. (a) FeAlSi alloy (grain p23-2); (b) enlarged view of the square in (a) showing inclusions within the alloy; (c) EDS analysis of the alloy in (a); (d) EDS analysis of 'inclusions' in (b) showing they have the same composition as the host.

$\delta^{13}C = -17.8‰$, whereas the later ones have $\delta^{13}C = -21.5$ to $-25.5‰$. These variations are interpreted as the result of evolution from a relatively reducing to an oxidizing environment (Dobrzhinetskaya et al., 2010). Nitrogen isotopes of diamonds from Kokchetav have average $\delta^{15}N$ values of $+5.9‰$ to $+8.5‰$, suggesting a crustal origin (Cartigny et al., 2001; Jacobsen et al., 2011).

Diamonds hosted in the felsic gneiss of the Kokchetav UHPM terrane contain a range of mineral inclusions such as SiO_2, TiO_2, Cr_2O_3, Al_2O_3, zircon, calcite and dolomite, as well as fluid inclusions (Dobrzhinetskaya, 2012). Those diamonds hosted in dolomite, marble and calcic-silicate gneiss mainly contain inclusions of calcite, dolomite, rutile and Fe_2O_3. Some inclusions in UHPM diamondsappear to have formed at depths

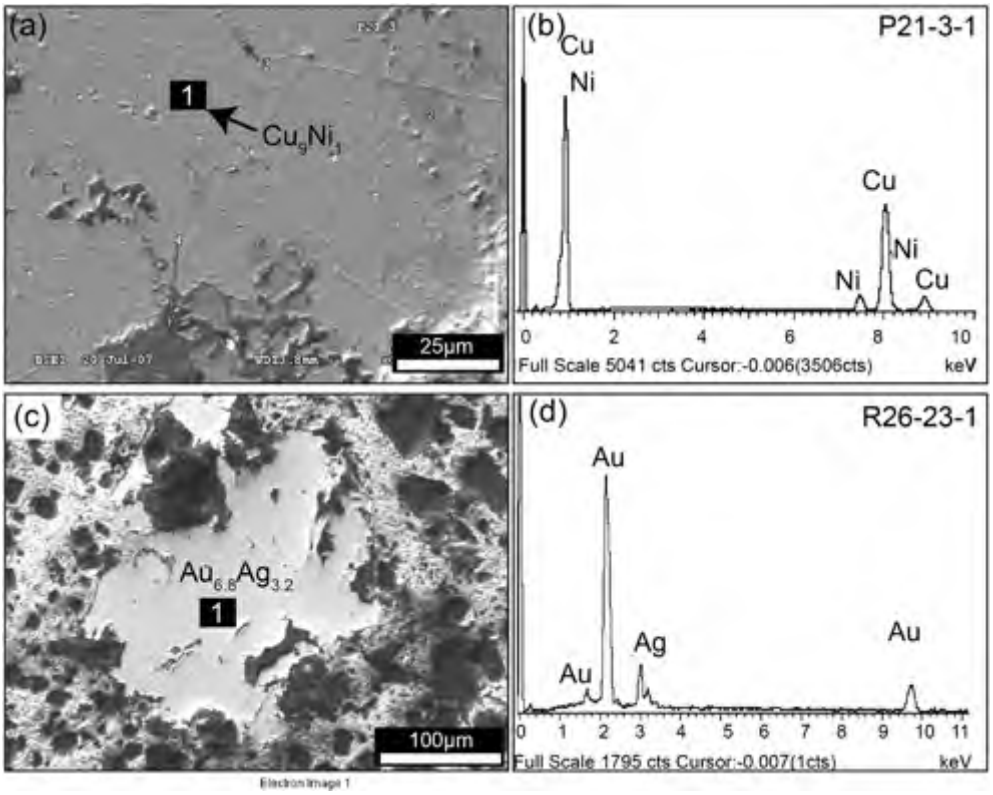

Fig. 21. SEM images and EDS analyses of CuNi alloy and AuAg alloy from the Ray-Iz chromitites. (a) SEM image of CuNi alloy; (b) EDS analysis of the grain in (a); (c) SEM image of AuAg alloy; (d) EDS analysis of the grain in (c).

Table 7
Chemical compositions of NiCu and AuAg alloys from the Ray-Iz chromitites.

Sample	wt.%							
	O	S	Mg	Ni	Cu	Ag	Au	Total
P21-3-1				9.84	90.16			100
P21-3-2	18.87				81.13			100
P21-3-3		23.87		66.3	9.84			100.01
P21-3-4	33.73		2.66	16.16	47.45			100
R26-23-1						20.42	79.58	100
	at.%							
	O	S	Mg	Ni	Cu	Ag	Au	Total
P21-3-1				10.57	89.43			100
P21-3-2	48.02				51.98			100
P21-3-3		36.7		55.67	7.63			100
P21-3-4	65.07		3.38	8.5	23.05			100
R26-23-1						31.9	68.1	100

>190–280 km, e.g., aragonite and magnesite, relics of majoritic garnet in the garnet peridotite, TiO_2II (rutile with a-PbO_2 structure in the diamond-bearing gneiss in the Erzgebirge terrane) (VanRoermund and Drury, 1998; Hwang et al., 2000; Katayama et al., 2000; Ye et al., 2000; Spengler et al., 2006; Dobrzhinetskaya et al., 2009; Masago et al., 2010).

Diamonds in meteorites or impact structures are relatively rare, but they have a clear genesis, and are called impact diamond (Koeberl et al., 1997; Karczemska et al., 2009). Impact diamond was found originally in the meteor impact pit in Arizona (Heymann et al., 1966). Impact diamond has also been reported from the Ries Crater in Germany (Goresy et al., 2001), the MWA 3140 meteorite in Morocco, and DaG 868 meteorite in Libya (Karczemska et al., 2009). In addition, very fine grains of diamond were discovered in siderolite on the Antarctic ice cover that is interpreted to have formed by collision between planets beyond the Earth (Goresy et al., 2001). Impact diamond has also been reported from many craters in Russia and Ukraine (Masaitis et al., 1972; Vishnevsky and Palchik, 1975; Masaitis et al., 1990; Masaitis, 1993; Gurov et al., 1995). In particular, the Popigai crater in Siberia, with a diameter of ca. 100 km and formation age of 35.7 Ma, contains abundant polycrystalline diamonds up to 1 cm in size (Masaitis et al., 1972). Koeberl et al. (1997) showed that the Popigai diamonds crystalized from a melt formed by the meteorite collision. These diamonds have $\delta^{13}C$ values of −12‰ to −17‰, which are much more depleted than values in kimberlite diamonds, but much enriched compared to organic sediments.

These three types of diamonds have different formational conditions and environments, but all formed at pressures above 5 GPa (>150 km depth) (Dobrzhinetskaya et al., 1995).

The occurrence of diamonds, both separated and in-situ grains, in two widely separated ophiolites of different ages and different tectonic regimes, suggest a new category of diamonds — here termed ophiolite-hosted diamonds (Yang et al., 2014). These diamonds occur in oceanic mantle rocks preserved in ophiolites and appear to be a characteristic feature of both podiform chromitites and the hosting peridotites. This interpretation is strongly supported by the presence of diamonds and other unusual minerals in peridotites of six ultramafic massifs along the 2000-km-long Yarlung–Zangbo suture and in both peridotites and chromitites of other ophiolites (Yang et al., 2011, 2013).

The ophiolite-hosted diamonds differ significantly from kimberlitic, metamorphic and meteoritic varieties. They have LREE-enriched trace-element patterns similar to those of some kimberlitic fibrous diamonds, but are characterized by strong negative anomalies in Sr, Sm, Eu and Yb. The trace element patterns are clearly distinct from those of synthetic diamonds and show striking differences from cratonic diamonds (Griffin et al., 2013). Many grains also contain micro-inclusions of $Ni_{70}Mn_{20}Co_5$ alloy and Mn-rich silicates, not found in other diamonds.

We suggest that ophiolite-hosted diamonds and their associated phases indicate a completely new environment for diamond formation in the mantle. The widespread occurrence of these minerals in ophiolites suggests that they may be a common feature of in situ oceanic lithosphere.

5.4. A new model for the formation of diamond-bearing ophiolitic peridotites and chromitites

The co-existence of UHP, highly reduced and crustal-type minerals in chromitites and peridotites of several ophiolites is difficult to explain. Clearly, these minerals do not represent any sort of equilibrium assemblage so they must reflect mixing of deep UHP and highly reduced minerals with crustal minerals from a relatively shallow source. The presence of coesite and clinopyroxene exsolution lamellae in some chromite grains suggests crystallization of a precursor with a calcium ferrite structure at a pressure >14 GPa, equivalent to a depth near the top of the transition zone (Yamamoto et al., 2009). It is clear that oceanic mantle peridotites contain abundant grains of chromite, most of which are relatively aluminous in composition. Several small micropods of chromitite have also been reported from in situ ocean mantle rocks (Arai and Matsukage, 1998; Abe, 2011; Payot et al., 2011) and larger bodies of chromitite may be present although this has yet to be confirmed. All of the chromitites recovered thus far from in situ oceanic peridotites are high-Al varieties with Cr# <60.

Seismic tomography provides graphic evidence for the subduction of oceanic lithosphere and even continental crust to the transition zone (410–660 km depth), and perhaps even to the core–mantle boundary (CMB) (2900 km depth) (Grand et al., 1997; Bijwaard et al., 1998; Zhao, 2004). An experimental study has also demonstrated that the subducted upper continental crust would not return to the surface once it reaches a depth of 250 km, because at that pressure the crust would develop a jadeite stishovitite lithology, which would continue to sink to the transition zone (Wu et al., 2009). It has been proposed that such crustal material may collect near the bottom of the MTZ to form 'a second continent' (Kawai et al., 2013).

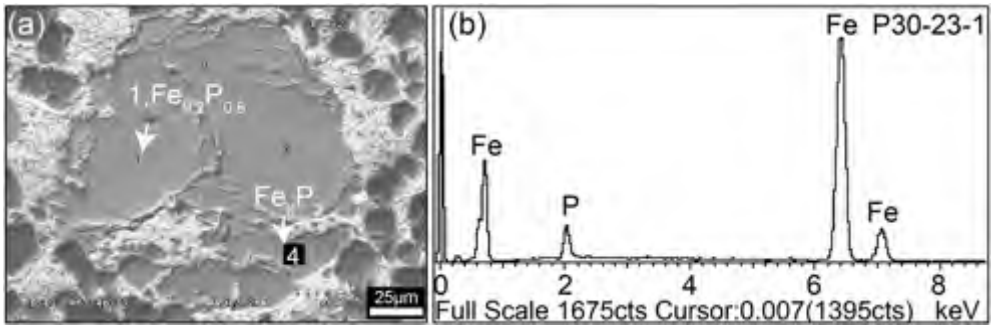

Fig. 22. SEM image and EDS analysis of FeP alloy from the Ray-Iz chromitite. (a) SEM image of an FeP alloy; (b) EDS analysis of the grain in (a).

Table 8
Summary of unusual minerals recovered from the Luobusa and Ray-Iz ophiolites.

Type	Luobusa	Ray-Iz
Native elements	Si, Fe, Zn, Pb, Al, Cr, Sn, Ni, Os, Ir, Ru, Rh, Pd, Au, Ag, W, Cu, S, Co, Ti, C (diamond, graphite)	Diamond, Cr, Ni, W, Cu, Si, Fe, Zn, Zr, Al, Ta, Pb, Co
Carbides	NiC, FeC, TiC, WC, (W, Co)C, SiC, Cr_3C_2, CrC, Cr_4C, Cr_3C, Cr_7C_3, Fe_4CrC_3, Fe_6CrC_3, Ni_6C_4	SiC, WC_2, W_2C_3, WC, $W_{4.4}C_{5.6}$, W_3C_7, $W_{3.5}C_{6.5}$, $W_{3.1-4}Co_{0.9-1.5}C_{4.9-5.8}$, $W_{0.8}Co_{6.6}C_{2.6}$, $W_{1.3}Co_{2.1}Fe_{0.5}Ni_{0.9}C_{5.1}$
Nitrides	Ti_2N, Ti_2N_3	
Metal alloys	Fe_3Si_7, Fe_2Si_3, FeSi, Fe_7Si_3, Fe_3Si_2, $Fe_4Ti_3Si_2P$, Ni_3Fe, Ni_7Fe_3, $Ni_5Fe_3Cr_2$, Fe_9Cr, Fe_2Ni, Ni(Fe, Ir), Ni_4FeIr, Ni_3Ir_2Fe, Ir_3Fe_2, IrFe, Ir_5Fe_2, Ir_7Fe_3, Pt_5Fe_2, NiIr, Ir_2Os, Ir_3Os_2, OsRu, Ru_3Os, Os_3RuIr, Pt_7Fe_3, $Pt_5Fe_3Pd_2$, Os_3Ir_2, Fe_2Ru, FeCo, Al_7Fe_2La, W_4Co, Fe_3Mn, Ag_6Au, Ag_8Sn_2, Ir_5Fe_4Ni, Si_2TiFe, NiFeSi, Ti_6W_4, Cu_3Zn, Fe_8CrNi, $Si_6CaAlFe$, $Si_7(Fe, Al)_3$, Si_7Ca_2Fe, Si_7Ca_3, Si_2Ca, $Si_5Fe_2Al_2Ca$, $Si_5Fe_{2.5}Ti_{2.5}$, Si_6CaCu	$Cu_{8.9}Ni_{1.1}$, $Pt_{5.6-7.1}Fe_{2.2-2.9}Ni_{0.3-0.5}Cu_{0.4-1}$, $Pt_{6.6-6.7}Rh_{0.4}Fe_{2.8}Ni_{0.1-0.2}$, $Pt_{5.2-6.2}Rh_{0.1-0.4}Fe_{2.4-2.7}Ni_{0.5-1}Cu_{0.3-1.3}$, $Pt_{4.8-5.2}Pd_{1.8-2.3}Fe_{2.7-2.8}Cu_{0.2-0.3}$, $Fe_{6.5-7.3}Cr_{1.6-2.8}Ni_{0.7-1.3}$, $Fe_{1.4}Cr_{6.7}Ni_{1.9}$, $Fe_{7.5}Cr_{2.4}Mn_{0.1}$, $Fe_8Cr_{1.8}Si_{0.2}$, $Fe_{2.3-3.7}Si_{6.3-7.7}$, $Fe_{6.4}Si_{3.6}$, $Fe_{1.7}Cr_{3.2}Ni_{1.7}Si_3Mg_{0.3}$, $Fe_{6.6-7.0}Cr_{1.7-1.9}Ni_{0.9}Si_{0.2-0.8}$, $Fe_{6.9-7.4}Cr_{1.4-2}Ni_{0.8-1.1}Mn_{0.1-0.3}$, $Fe_{6.7-7}Cr_{1.7-1.9}Ni_{0.9-1.1}Mn_{0.2}Si_{0.2}$, $Fe_{6.5-6.8}Cr_{1.8-1.9}Ni_{0.9-1}Mn_{0-0.2}Ti_{0.1-0.8}$, $Fe_{3.9-6}Al_{2.3-3.5}Si_{1.6-2.6}$, $Fe_{8.2-8.3}Al_{0.1}Si_{1.6-1.7}$, $Ag_{2.4-3.8}Au_{6.2-7.6}$, $Ag_{0.9}Au_{9.1}$, $Ag_{2.2}Au_{5.9}Fe_{1.2}Ni_{0.2}Cu_{0.3}Zn_{0.2}$, $Os_{2.2-3.3}Ir_{2.5-4.1}Ru_{2.2-5.2}$, $Os_{1.0-2.2}Ir_{0.3-0.6}Ru_{6-7.6}Fe_{0.5-0.9}Ni_{0.5-0.6}$, $Os_{5.1-5.2}Ir_{4.1-4.2}Ru_{0.6-0.8}$, $Os_{5.9}Ir_{1.7}Ru_{2.4}$, $Os_{2.3-4.1}Ir_{2.0-3.2}Ru_{1.8-5}Cu_{0.8-0.9}$, $Os_{3.2}Ir_{3.2}Ru_{2.6}Fe_{0.3}Cu_{0.7}$, $Os_{3.9}Ir_{3.6}Ru_{2.3}Fe_{0.2}$, $Pb_{4.5}Sn_{5.5}$, $Sn_7Zn_{2.6}Ag_{0.4}$, $Sn_{5.4}Ag_{4.6}$, $Pb_{4.8}Zn_{1.9}Cu_{2.8}Fe_{0.5}$, $Ta_{5.4}Co_{4.5}$, $Fe_{8.5}P_{1.3}As_{0.2}$, $Fe_{7.9-9.4}P_{0.6-2.1}$, $Ni_{7.3}As_{2.7}$

Thus, subduction of oceanic lithosphere and continental crustal material can provide a mechanism for mixing deep mantle and crustal phases. Subduction of oceanic crust also provides a mechanism for introducing organic carbon with $\delta^{13}C_{PDB}$ values in the range of the measured values in both diamond and moissanite from ophiolitic chromitites and peridotites (−17 to −28) (Walter et al., 2011).

Here, we propose a 3-stage model that provides a coherent explanation for the origin of podiform chromitites and oceanic peridotites, and the exotic minerals they contain.

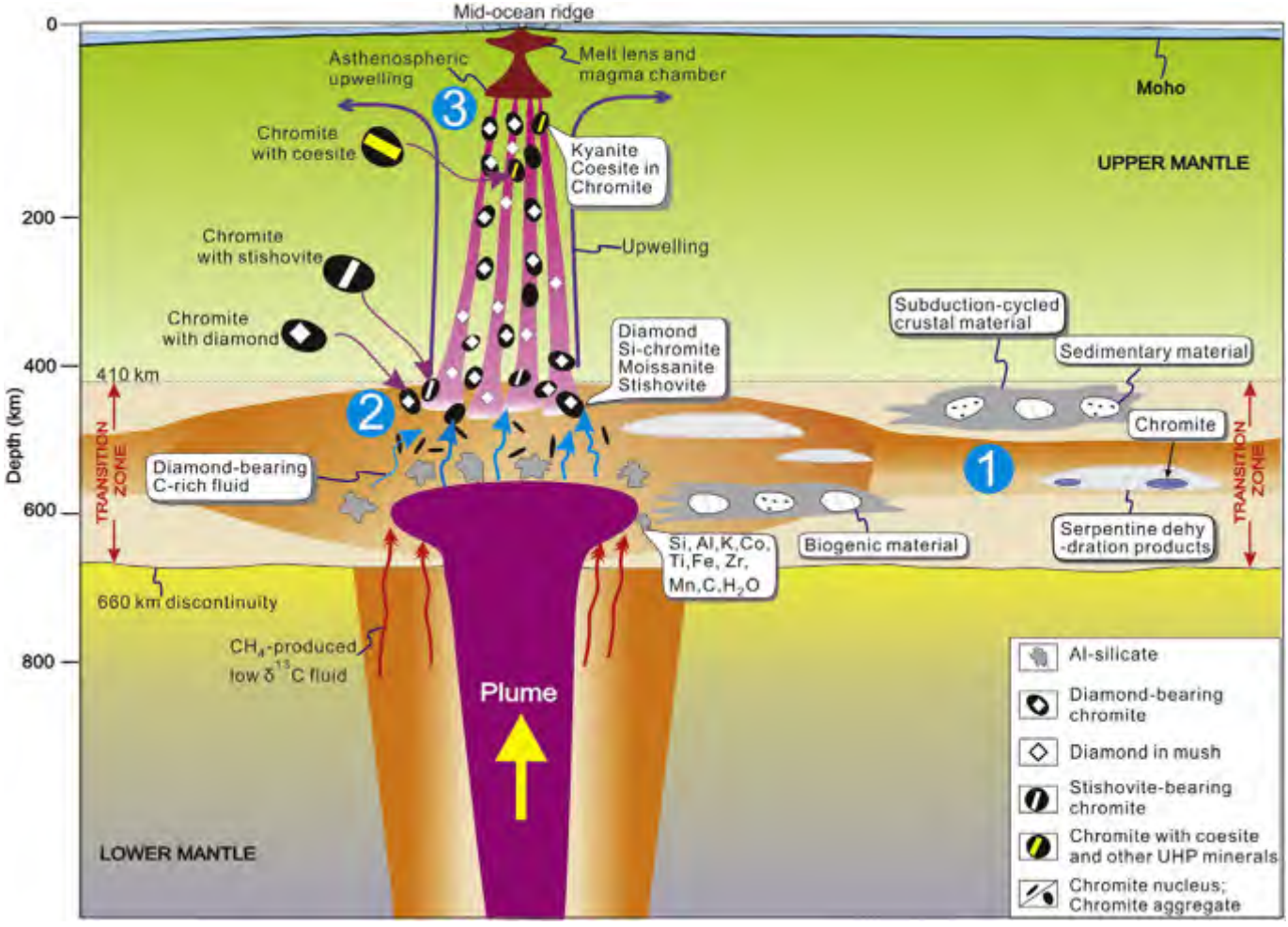

Fig. 23. A model for the formation of ophiolitic diamonds. Previously subducted slabs of continental and oceanic crust lying in the lower part of the transition zone between the upper and lower mantle are partially melted at high temperatures in a highly reduced environment. H_2O, CO_2 and other fluids are released from the rocks and some of them are reduced to single element material, such as C and H. The melts then rise through the mantle to the top of, or above, the transition zone, where diamonds can be encapsulated in high-pressure chromite (with dissolved Si) and stishovite may crystallize from the melts or fluids. With continued upwelling, coesite exsolution lamellae form in the chromite grains and stishovite is replaced by coesite, but the diamonds are preserved as inclusions in chromite grains. This new model challenges the concept that MORB-type ophiolites form only at shallow depth in mantle.

5.4.1. Stage one

Mantle convection causes continuous recycling of oceanic lithosphere with upwelling beneath spreading ridges and downwelling at subduction zones (Fig. 23). Subduction and recycling carries upper mantle peridotites, including chromite grains and any chromitites that may be present, as well as crustal materials to the transition zone. The ambient conditions within the transition zone would be ~15–16 GPa and ~1600 °C. Under such conditions, slabs of oceanic lithosphere, including dense eclogites, may undergo partial melting (Maruyama et al., 2007) or at least become plastic. It has recently been suggested that the transition zone can contain 1–1.5 wt.% water (Pearson et al., 2014), which would certainly facilitate partial melting. Chromite grains under these conditions would break down to a new phase with a Ca ferrite structure (Xu et al., 2013). Most crustal minerals subducted to the transition zone would either break down or react with the highly reduced phases (e.g., coesite and kyanite rimming Ti–Fe alloy; Yang et al., 2007), although some more resistant grains, such as zircon, might survive. However, we suggest that any subducted material entering the transition zone would become highly deformed, dismembered and redistributed.

Material transported to the transition zone would be mixed with highly reduced and UHP phases, presumably derived from even greater depths, or from zones with extremely low fO_2, as required for the formation of moissanite and the numerous native elements. Thus far, no diamonds in ophiolites have been found with inclusions of chromite, suggesting that they crystallized at depths below the chromite stability field (~14 GPa).

5.4.2. Stage two

Partially melted material in the transition zone becomes more buoyant and moves upward beneath oceanic spreading centers. Near the top of the transition zone (>300 km depth), UHP chromite (with dissolved Si) begins to crystallize, encapsulating diamond, moissanite, and other highly reduced phases (Robinson et al., 2004; Trumbull et al., 2009). The association of in situ diamondswith spherical patches of amorphous carbon suggests that they grew in a carbon-rich fluid that also contained metallic alloys, stishovite/coesite, and Mn-rich phases, all of which occur as inclusions in the diamonds (Yang et al., 2011, 2014). Patches of amorphous carbon that host moissanite and corundum in the peridotites presumably formed at the same time.

5.4.3. Stage three

As the mantle peridotites continue to rise, they carry with them the minerals that formed at depth. With continued upwelling, coesite exsolution lamellae form in the chromite grains and stishovite is replaced by coesite, but the diamonds and highly reduced minerals are preserved as inclusions in chromite grains (Yang et al., 2007; Yamamoto et al., 2009). Partial melting of the rising peridotites at shallow mantle depths may cause redistribution of chromite grains and the formation of small chromitite pods. The majorityof the mantle peridotites that reach the lithospheric mantle get subducted back into the mantle, but some may be trapped as mantle wedges above subduction zones where they are partially melted and modified by arc tholeiite and boninite magmas generated within the wedge (Dilek and Robinson, 2003; Dilek and Furnes, 2009; Dilek and Thy, 2009; Morishita et al., 2011; Uysal et al., 2014). These migrating melts and fluids redistribute, chemically modify and redeposit the chromite grains into larger podiform chromitites with typically high-Cr compositions (Xu et al., 2009, 2011; Xiong et al., 2014).

Crustal minerals may also be incorporated into the melt regime of the peridotites and chromitites in the wedge from the subducted slab (Robinson et al., 2014; Zhou et al., 2014). When such suprasubduction zone mantle wedges are underplated by less dense continental crustal material during trench–continent collisions they can be emplaced on land as ophiolites (Wakabayashi and Dilek, 2003; Dilek, 2006).

This model provides a means of reconcilingthe need for deep crystallization of chromite grains to entrain the UHP and highly reduced minerals with the clear evidence for the redistribution and reprecipitation of high-Cr chromite to form chromitites in suprasubduction zone environments (Stockman and Hlava, 1984; Talkington et al., 1984; Zhou et al., 1996; Edwards et al., 2000; Rollinson, 2005, 2008; Rollinson and Adetunji, 2013).

6. Conclusions

Ophiolites of the Yarlung–Zangbo suture zone of southern Tibet and the Polar Urals differ significantly in age and tectonic setting, but have similar assemblages of UHP and highly reduced minerals, hosted in both peridotites and podiform chromitites. The in-situ occurrence of the diamonds and some of the other minerals prove that they are natural in origin. These diamonds have different mineral inclusions and trace element compositions than those from kimberlites,UHP metamorphic rocks and meteorite impact structures, and constitute a new class of diamonds known thus far only in oceanic mantle sections of ophiolites. However, the widespread occurrence of the ophiolite-hosted diamonds and associated minerals suggests that they may be a common feature of in-situ oceanic mantle. In-situ diamonds and UHP crustal minerals in ophiolitic peridotites and chromitites likely formed in the mantle transition zone and were then encapsulated as inclusions in solid chromitite that crystallized near the top of the transition zone. The rising asthenosphere brought these diamond-carrying chromitites and peridotites to shallow mantle depths, where partial melting processes redistributed and disseminated them in the oceanic mantle beneath the spreading axes and/or subduction-derived fluids interacted with them to form podiform chromitites in the mantle wedge.

Acknowledgments

Professor Qingsong Fang (deceased) is gratefully acknowledged for his careful work in selecting diamonds from heavy mineral separates and his fieldwork. We thank Songyong Chen, Wenji Bai, and N. Makeyev for assistance with the field work and sampling, and Larissa Dobrzhinetskaya with the laboratory work. This research was funded by grants from SinoProbe-05, the NSF China (40930313, 40921001, 41221061), the MST China (2014DFR2127C) and the China Geological Survey (12120114061801). The authors acknowledge the facilities, and the scientific and technical assistance of the Institute of Multipurpose Utilization of Mineral Resources, Chinese Academy of Geological Sciences, Zhengzhou, the Beijing General Research Institute of Mining and Metallurgy, and the Key Laboratory of Nuclear Resources and Environment (East China Institute of Technology). Gary Ernst and Juhn-Guang Liou are gratefully acknowledged for their critical and constructive reviews for Gondwana Research. Mei-Fu Zhou's careful comments on the latest version of the manuscript helped us further improve the paper.

References

Abe, N., 2011. Petrology of podiform chromitite from the ocean floor at the 15°20′N FZ in the MAR, Site 1271, ODP Leg 209. Journal of Mineralogical and Petrological Sciences 106, 97–102.

Arai, S., 1997. Origin of podiform chromitites. Journal of Asian Earth Sciences 15, 303–310.

Arai, S., Matsukage, K., 1998. Petrology of a chromitite micropod from Hess Deep, equatorial Pacific: a comparison between the abyssal and alpine-type podiform chromitites. Lithos 43, 1–14.

Bai, W.-J., Robinson, P.T., Fang, Q., Hu, X.-F., Zhou, M.-F., 2000a. Origin of PGE and base metal alloys in podiform chromitites of the Luobusa ophiolite, southern Tibet. Canadian Mineralogist 38, 585–598.

Bai, W.J., Zhou, M.F., Robinson, P.T., Fang, Q.S., Zhang, Z.M., Yan, B.G., Hu, X.F., Yang, J.S., 2000b. Origin of Podiform Chromitites, Diamond and Associated Mineral Assemblage in the Luobusa Ophiolite, Tibet. Seismological Press, Beijing, (in Chinese).

Bai, W.J., Yang, J.S., Fang, Q.S., Yan, B.G., Zhang, Z.M., 2001. Study on a storehouse of ultrahigh pressure mantle minerals — podiform chromite deposits. Earth Science Frontiers 8, 111–121 (in Chinese with English abstract).

Bai, W.J., Yang, J.S., Fang, Q.S., Yan, B.G., Shi, N.C., 2003. An unusual mantle mineral group in ophiolites of Tibet. Geology in China 30, 144–151 (in Chinese with English abstract).
Bai, W.J., Yang, J.S., Fang, Q.S., Yan, B.G., Zhang, Z.M., Ren, Y.F., Shi, N.C., Ma, Z.S., Dai, M.Q., 2004. Some native metals from ophiolitic chromitites in Tibet. Earth Science Frontiers 11, 179–187 (in Chinese with English abstract).
Bai, W.J., Ren, Y.F., Yang, J.S., Fang, Q.S., Yan, B.G., Rong, H., 2006. The native iron and wüstite assemblage: records of oxygen element from the mantle. Acta Geoscientica Sinica 27, 43–49 (in Chinese with English abstract).
Bai, W.J., Tao, S.F., Yang, J.S., Fang, Q.S., Shi, N.C., Li, G.W., 2007a. A mineral assemblage of sulfides and sulfo-arsenides from the ophiolite mantle in Tibet. Acta Petrologica Et Mineralogica 26, 41–428 (in Chinese with English abstract).
Bai, W.J., Shi, N.C., Yang, J.S., Fang, Q.S., Ren, Y.F., Rong, H., Li, G.W., Ma, Z.S., 2007b. An sssemblage of dimple oxide minerals from ophiolitic podiform chromitites in Tibet and their ultrahigh pressure origin. Acta Geologica Sinica 81, 1538–1549 (in Chinese with English abstract).
Basu, S., Jones, A.P., Verchovsky, A.B., Kelley, S., Stuart, F.M., 2013. An overview of noble gas (He, Ne, Ar, Xe) contents and isotope signals in terrestrial diamond. Earth-Science Reviews 126, 235–249.
Bijwaard, H., Spakman, W., Engdahl, E., 1998. Closing the gap between regional and global travel time tomography. Journal of Geophysical Research 103, 30055–30078.
Brown, D., Juhlin, C., Alvarez-Marron, J., Perez-Estaun, A., Oslianski, A., 1998. Crustal-scale structure and evolution of an arc–continent collisionzone in the southern Urals, Russia. Tectonics 17, 158–171.
Bulanova, G.P., et al., 2002. Carbon and nitrogen isotope systematics within a sector-growth diamond from the Mir kimberlite, Yakutia. Chemical Geology 188 (1–2), 105–123.
Burgess, R., Cartigny, P., Harrison, D., Hobson, E., Harris, J., 2009. Volatile composition of microinclusions in diamonds from the Panda kimberlite, Canada: implications for chemical and isotopic heterogeneity in the mantle. Geochimica et Cosmochimica Acta 73, 1779–1794.
Cartigny, P., 2005. Stable isotopes and the origin of diamond. Elements 1, 79–84.
Cartigny, P., DeCorte, K., Shatsky, V.S., Ader, M., De Paepe, P., Sobolevn, V., Javoy, M., 2001. The origin and formation of metamorphic microdiamonds from the Kokchetav massif, Kazakhstan: a nitrogen and carbon isotopic study. Chemical Geology 176, 267–283.
Chemenda, A., Matte, O., Sokolov, V., 1997. A model of Paleozoic obduction and exhumation of high-pressure/low-temperature in rocks in the southern Urals. Tectonophysics 276, 217–227.
Coleman, R.G., 1977. Ophiolites, Ancient Oceanic Lithosphere? Spinger, New York, p. 229.
Davydov, M.P., Aleksandrov, P.A., 2001. Native aluminium in metasomatized sediments of the East Pacific Rise, 13° N. Earth Sciences Section. 379. Doklady Academy of Science, Russia, pp. 567–570.
Deines, P., 1980. The carbon isotopic compositions of diamonds: relationship to diamond shape, color, occurrence and vapor composition. Geochimica et Cosmochimica Acta 44, 943–961.
Deines, P., Stachel, T., Harris, J.W., 2009. Systematic regional variations in diamond carbon isotopic composition and inclusion chemistry beneath the Orapa kimberlite cluster, in Botswana. Lithos 112, 776–784.
Dilek, Y., 2003. Ophiolite concept and its evolution. Geological Society of America, Special Paper 373, 1–16.
Dilek, Y., 2006. Collision tectonics of the Eastern Mediterranean region: causes and consequences. Geological Society of America, Special Paper 409, 1–13.
Dilek, Y., Flower, M.F.J., 2003. Arc–trench rollback and forearc accretion: 2. Model template for Albania, Cyprus, and Oman. In: Dilek, Y., Robinson, P.T. (Eds.), Ophiolites in Earth History. Geological Society of London Special Publication. 218, pp. 43–68.
Dilek, Y., Furnes, H., 2009. Structure and geochemistry of Tethyan ophiolites and their petrogenesis in subduction rollback systems. Lithos 113, 1–20.
Dilek, Y., Furnes, H., 2011. Ophiolite genesis and global tectonics: geochemical and tectonic fingerprinting of ancient oceanic lithosphere. Geological Society of America Bulletin 123, 387–411.
Dilek, Y., Furnes, H., 2014. Ophiolites and their origins. Elements 10, 93–100. http://dx.doi.org/10.2113/gselements.10.2.93.
Dilek, Y., Robinson, P.T., 2003. Ophiolites in Earth history: introduction. In: Dilek, Y., Robinson, P.T. (Eds.), Ophiolites in Earth History. Geological Society of London Special Publication. 218, pp. 1–8.
Dilek, Y., Thy, P., 2009. Island arc tholeiite to boninitic melt evolution of the Cretaceous Kizildag (Turkey) ophiolite: model for multi-stage early arc–forearc magmatism in Tethyan subduction factories. Lithos 113, 68–87. http://dx.doi.org/10.1016/j.lithos.2009.05.044.
Dilek, Y., Thy, P., Hacker, B., Grundvig, S., 1999. Structure and petrology of Tauride ophiolites and mafic dike intrusions (Turkey): implications for the Neo-Tethyan ocean. Bulletin of the Geological Society of America 111, 1192–1216.
Dobretsov, N.L., 1991. Blueschists and eclogites: a possible plate tectonic mechanism for their emplacement from the upper mantle. Tectonophysics 186, 253–268.
Dobrzhinetskaya, L.F., 2012. Microdiamonds — frontier of ultrahigh-pressure metamorphism: a review. Gondwana Research 21, 207–223.
Dobrzhinetskaya, L.F., Eide, E.A., Larsen, R.B., Sturt, B.A., Trønnes, R.G., Smith, D.C., Taylor, W.R., Posukhova, T.V., 1995. Microdiamond in high-grade metamorphic rocks of the Western Gneiss region, Norway. Geology 23, 597–600.
Dobrzhinetskaya, L.F., Wirth, R., Yang, J.S., Hutcheon, Ian D., Weber, P.K., Green II, Harry W., 2009. High-pressure highly reduced nitrides and oxides from chromitite of a Tibetan ophiolite, Early Edition. Proceeding of the National Academy of Sciences, pp. 1–6.
Dobrzhinetskaya, L.F., Green, H.W., Takahata, N., Sano, Y., Shirai, K., 2010. Crustal signature of $\delta^{13}C$ and nitrogen content in microdiamonds from Erzgebirge, Germany: ion microprobe studies. Journal of Earth Science 21, 623–634.
Edwards, S.J., Pearce, J.A., Freeman, J., 2000. New insights concerning the influence of water during the formation of podiform chromite. In: Dilek, Y., Moores, E.M., Elthon, D., Nicolas, A. (Eds.), Ophiolites and Oceanic Crust: New Insights From Field Studies and the Ocean Drilling Program. Geological Society of America Special Paper. 49, pp. 139–147.
Fang, Q.S., Bai, W.J., Yang, J.S., Xu, X.Z., Li, G.W., Shi, N.C., Xiong, M., Rong, H., 2009. Qusongite (WC): a new mineral. American Mineralogist 94, 387–390.
Fedortchouk, Y., Matveev, S., Carlson, J.A., 2010. H_2O and CO_2 in kimberlitic fluid as recorded by diamonds and olivines in several Ekati Diamond Mine kimberlites, Northwest Territories, Canada. Earth and Planetary Science Letters 289 (3–4), 549–559.
Field, M., Stiefenhofer, J., Bobey, J., Kurszlaukis, S., 2008. Kimberlite-hosted diamond deposits of southern Africa: a review. Ore Geology Reviews 34, 33–75.
Filimonova, L.G., Trubkin, N.V., 1996. Native aluminium in potash rhyolites of Dukat ore-field. Proceedings of the Russian Mineralogical Society 125, 69–71.
Flower, M.F.J., Dilek, Y., 2003. Arc–trench rollback and forearc accretion: 1. A collision-induced mantle flow model for Tethyan ophiolites. In: Dilek, Y., Robinson, P.T. (Eds.), Ophiolites in Earth History. Geological Society of London Special Publication. 218, pp. 21–42.
Frost, D.J., McCammon, C.A., 2008. The redox state of Earth's mantle. Annual Review of Earth and Planetary Sciences 36, 389–420.
Furnes, H., Dilek, Y., de Wit, M., 2014a. Precambrian greenstone sequences represent different ophiolite type. Gondwana Research http://dx.doi.org/10.1016/j.gr.2013.06.004.
Furnes, de Wit, M., Dilek, Y., 2014b. Four billion years of ophiolites reveal secular trends in oceanic crust formation. Geoscience Frontiers 5, 571–603.
Garutis, G., Zaccarini, F., Moloshag, V., Alimov, V., 1999. Platinum-group minerals as indications of sulfur fugacity in ophiolitic upper mantle: an example from chromitites of the Ray-Is ultramafic complex, Polar Urals, Russia. The Canadian Mineralogist 37, 1099–1115.
Glodny, J., Pease, V., Montero, P., 2000. The Marun Keu metamorphic complex, Polar Urals: protolith evolution and its geodynamics significance. Abstracts INTAS Europrobe Timpebar–Uralides Workshop, October 13–14, St Petersburg, Russia.
Glodny, J., Austrheim, H., Molina, J.F., et al., 2003. Rb/Sr record of fluid–rock interaction in eclogites: the Marun–Keu complex, Polar Urals, Russia. Geochimica et Cosmochimica Acta 67, 4353–4371.
Goodenough, K.M., Thomas, R.J., Styles, M.T., Schofield, D.I., MacLeod, C.J., 2014. Records of ocean growth and destruction in the Oman–UAE ophiolite. Elements 10, 109–114.
Goresy, A.E., Gillet, P., Chen, M., Kunstler, F., Graup, G., Stahle, V., 2001. In situ discovery of shock-induced graphite-diamond phase transition in gneisses from the Ries Crater, Germany. American Mineralogist 86, 611–621.
Grand, S., van der Hilst, R., Widiyantoro, S., 1997. Global seismic tomography: a snapshot of convection in the Earth. GSA Today 7, 1–7.
Griffin, W.L., Yang, J.S., Robinson, P.T., Howell, D., Shi, R., O Reilly, S.Y., Pearson, N.J., 2013. Going up or going down? Diamonds and super-reducing UHP assemblages in ophiolitic mantle. Goldschmidt 2013 Conference Abstracts, p. 1215.
Gurney, J.J., 1989. Diamonds. Geological Society of Australia Special Publication 14, 935–965.
Gurney, J.J., Helmstaedt, H.H., Le Roux, A.P., Nowicki, T.R., Richardson, S.H., Westerlund, K.J., 2005. Diamonds: crust distribution and formation processes in time and space and an interated deposit model. Economic Geology,pp. 143–177, (100th Anniv. Vol.).
Gurney, J.J., Helmstaedt, H.H., Richardson, S.H., Shirey, S.B., 2010. Diamonds through time. Economic Geology 105, 689–712.
Gurov, E.P., Gurova, E.P., Rakitskaya, R.B., 1995. Impact diamonds in the craters of the Ukrainian shield. Meteoritics 30, 515–516.
Gurskaya, L.P., Smelova, L.V., 2003. PGE mineral formation and the structure of the Syum–Keu massif (Polar Urals). Geology of Ore Deposits 45, 309–325.
Harris, D.C., Cabri, L.J., 1991. Nomenclature of platinum-group element alloys: review and revision. Canadian Mineralogist 29, 231–237.
Harte, B., 2010. Diamond formation in the deep mantle: the record of mineral inclusions and their distribution in relation to mantle dehydration zones. Mineralogical Magazine 74 (2), 189–215.
Harte, B., Harris, J.W., 1994. Lower mantle mineral association preserved in diamonds. Mineralogical Magazine 58A, 384–385.
Hayman, P.C., Kopylova, M.G., Kaminsky, F.V., 2005. Lower mantle diamonds from Rio Soriso (Juina, Brazil). Contributions to Mineralogy and Petrology 149, 430–445.
Heymann, D., Lipschutz, M.E., Nielson, B., Anders, E., 1966. Canyon Diablo meteorite: metallographic and mass-spectrometric study of 56 fragments. Journal of Geophysical Research 71, 619–641.
Hoeck, V., Koller, F., Meisel, T., Onuzi, K., Kneringer, E., 2002. The Jurassic South Albanian ophiolites: MOR- vs. SSZ-type ophiolites. Lithos 65, 143–164.
Hough, R.M., Gilmour, I., Pillinger, C.T., Arden, J.W., Gilkes, K.W.R., Yuan, J., Milledge, H.J., 1995. Diamond and silicon carbide in suevite from the Nördlinger Ries impact crater. Nature 378, 41–44.
Hough, R.M., Langenhorst, F., Montanari, A., Pillinger, C.T., Gilmour, I., 1997. Diamonds from the iridium-rich K–T boundary layer at Arroyo el Mimbral, Tamaulipas, Mexico. Geology 25, 1019–1022.
Hu, X.F., 1999. Origin of Diamonds in Chromitites of the Luobusa Ophiolite, Southern Tibet, China. (MSc Thesis) Dalhousie University, p. 151.
Hwang, S.L., Shen, P., Chu, H.T., Yui, T.F., 2000. Nanometer-size αPbO_2-type TiO_2 in garnet: a thermobarometer for ultrahigh-pressure metamorphism. Science 288, 321–324.
Institute of Geology, Chinese Academy of Geological Sciences, 1981. The discovery of alpine-type diamond bearing ultrabasic intrusions in Xizang (Tibet). Geological Review 27, 445–447 (in Chinese).
Iyer, S.D., Mascarenhas-Pereira, M.B.L., Nath, B.N., 2007. Native aluminium (spherules and particles) in the Central Indian Basin sediments: implications on the occurrence of hydrothermal events. Marine Geology 240, 177–184.

Jacobsen, B., Matzel, J., Hutcheon, I.D., Green, H.W., Dobrzhinetskaya, L.F., 2011. Diamond-graphite transformation: a NanoSIMS isotope study of diamond–graphite inclusion in zircon from the Kochetav massif. Abstract, Goldscmidt Conference.
Jaques, A.L., Hall, A.E., Sheraton, J.W., Smith, C.B., Sun, S.S., Drew, R.M., Foudoulis, C., Ellingsen, K., 1989. In: Ross, J., Jaques, A.L., Ferguson, J., Green, D.H., O'Reilly, S.Y., Danchin, R.V., Janse, A.J.A. (Eds.), Composition of Crystalline Inclusions and C-isotope Composition of Argyle and Ellendale Diamonds. Kimberlites and Related Rocks. 2. Blackwell Scientific, Cambridge, England, pp. 966–989.
Kaminsky, F., 2012. Mineralogy of the lower mantle: a review of 'super-deep'mineral inclusions in diamond. Earth-Science Reviews 110, 127–147.
Kaminsky, F., Wirth, R., Matsyuk, S., Schreiber, A., Thomas, R., 2009. Nyerereite and nahcolite inclusions in diamond: evidence for lower-mantle carbonatitic magmas. Mineralogical Magazine 73, 797–816.
Karczemska, A., Jakubowski, T., Vergas, F., 2009. Different diamonds in meteorites — DaG 868 and NWA 3140 ureilites. Journal of Achievements in Materials and Manufacturing Engineering 37 (2), 292–297.
Katayama, I., Parkinson, C.D., Okamoto, K., Nakajima, Y., Maruyama, S., 2000. Supersilicic clinopyroxene and silica exolution in UHPM eclogite and pelitic gneiss from the Kokchetav massif, Kazakhstan. American Mineralogist 85, 1368–1374.
Kawai, K., Yamamoto, S., Tsuchiya, T., Maruyama, S., 2013. The second continent: existence of granitic continental materials around the bottom of the mantle transition zone. Geoscience Frontiers 4, 1–6.
Kazak, A.P., Dobretsov, N.L., Moldavantsev, Yu.E., 1976. Glaucophane schists, jadeitites, vesuvianites and nephrites of the ultrabasitic Rai-Iz massif. Geology and Geophysics 2, 60–66.
Klein-BenDavid, O., Wirth, R., Navon, O., 2007. Micrometer-scale cavities infibrous and cloudy diamonds—a glance into diamond dissolution events. Earth and Planetary Science Letters 264, 89–103.
Koeberl, C., Masaitis, V.L., Shafranovsky, G.I., Gilmour, I., Langenhorst, F., Schrauder, M., 1997. Diamonds from the Popigai impact structure, Russia. Geology 25, 967–970.
Leech, M.L., Ernst, W.G., 1998. Graphite pseudomorphs after diamond? A carbon isotope and spectroscopic study of graphite cuboids from the Maksyutov Complex, south Ural Mountains, Russia. Geochimica et Cosmochimica Acta 62, 2143–2154.
Leech, M.L., Ernst, W.G., 2000. Petrotectonic evolution of the high- to ultrahigh-pressure Maksyutov Complex, Karayanova area, south Ural Mountains: structural and oxygen isotope constraints. Lithos 52, 235–252.
Leung, I., Guo, W., Freidman, I., Gleason, J., 1990. Natural occurrence of silicon carbide in a diamondiferous kimberlite from Fuxian. Nature 346, 352–354.
Liou, J.G., Ernst, W.G., Zhang, R.Y., Tsujimori, T., Jahn, B.M., 2009. Ultrahigh-pressure minerals and metamorphic terranes — the view from China. Journal of Asian Earth Sciences 35, 199–231.
Makeev, A.B., 2000. Interview with diamond — a new hypothesis of formation of natural diamond. Vest. Institute of Geology 4, 25–30.
Makeev, A.B., 2010. Information implications of study of minerals associated with diamond. Russian Chemistry Journal 54, 62–72.
Makeev, A.B., Kriulina, G.Y., 2012. Metal films on the surfaces and within diamond crystals from Arkhangelskaya and Yakutian diamond provinces. Geology of Ore Deposits 54, 663–673.
Makeyev, A.B., 1992. Mineralogy of Alpine-type Ultramafics in the Ural. Nauka, St. Petersburg, pp. 1–195, (in Russian).
Makeyev, A.B., Braynchaninova, N.I., 1999. Topomineralogy of Ultramafics in the Polar Ural. Nauka, St. Petersburg, pp. 1–122, (in Russian).
Makeyev, A.B., Perevozchikov, B.V., Afanacyev, A.K., 1985. Chromite in the Polar Urals. Komi Branch of the Academy of Sciences of USSR, Syktyvkar, Russia, pp. 1–152, (in Russian).
Maruyama, S., Santosh, M., Zhao, D., 2007. Superplume, supercontinent, and post-perovskite: mantle dynamics and anti-plate tectonics on the core–mantle boundary. Gondwana Research 11, 7–37.
Masago, H., Omori, S., Maruyama, S., 2010. Significance of retrograde hydration in collisional metamorphism: a case study of water infiltration in the Kokchetav ultrahigh-pressure metamorphic rocks, northern Kazakhstan. Gondwana Research 18, 205–212.
Masaitis, V.L., 1993. Diamond-bearing impactites, their distribution and petrogenesis. Regionalnaya Geologiai Metallogenia 1, 121–134 (in Russian).
Masaitis, V.L., Futergendler, S.I., Gnevushev, M.A., 1972. Diamonds in impactites of the Popigai meteorite crater. All-Union Mineralogical Society Proceedings 1, 108–112 (in Russian).
Masaitis, V.L., Shafranovsky, G.I., Yezersky, V.A., Reshetnyak, N.B., 1990. Impact diamonds in ureilites and impactites. Meteoritika 49, 180–196 (in Russian).
Massonne, H.J., 1999. A new occurrence of microdiamonds in quartzofeldspathic rocks of the Saxonian Erzgebirge, Germany, and their metamorphic evolution. In: Gurney, J., Gurney, J.L., Pascoe, M.D., Richardson, S.H. (Eds.), The P.H. Nixon Volume. Proceedings of 7th International Kimberlitic Conference, Capetown, pp. 533–539.
Mathez, E.A., Fogel, R.A., Hutcheon, I.D., Marshintsev, V.K., 1995. Carbon isotopic composition and origin of SiC from kimberlites of Yakutia, Russia. Geochimica et Cosmochimica Acta 59, 781–791.
Matte, Ph., 1995. Southern Uralides and Variscides: comparison of their anatomies and evolution. Geologische Mijnbouw 74, 151–166.
Melcher, F., Grum, W., Simon, G., 1997. Petrogenesis of the ophiolitic giant chromite deposits of Kempirsai, Kazakhstan: a study of solid and fluid inclusions in chromite. Journal of Petrology 38, 1419–1458.
Melton, G.L., Stachel, T., Stern, R.A., Carlson, J., Harris, J.W., 2013. Infrared spectral and carbon isotopic characteristics of micro- and macro-diamonds from the Panda kimberlite, Central Slave Craton, Canada. Lithos 177, 110–119.
Meyer, H.O.A., MccaUum, M.E., 1986. Mineral inclusions in diamonds from the Sloan kimberlites, Colorado. Journal of Geology 94, 600–612.
Moghadam, H.S., Stern, R.J., Rahgoshay, M., 2010. The Dehshir ophiolite (central Iran): geochemical constraints on the origin and evolution of the Inner Zagros ophiolite belt. Geological Society of America Bulletin 122, 1516–1547. http://dx.doi.org/10.1130/B30066.1.
Moldavantsev, Yu.E., Kazak, A.P., 1977. Rai-Iz Massif. In: Sobolev, V.S., Dobretsov, N.L. (Eds.), Nauka, Novosibirsk, pp. 38–59 (in Russian).
Moore, R.O., Gurney, J.J., 1989. In: Ross, J., Jaques, A.L., Ferguson, J., Green, D.H., O'Reilly, S.Y., Danchin, R.V., Janse, A.J.A. (Eds.), Mineral Inclusions in Diamond from the Monastery Kimberlite, South AfricaKimberlites and Related Rocks. 2. Blackwell Scientific, Cambridge, England, pp. 1029–1041.
Morishita, T., Dilek, Y., Shallo, M., Tamura, A., Arai, S., 2011. Insight into the uppermost mantle section of a maturing arc: the Eastern Mirdita ophiolite, Albania. Lithos 124, 215–226. http://dx.doi.org/10.1016/j.lithos.2010.10.003.
Mposkos, E.D., Kostopoulos, D.K., 2001. Diamond, former coesite and supersilicic garnet in metasedimentary rocks from the Greek Rhodope: a new ultrahigh-pressure metamorphic province established. Earth and Planetary Science Letters 192, 497–506.
Nakagawa, M., Franco, H.E.A., 1997. Placer Os–Ir–Ru alloys and sulfides: indicators of sulfur fugacity in an ophiolite? The Canadian Mineralogist 35, 1441–1452.
Nicolas, A., 1989. Structures of Ophiolites and Dynamics of Oceanic Lithosphere. 4. Kluwer Academic Publishers, Dordrecht and Boston, p. 367.
Novgorodova, M.I., Blokhina, N.A., Gorshkov, A.I., Trubkin, N.V., 1982. Structurally ordered native aluminum in skarns. Doklady Academy of Science USSR 256, 109–111 (in Russian).
Ogasawara, Y., 2005. Microdiamonds in ultrahigh-pressure metamorphic rocks. Elements 1, 91–96.
Okrugin, A.V., Oleynikov, B.V., Zayakina, N.V., Leskova, N.V., 1981. Native metals in the Siberian Platform traps. Zapiski Vsesoyuznogo Mineralogicheskogo Obshchestva (Reports of All-union Mineralogical Society). 110, pp. 186–204, (in Russian).
Ono, S., 1999. High temperature stability of phase "Egg", $AlSiO_3(OH)$. Contributions to Mineralogy and Petrology 137, 83–89.
Pasava, J., Knesl, I., Vymazalova, A., Vavrin, I., Gurskaya, L.I., Kolbantsev, L.R., 2011. Geochemistry and mineralogy of platinum-group elements (PGE) in chromites from Centralnoye I, Polar Urals, Russia. Geoscience Frontiers 2, 81–85.
Payot, B.D., Arai, S., Dick, H.J.B., Abe, N., 2011. Podiform chromities in dunites from the Southwest Indian Ridge (SWIR). Abstract 24th Annula Geological Convention of the Geological Society of the Philippines.
Pearce, J.A., 2003. Supra-subduction zone ophiolites: the search for modern analogues. Geological Society of America, Special Paper 373, 269–293.
Pearce, J.A., Lippard, S.J., Roberts, S., 1984. Characteristics and tectonic significance of supra-subduction zone ophiolites. Geological Society, London, Special Publications 16, 77–94.
Pearson, D.G., Brenker, F.E., Nestola, F., McNeill, J., Nasdala, L., Hutchison, M.T., Matveev, S., Mather, K., Silversmit, G., Schmitz, S., Vekemans, B., Vincze, L., 2014. Hydrous mantle transition zone indicated by ringwoodite included within diamond. Nature 507, 221–224.
Perevozchikov, B.V., Chashchukhin, I.S., Tsritsyn, E.P., 1990a. Metamorphism of ultramafic rocks massif and their primal composition. In: Puchkov, V.N., Shteinberg, D.S. (Eds.), Structure, Evolution and Minerogenesis of the Rai-Iz Ultramafic Massif. The Ural Branch of the Academy of Sciences of USSR, Sverdlovsk, Russia, pp. 29–57 (in Russian).
Perevozchikov, B.V., Alimov, V.Yu, Tsritsyn, E.P., Chashchukhin, I.S., Sherstobitova, L.A., 1990b. Chromic spinel and chromic mineralization of massif. In: Puchkov, V.N., Shteinberg, D.S. (Eds.), Structure, Evolution and Minerogenesis of the Rai-Iz Ultramafic Massif. The Ural Branch of the Academy of Sciences of USSR, Sverdlovsk, Russia, pp. 145–194 (in Russian).
Perevozchikov, B.V., Kenig, V.V., Lukin, A.A., Ovechkin, A.M., 2005. Chromites of the Rai-Iz massif in the Polar Urals (Russia). Geology of Ore Deposits 47, 206.
Proenza, J., Gervilla, F., Melgarejo, J., Bodinier, J.L., 1999. Al and Cr rich chromitites from the Mayarí–Baracoa Ophiolitic Belt, (eastern Cuba): consequence of interaction between volatile-rich melts and peridotites in suprasubduction mantle. Economic Geology 94, 547–566.
Puchkov, V.N., 1990. Tectonic position and geological feature of massif. In: Puchkov, V.N., Shteinberg, D.S. (Eds.), Structure, Evolution and Minerogenesis of the Rai-Iz Ultramafic Massif. The Ural Branch of the Academy of Sciences of USSR, Sverdlovsk, Russia, pp. 4–10 (in Russian).
Ren, Y.F., Fei, Y.W., Yang, J.S., Bai, W.J., Xu, Z.Q., 2009. SiO_2 solubility in rutile at high temperature and pressure. Journal of Earth Science 20, 274–283.
Richardson, S.H., Gurney, J.J., Erlank, A.J., Harris, J.W., 1984. Origin of diamonds in old enriched mantle. Nature 310, 198–202.
Robinson, P.T., Bai, W., Malpas, J., Yang, J., Zhou, M., Fang, Q., Hu, X., Cameron, S., Staudigel, H., 2004. Ultra-high pressure minerals in the Luobusa Ophiolite, Tibet, and their tectonic implications. Geological Society, London, Special Publications 226, 247–271.
Robinson, P.T., Trumbull, R., Schmitt, A., Erzinger, J., Yang, J.-S., Li, J.-W., Zhou, M.-F., Erzinger, J., Dare, S., Xiong, F., 2014. The origin and significance of crustal minerals in ophiolitic chromitites and peridotites, (in this issue).
Rollinson, H., 2005. Chromite in the mantle section of the Oman ophiolite: a new genetic model. The Island Arc 14, 542–550.
Rollinson, H., 2008. The geochemistry of mantle chromitites from the northern part of the Oman ophiolite: inferred parental melt compositions. Contributions to Mineralogy and Petrology 156, 273–288.
Rollinson, H., Adetunji, J., 2013. Mantle podiform chromitites do not form beneath mid-ocean ridges: a case study from the Moho transition zone of the Oman ophiolite. Lithos 177, 314–327.

Ronkin, Y.L., Priamonocov, A.P., Telegina, T.V., Lepehina, O.P., 2000. Dunite–harzburgite, dunite–wehrlite–clinopyroxenite–gabbro complex of Polar Urals: REE, Sr–Nd constraints. Isotopic Dating of Geological Process: New Methods and Results. Abstract of Report I Russian Conference on Isotopic Geochronology, pp. 302–305 (Moscow, in Russian).

Saccani, E., Photiades, A., 2004. Mid-ocean ridge and supra-subduction affinities in the Pindos ophiolites (Greece): implications for magma genesis in a forearc setting. Lithos 73, 229–253.

Sano, A., Ohtani, E., Kubo, T., Finakoshi, K., 2004. In situ X-ray observation of decomposition of hydrous aluminum silicate $AlSiO_3OH$ and aluminum oxide hydroxide d-AlOOH at high pressure and temperature. Journal of Physics and Chemistry of Solids 65, 1547–1554.

Sarifakioglu, E., Dilek, Y., Sevin, M., 2014. Jurassic–Paleogene intra-oceanic magmatic evolution of the Ankara Mélange, north-central Anatolia, Turkey. Solid Earth 5, 77–108. http://dx.doi.org/10.5194/se-5-77-2014.

Savelieva, G.N., 1987. Gabbro-ultrabasite assemblages of the Urals ophiolites and their analogues in modern oceanic crust. Transactions of the Geological Institute RAS 404, 246.

Savelieva, G.N., Nesbitt, R.W., 1996. A synthesis of the stratigraphic and tectonic setting of the Uralian ophiolites. Journal of the Geological Society 153, 525–537.

Savelieva, G.N., Pertsev, A.N., Astrakhantsev, O.V., et al., 1999. Kytlym pluton, north Urals: structure and emplacement history. Geotectonics 33, 119–141.

Savelieva, G.N., Suslov, P.V., Larionov, A.N., et al., 2006. Age of zircons from chromites in the residual ophiolitic rocks as a reflection of upper mantle magmatic events. Doklady Earth Sciences. 411. MAIK Nauka/Interperiodica, pp. 1401–1406.

Schmidt, M.W., Finger, L.W., Ross, R.J., Dinnebier, R.E., 1998. Synthesis, crystal structure, and phase relations of $AlSiO_3OH$, a high-pressure hydrous phase. American Mineralogist 83, 881–888.

Sharma, M., Wasserburg, G.J., Papanastassiou, D.A., et al., 1995. High $^{143}Nd/^{144}Nd$ in extremely depleted mantle mocks. Earth and Planetary Science Letters 135, 101–114.

Shirey, S.B., Richardson, S.H., Harris, J.W., 2004. Integrated models of diamond formation and craton evolution. Lithos 77, 923–944.

Shiryaev, A.A., Griffin, W.L., Stoyanov, E., 2011. Moissanite (SiC) from kimberlites: polytypes, trace elements, inclusions and speculations on origin. Lithos 122, 152–164.

Shmelev, V.R., 2011. Mantle ultrabasites of ophiolite complexes in the Polar Urals: petrogenesis and geodynamic environments. Petrology 19, 618–640.

Shmelev, V.R., Meng, F.C., 2013. Thenature and age of basic rocks of the Rai-Iz ophiolite massif (Polar Urals). Doklady Earth Sciences 451, 758–761.

Shmelev, V.P., Goncharenko, A.I., Chernyshev, A.I., Puchkov, V.N., Perevozchikov, B.V., 1990. Tectonics of ultramafic and gabbroic rocks. In: Puchkov, V.N., Shteinberg, D.S. (Eds.), Structure, Evolution and Minerogenesis of the Rai-Iz Ultramafic Massif. The Ural Branch of the Academy of Sciences of USSR, Sverdlovsk, Russia, pp. 88–148 (in Russian).

Skuzovatov, S.Y., Zedgenizov, D.A., Ragozin, A.L., Shatsky, V.S., 2012. Growth medium composition of coated diamonds from the Sytykanskaya kimberlite pipe (Yakutia). Russian Geology and Geophysics 53, 1197–1208.

Sobolev, N.V., Shatsky, V.S., 1990. Diamond inclusions in garnets from metamorphic rocks; a new environment for diamond formation. Nature 343, 742–746.

Sobolev, N.V., Ephimova, E.S., Pospelova, L.I., 1981. Native iron in Yakutian diamonds and its paragenesis. Geologiya i Geofizika 22, 25–28 (inRussian).

Sobolev, N.V., Kaminsky, F.V., Griffin, W.L., Yefimova, E.S., Win, T.T., Ryan, C.G., Botkunov, A.I., 1997. Mineral inclusions in diamonds from the Sputnik kimberlite pipe, Yakutia. Lithos 39, 135–157.

Spadea, P., Zanetti, A., Vannucci, R., 2003. Mineral chemistry of ultramafic massifs in the Southern Uralides orogenic belt (Russia) and the petrogenesis of the Lower Palaeozoic ophiolites of the Uralian Ocean. In: Dilek, Y., Robinson, P.T. (Eds.), Ophiolites in Earth History. Geological Society of London Special Publications. 218, pp. 567–596.

Spengler, D.V., Roermund, H.L.M., Drury, M., Ottolini, L., Maso, P.R.D., Davies, G., 2006. Deep origin and hot melting of an Archaean orogenic peridotite massif in Norway. Nature 440, 913–917.

Stachel, T., Harris, J.W., Brey, G.P., 1999. REE patterns of peridotitic and eclogitic inclusions in diamonds from Mwadui (Tanzania). Proceedings of the VIIth International Kimberlite Conference, Cape Town. 2, pp. 829–835.

Stachel, T., Brey, G.P., Harris, J.W., 2000. Kankan diamonds (Guinea) I: from the lithosphere down to the transition zone. Contributions to Mineralogy and Petrology 140, 16–27.

Stachel, T., Brey, G.P., Harris, J.W., 2005. Inclusions in sublithospheric diamonds: glimpses of deep Earth. Elements 1, 73–78.

Stockman, H.W., Hlava, P.F., 1984. Platinum-group minerals in Alpine chromitites from southwestern orogen. Economic Geology 79, 491–508.

Talkington, R.W., Watkinson, D.H., Whittaker, P.J., Jones, P.C., 1984. Platinum-group minerals and other solid inclusions in chromite of ophiolitic complexes: occurrence and petrological significance. Tschermaks Mineralogische und Petrographische Mitteilungen 32, 285–301.

Tappert, R., Stachel, T., Harris, J.W., Muehlenbachs, K., Ludwig, T., Brey, G.P., 2005. Diamonds from Jagersfontein (South Africa): messagers from the sublithospheric mantle. Contributions to Mineralogy and Petrology 150, 505–522.

Tappert, R., Foden, J., Stachel, T., Muehlenbachs, K., Tappert, M., Wills, K., 2009. The diamonds of South Australia. Lithos 112S, 806–821.

Tektonika, U., 1977. (Ob'yasnitel'naya zapiska k tektonicheskoi karte Urala masshtaba 1: 1,000,000)(Tectonics of the Urals: Explanatory Notes to the 1:1,000,000 Tectonic Map of the Urals), Yanshin, A.L., Ed., Moscow: Nauka.

Trumbull, R.B., Yang, J.S., Robinson, P.T., Di Pierro, S., Vennemann, T., Wiedenbeck, M., 2009. The carbon isotope composition of natural SiC (moissanite) from the Earth's mantle: new discoveries from ophiolites. Lithos 113, 612–620.

Uysal, I., Ersoy, E.Y., Dilek, Y., Escayola, M., Sarifakioglu, E., Saka, S., Hirata, T., 2014. Depletion and refertilization of the Tethyan oceanic upper mantle as revealed by the early Jurassic Refahiye ophiolite, NE Anatolia — Turkey. Gondwana Research http://dx.doi.org/10.1016/j.gr.2013.09.008.

Vakhrusheva, N.V., 2007. Non-serpentinized harzburgites and websterites of the Voikar–Syn'ya Massif: mineralogy, geochemistry, and Sm–Nd age. Ul'trabazit-bazitovye kompleksy skladchatykh oblastei (Ultramafic–Mafic Complexes of Fold Systems). Izd-vo IrGTU, Irkutsk, pp. 293–296.

Vanpeteghem, C., Ohtani, E., Kondo, T., Takemura, K., Kikegawa, T., 2003. Compressibility of phase Egg $AlSiO_3OH$: equation of state and role of water at high pressure. American Mineralogist 88, 1408–1411.

VanRoermund, H.L.M., Drury, M.R., 1998. Ultra-high pressure (P > 6 GPa) garnet peridotites in Western Norway: exhumation of mantle rocks from 185 km depth. Terra Nova 10, 295–301.

Vishnevsky, S.A., Palchik, N.A., 1975. Graphite in the rocks of Popigai structure: destruction and transformation to other phases of the carbon system. Geologiya i Geofizika 1, 7–75.

Wakabayashi, J., Dilek, Y., 2003. What constitutes "emplacement" of an ophiolite? Mechanisms and relationship to subduction initiation and formation of metamorphic soles. In: Dilek, Y., Robinson, P.T. (Eds.), Ophiolites in Earth History. Geological Society of London Special Publication. 218, pp. 427–448.

Walker, R.J., Prichard, H.M., Ishiwatari, A., Pimentel, M., 2002. The osmium isotopic composition of convecting upper mantle deduced from ophiolite chromites. Geochimica et Cosmochimica Acta 66, 329–345.

Walter, M.J., Kohn, S.C., Araujo, D., Bulanova, G.P., Smith, C.B., Gaillou, E., Wang, J., Steele, A., Shirey, S.B., 2011. Deep mantle cycling of oceanic crust: evidence from diamonds and their mineral inclusions. Science 334, 54–57.

Wirth, R., Vollmer, C., Brenker, F., Matsyuk, S., Kaminsky, F., 2007. Nanocrystalline hydrous aluminium silicate in superdeep diamonds from Juina (Mato Grosso State, Brazil). Earth and Planetary Science Letters 259, 384–399.

Wirth, R., Kaminsky, F., Matsyuk, S., Schreiber, A., 2009. Unusual micro- and nano-inclusions in diamonds from the Juina Area, Brazil. Earth and Planetary Science Letters 286, 292–303.

Wu, Y., Fei, Y., Jin, Z., Liu, X., 2009. The fate of subducted upper continental crust: an experimental study. Earth and Planetary Science Letters 282, 275–284.

Xiong, F.H., Yang, J.S., Liang, F.H., Ba, D.Z., Zhang, J., Xu, X.Z., Li, Y., Liu, Z., 2011. Zircon U–Pb ages of the Dongbo ophiolite in the western Yarlung Zangbo suture zone and their geological significance. Acta Petrologica Sinica 27, 3223–3238 (in Chinese with English abstract).

Xiong, F.H., Yang, J.S., Robinson, P.T., Xu, X.Z., Liu, Z., Li, Y., Li, J.Y., Chen, S.Y., 2014. Origin of podiform chromitite: a new model based on the Luobusa ophiolite, Tibet. Gondwana Research http://dx.doi.org/10.1016/j.gr.2014.04.008.

Xu, M.J., Jin, Z.M., Wu, Y., 2013. Experimental constraints on the origin of podiform chromitite. Acta Geologica Sinica 87, 196 (supp.).

Xu, S.T., Okay, A.I., Ji, S.Y., Sengor, A.M.C., Su, W., Liu, Y.C., Jiang, L.L., 1992. Diamond from the Dabie Shan metamorphic rocks and its implication for tectonic setting. Science 256, 80–82.

Xu, X.Z., Yang, J.S., Ba, D.Z., Chen, S.Y., Fang, Q.S., Bai, W.J., 2008. Diamond discovered from the Kangjinla chromitite in the Yarlung Zangbo ophiolite belt, Tibet. Acta Petrologica Sinica 24 (7), 1453–1462 (in Chinese with English abstract).

Xu, X.Z., Yang, J.S., Chen, S.Y., Fang, Q.S., Bai, W.J., Ba, D.Z., 2009. Unusual mantle mineral group from chromitite orebody Cr-11 in Luobusa ophiolite of the Yarlung–Zangbo suture zone, Tibet. Journal of Earth Science 20, 284–302.

Xu, X.Z., Yang, J.S., Guo, G.L., Li, J.Y., 2011. Lithological research on the Purang mantle peridotite in western Yarlung–Zangbo suture zone in Tibet. Acta Petrologica Sinica 27, 3179–3196 (in Chinese with English abstract).

Xu, X.Z., Yang, J.S., Robinson, P.T., Xiong, F.H., Ba, D.Z., Guo, G.L., 2014. Origin of ultrahigh pressure and highly reduced minerals in podiform chromitites and associated mantle peridotites of the Luobusa ophiolite, Tibet. Gondwana Research http://dx.doi.org/10.1016/j.gr.2014.05.010.

Yamamoto, S., Komiya, T., Hirose, K., Maruyama, S., 2009. Coesite and clinopyroxene exsolution lamellae in chromites: in-situ ultrahigh-pressure evidence from podiform chromitites in the Luobusa ophiolite, southern Tibet. Lithos 109, 314–322.

Yang, J.S., Robinson, P.T., 2011. In-situ diamonds and moissanite in podiform chromitites of the Luobusa and Ray-Iz ophiolites, Tibet and Russia. Goldschmidt Conference Abstracts, p. A2209.

Yang, J.S., Xu, Z.Q., Song, S.G., Zhang, J.X., Wu, C.L., Shi, R.D., Li, H.B., Brunel, M., 2001. Discovery of coesite in the North Qaidam Early Paleozoic ultrahigh pressure (UHP) metamorphic belt, NW China. Comptes Rendus de l'Académie des Sciences de la Terre et des Planets/ Earth and Planetary Sciences 333, 719–724.

Yang, J.S., Bai, W.J., Fang, Q.S., Yan, B.G., Shi, N.C., Ma, Z.S., Dai, M.Q., Xiong, M., 2003. Silicon-rutile—an ultrahigh pressure (UHP) mineral from an ophiolite. Progress in Natural Science 13, 528–531.

Yang, J.S., Bai, W.J., Rong, H., Zhang, Z.M., Xu, Z.Q., Fang, Q.S., Yan, B.G., Li, T.F., Ren, Y.F., Chen, S.Y., Hu, J., Su, J., Mao, H.K., 2005. Discovery of Fe_2P alloy in garnet peridotite from the Chinese Continental Scientific Drilling Project (CCSD) main hole. Acta Petrologica Sinica 21, 271–276 (in Chinese with English abstract).

Yang, J.S., Dobrzhinetskaya, L., Bai, W.J., Fang, Q.-S., Robinson, P.T., Zhang, J., Green, H., 2007. Diamond- and coesite-bearing chromitites from the Luobusa ophiolite, Tibet. Geology 35, 875–878.

Yang, J.S., Bai, W.J., Fang, Q.S., Rong, H., 2008. Ultrahigh-pressure minerals and mew minerals from the Luobusa ophiolitic chromitites in Tibet: a review. Acta Geoscientica Sinica 29, 263–274 (in Chinese with English abstract).

Yang, J.S., Bai, W.J., Dobrzhinetskaya, L., Makeev, A.B., 2009. In situ diamonds in polished chromitite fragments from the chromite deposits in Polar Ural and Tibet. American Geophysical Union, Fall Meeting Abstracts, #V54B-08.

Yang, J.S., Xu, X.Z., Li, Y., Li, J.Y., R. H., Ba, D.Z., Zhang, Z.M., 2011. Diamonds recovered from peridotite of the Purang ophiolite in the Yarlung–Zangbo suture of Tibet: a proposal for a new type of diamond occurrence. Acta Petrologica Sinica 27, 3207–3222 (in Chinese with English abstract).

Yang, J.S., Robinson, P.T., Xu, X.Z., Dilek, Y., 2013. Ophiolite-type diamond: a new occurrence of diamond on the Earth. Abstract European Geosciences Union General Assembly 2013, Vienna, Austria.

Yang, J.S., Robinson, P.T., Dilek, Y., 2014. Diamonds in ophiolites. Elements 10, 127–130.

Ye, K., Cong, B., De, E., 2000. The possible subduction of continental material to depth greater than 200 km. Nature 407, 734–736.

Yumul, G.P., 2001. The Acoje block platiniferous dunite horizon, Zambales ophiolite complex, Philippines: melt type and associated geochemical controls. Resource Geology 51, 165–174.

Zavaritsky, A.N., 1932. Peridotite Massif Rai-Iz in Polar Urals. ONTI, Moscow, p. 220, (in Russian).

Zedgenizov, D.A., Ragozin, A.L., Shatsky, V.S., Araujo, D., Griffin, W.L., Kagi, H., 2009. Mg and Fe-rich carbonate–silicate high-density fluids in cuboid diamonds from the Internationalnaya kimberlite pipe (Yakutia). Lithos 112, 638–647.

Zhao, D., 2004. Global tomographic images of mantle plumes and subductingslabs: insight into deep earth dynamics. Physics of the Earth and Planetary Interiors 146, 3–34.

Zhou, M.F., Robinson, P.T., Bai, W.J., 1994. Formation of podiform chromitites by melt/rock interaction in the upper mantle. Mineralium Deposita 29, 98–101.

Zhou, M.F., Robinson, P.T., Malpas, J., Li, Z., 1996. Podiform chromitites in the Luobusa Ophiolite (southern Tibet); implications for melt–rock interaction and chromite segregation in the upper mantle. Journal of Petrology 37, 3–21.

Zhou, M.F., Robinson, P.T., Su, B.X., Gao, J.F., Li, J.W., Yang, J.S., Malpas, J., 2014. Compositions of chromite, associated minerals, and parental magmas of podiform chromite deposits: the role of slab contamination of contamination of asthenospheric melts in supersubduction zone environments. Gondwana Research http://dx.doi.org/10.1016/j.gr.2013.12.011.

Zhu, M.Y., Liu, Y., 1981. Discovery of native chromium in Xizang (Tibet). Chinese Science Bulletin 26, 1014–1017.

Zhu, M.Y., Liu, Y.X., Zhou, X.C., Mao, S.H., 1981. Discovery of native chromium in Tibet. Chinese Science Bulletin 15, 936–938 (in Chinese).